

UNCLASSIFIED

AD NUMBER
AD467728
NEW LIMITATION CHANGE
TO Approved for public release, distribution unlimited
FROM Distribution authorized to U.S. Gov't. agencies and their contractors; Administrative/Operational Use; Jun 1965. Other requests shall be referred to Office of Naval Research, Arlington, VA 22217.
AUTHORITY
ONR, D/a ltr, 26 Oct 1972

THIS PAGE IS UNCLASSIFIED

SECURITY

MARKING

The classified or limited status of this report applies to each page, unless otherwise marked.

Separate page printouts MUST be marked accordingly.

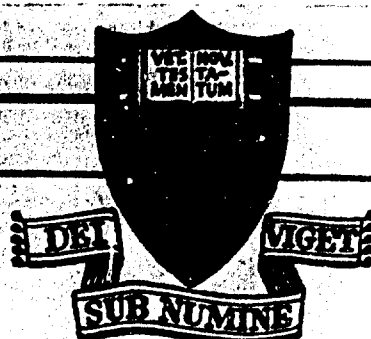
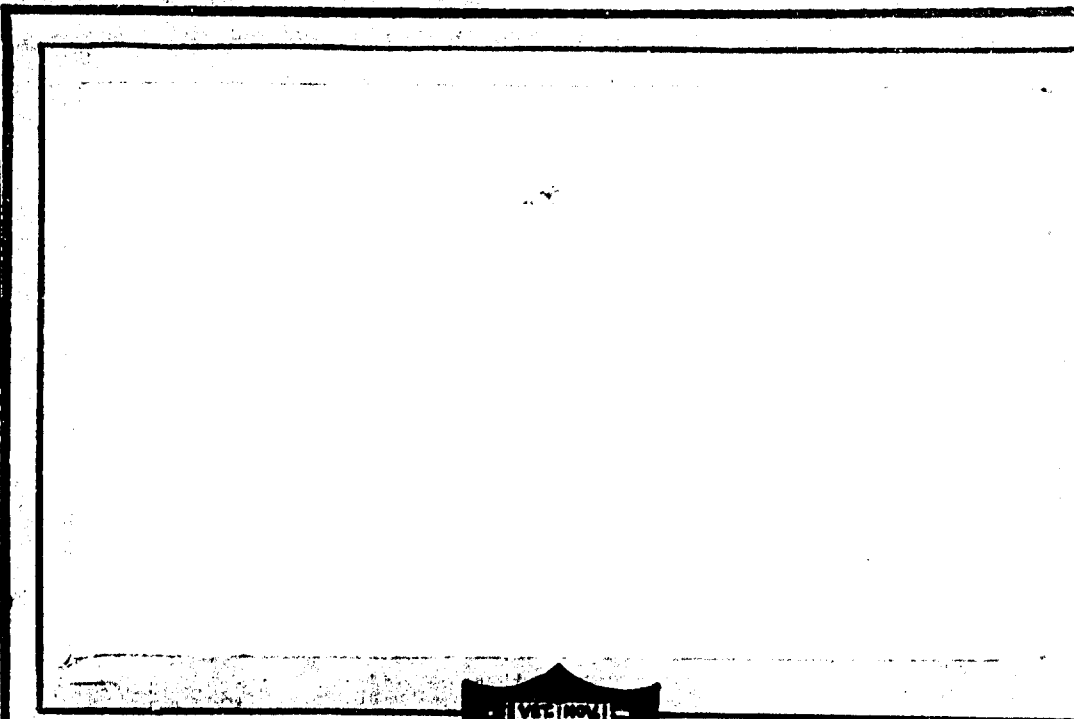
THIS DOCUMENT CONTAINS INFORMATION AFFECTING THE NATIONAL DEFENSE OF THE UNITED STATES WITHIN THE MEANING OF THE ESPIONAGE LAWS, TITLE 18, U.S.C., SECTIONS 793 AND 794. THE TRANSMISSION OR THE REVELATION OF ITS CONTENTS IN ANY MANNER TO AN UNAUTHORIZED PERSON IS PROHIBITED BY LAW.

NOTICE: When government or other drawings, specifications or other data are used for any purpose other than in connection with a definitely related government procurement operation, the U. S. Government thereby incurs no responsibility, nor any obligation whatsoever; and the fact that the Government may have formulated, furnished, or in any way supplied the said drawings, specifications, or other data is not to be regarded by implication or otherwise as in any manner licensing the holder or any other person or corporation, or conveying any rights or permission to manufacture, use or sell any patented invention that may in any way be related thereto.

CATALOGED BY: DDG

467728

AS AD NO.



PRINCETON UNIVERSITY

DEPARTMENT OF
AEROSPACE AND MECHANICAL SCIENCES

Best Available Copy

DEPARTMENT OF THE NAVY
OFFICE OF NAVAL RESEARCH
POWER BRANCH

Contract Nonr 1858(32)
Task No. (NR - 092-516)
ARPA Order No. 23

SOLID PROPELLANT COMBUSTION

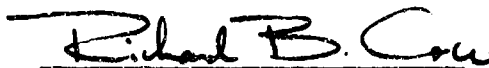
MECHANISM STUDIES

Fifteenth and Sixteenth Progress Report

For the Period 1 October 1963 to 31 March 1964

Aerospace and Mechanical Sciences Report No. 446-o

by



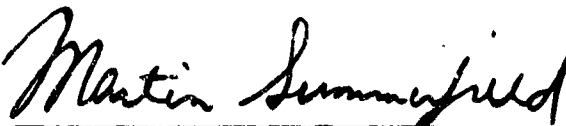
Richard B. Cole - Air Reduction Company Fellow

and



Joseph Wenograd - Research Engineer

Transmitted by:



Martin Summerfield
Principal Investigator

Reproduction, translation, publication, use and disposal in
whole or in part by or for the United States Government is
permitted.

17 June 1965

Guggenheim Laboratories for the Aerospace Propulsion Sciences
Department of Aerospace and Mechanical Sciences
PRINCETON UNIVERSITY
Princeton, New Jersey

The contents of this report have been submitted in partial fulfillment of the requirements for the degree of Master of Science in Engineering from Princeton University, 1965.

ACKNOWLEDGEMENTS

The writer would like to acknowledge the assistance and advice of a number of persons who substantially contributed to the progress of this research work.

Dr. Martin Summerfield, Professor of Aeronautical Engineering, lent notable guidance and direction to this work in his capacity of thesis advisor, and his enthusiasm for solid propellant combustion research never failed to communicate itself. The insights and inspiration which Dr. Summerfield provided are gratefully acknowledged.

The author is also pleased to acknowledge the cooperation, guidance, patience, and support offered him by Dr. Joseph Wenograd. Dr. Wenograd's experience in the areas of chemistry and experimental techniques contributed significantly to the author's research effort and experience.

Finally, the author would like to acknowledge the assistance of Messrs. Sylvester Hight and Keith Donaldson in optics and photographic technique development, Messrs. Lubomyr Kurylko and Chris Felsheim for their efforts in propellant processing, and Mr. Fran Michot during development and construction of experimental apparatus.

TABLE OF CONTENTS

	<u>Page</u>
TITLE PAGE	i
ACKNOWLEDGEMENTS	ii
TABLE OF CONTENTS	iii
ABSTRACT	vi
CHAPTER I - Introduction	1
CHAPTER II - Composite Solid Propellant Burning Surface Photography	7
A. Background	7
B. Experimental Program	11
1. Approach	11
2. Concept Feasibility	11
3. Apparatus	12
a. Optical Strand Burner	13
b. Optical System	15
(1) "Depth-of-Field" vs. "Resolution"	15
(2) Optical System Analysis and Results	18
(3) Optical System Details	19
c. Photographic Light Source	20
4. Procedure	26
a. Strand Preparation	26
b. Flash Synchronization	27
c. Firing Procedure	28
d. Interference by Carbon Continuum Radiation	29

TABLE OF CONTENTS

	<u>Page</u>
Chapter II (continued)	
C. Results and Discussion	32
D. Conclusions and Recommendations	39
CHAPTER III - Composite Solid Propellant Burning Studies at Low Pressures	41
A. Background	41
B. Previous Subatmospheric Composite Propellant Combustion Studies	43
C. Previous Studies of Particle Size Effects in Composite Solid Propellant Combustion at Low Pressures	44
D. Experimental Program	52
1. Scope of Work	52
2. Apparatus	52
a. Subatmospheric Pressure Strand Burner	52
b. Instrumentation	55
c. Subatmospheric Strand Burner Operation	57
3. Procedure	59
4. Measurement Errors and Data Reduction	61
5. Results	65
6. Discussion	67
7. Conclusions and Recommendations	71
REFERENCES	74
APPENDICES A - NOMENCLATURE	A-18
REFERENCES	A-20
LIST OF FIGURES	A-21
B	

FIGURES

LIST OF FIGURES

- Figure 1 Apparatus for Burning Surface Photography at Atmospheric Pressure
- Figure 2 Surface of Polyester-Styrene Propellant Photographed While Burning (1 atm. press. in N_2)
- Figure 3 Optical Strand Burner for Photography of Burning Solid Propellant Strands
- Figure 4 Detail Crosssection of Strand Location in Optical Strand Burner
- Figure 5 Optical System for Solid Propellant Burning Surface Photography
- Figure 6 Photoelectric Trigger Sensor Assembly for Sensing Presence of Burning Surface in Photographic Field-of-View
- Figure 7 Photoelectric Trigger Circuit
- Figure 8 PBAA Propellant Burning at 250 psig
- Figure 9 LP-3 Propellant Burning at 300 psig
- Figure 10 Low Pressure Burning Rates of Several Composite Solid Propellants of Narrow, Unimodal Particle Size Distributions
- Figure 11 Surface of Polysulfide-Ammonium Perchlorate Propellant Burning at 20 psig
- Figure 12 Surface of Polysulfide-Ammonium Perchlorate Propellant Burning at 100 psig
- Figure 13 Collected Subatmospheric Pressure Composite Solid Propellant Burning Rates
- Figure 14 Modes of Combustion (Polysulfide Propellants, Unimodal Particle Size Distributions)
- Figure 15 Burning Rate vs Pressure for Polysulfide Propellants, Narrow Unimodal Particle Size Distributions
- Figure 16 Burning Rate vs Particle Size, Polysulfide Propellants, Narrow Unimodal Particle Size Distributions
- Figure 17 Burning Rate vs Particle Size, Polyester-Styrene Propellants, Unimodal Particle Size Distributions
- Figure 18 Diffusion Time Parameter "b" vs Particle Size, Polysulfide Propellants, Narrow Unimodal Particle Size Distributions
- Figure 19 P/r vs $P^{2/3}$, Polysulfide Propellants, Narrow Unimodal Particle Size Distributions
- Figure 20 Subatmospheric Strand Burner
- Figure 21 Subatmospheric Strand Burner Flow System
- Figure 22 Photographic Burning Rate Measurement Optical System
- Figure 23 Typical Film Record Used for Propellant Burning Rate Determination

ABSTRACT

Two composite solid propellant combustion experiments aimed at further elucidation of combustion mechanism are reported; one deals with burning surface photomacroscopy, the other, with low pressure combustion and oxidizer particle size influences on it.

The first investigation involved photography of the surfaces of 1/4 inch square polysulfide-ammonium perchlorate (unmetallized) propellant strands during combustion in a coaxially-flowing nitrogen environment. Intense electronic flash illumination was used to render the luminosity of the flame photographically negligible, and the externally-lighted surface was thereby viewed obliquely through the propellant flame zone at up to seven times magnification. Apparatus is described in detail, and an appendix of first-order analytical studies of the resolution-"depth-of-field" trade-off in photomacroscopic systems is included. Useful combustion pressures for high resolution surface photography of burning strands were found to be limited to less than about 500 psig, due to increasing carbon continuum radiation and the image-degrading temperature inhomogeneities of the flame zone at higher pressures. Observations on polybutadiene-acrylic acid-ammonium perchlorate and polyester-ammonium perchlorate propellants indicated an even lower pressure limit on high resolution burning surface photomacrography. Results include single frame black-and-white photographs displaying the combustion of the large oxidizer particles of a bimodal blend

within crater-like surface depressions and cloud-like haze patches over some individual large oxidizer particles. Liquid-phase agglomerates were also photographed when potassium perchlorate was substituted for ammonium perchlorate in the polysulfide propellant.

The second investigation dealt with the dependence of the sub-atmospheric pressure burning rates of 1/4 inch square strands of ammonium perchlorate (polybutadiene-acrylic acid and polysulfide, unmetallized) propellants on pressure and oxidizer particle size. An apparatus providing for burning rate determination by sequence photography of the strands burning in an essentially stagnant nitrogen environment is detailed, and burning rate versus pressure results are reported for two propellants containing narrow, unimodal oxidizer cuts with mean particle sizes of 13 and 165 microns. On the basis of these and the earlier data of Bastress, it is suggested that mass diffusion may be an insufficient basis for an explanation of particle size effects in composite propellant combustion and that current analytical formulations of mass diffusion concepts are not supported by the observed trends of burning rate data at low pressures. Several possible alternatives to mass diffusion explanations of particle size effects are mentioned and include locally unsteady burning and the particle size dependence of ammonium perchlorate thermal decomposition. In the light of this study using a nearly-stagnant environment a different apparatus arrangement providing a coaxial purge-flow environment was judged necessary for low pressure flame spectroscopy or surface photography because of optical interference by the white smoke typically produced during low pressure combustion.

CHAPTER I

INTRODUCTION

In the midst of a large body of published experimental data on the many aspects of the combustion of composite solid propellants appears a considerable discussion and presentation of theories regarding the steady-state combustion mechanism of these propellants. Several reviews have been directed at surveying the status both of these combustion mechanism theories and of the associated experimental results bearing upon them (5) (6) (7)*. While it is not the aim of this thesis to deal directly and in detail with these various hypotheses of burning mechanism, nonetheless, some mention of them serves to clarify the aspects of combustion mechanism dealt with herein. Not considered here are the several propellant theories involving homogeneous propellant models despite possible and suggested application of these theories (35) to composite propellants with either so-called "inert" binders or those with separately-reactive binders.

Current theories of solid propellant combustion mechanism deal almost exclusively with the prediction of the propellant burning rate (linear regression rate of the burning surface) as a function of combustion pressure. The ballistic implications of such a relation between mass rate of combustion and chamber pressure are well known (8) (34) (36).

The various heterogeneous propellant burning rate theories deal with several important physical processes and combine these within the following phenomenological view of the combustion process: Gas-phase

*Numbers in parentheses refer to references listed on page 74

reaction of fuel and oxidizer initially unmixed and streaming separately from the burning surface serves as a source for heat feedback to the surface; this heat feedback provides energy to support gasification and any endothermic reaction in the solid phase and at the surface. The heat feedback also serves to raise the propellant from its initial sensible enthalpy level to a higher level corresponding to the higher temperature of the burning surface.

In the sense that heat transfer is presumed to be the mechanism of flame propagation into the solid, the various composite propellant burning theories are so-called "thermal theories" of flame propagation. In the sense that heat release through gas phase reaction is assumed to depend upon mixing of gaseous reactants (which are initially unmixed at the burning surface), the theories are largely for so-called "diffusion flames" either controlled by the rates of mass diffusion transverse to the burning surface (as contrasted to control by chemical reaction rates) or at least strongly influenced by such diffusion rates. The sole exception to this is the oxidizer-decomposition-controlled model of Chaiken's theory (2).

In the face of the obvious difficulties and complexities encountered in any attempt at complete analytical description of the composite propellant combustion zone, current burning rate theories deal with postulates of simplified, controlling processes, i.e., heat feedback by conduction only (either quasi-one-dimensional (1) (4),

two-dimensional (3), or three-dimensional (2)) with either gasification and diffusion controlling (1), chemical kinetics controlling (2), or a combination of chemical kinetics and diffusion (4) controlling heat release.

Analytical treatments in current composite propellant theories typically deal with gas phase processes via the equation of energy conservation in a convective flow field. Expressions for burning rates as functions of pressure particle size, flame temperature, etc. are determined either by use of an integrated energy equation form wherein energy conservation at the plane of the burning surface is expressed in terms of mass flux, surface and flame temperatures, and flame stand-off distance from the surface (1)(2)(4) or by actual integration of the appropriate differential equation for energy conservation in a flow field with given temperature and composition boundary conditions both at the surface and downstream at infinity (3). In all cases the dimensional scale of solid phase inhomogeneity (say, mean oxidizer particle size) is introduced into the energy equation formulations. Typically, this scale of inhomogeneity is related to flame stand-off distance from the surface (quasi-one-dimensional, concentrated flame zones) or, in more general terms (for non-concentrated, multi-dimensional flame zones), to the characteristic physical scale of the gas phase temperature profile. This relation is typically the result of considering either diffusion resulting from gas phase composition heterogeneity (1)(3)(4) or

burning surface configuration (2)(3). Inherent in all treatments is the modeling of the burning surface in some simple manner which is not justifiable *a priori* but is only supportable in the light of experimental observations. Further, in all cases, the burning surface temperature enters the energy equation either as a constant or as a dependent variable determined by simultaneous solution of the energy conservation equation and pyrolysis rate expressions* for burning surface gasification rate.

One quickly observes in the light of the preceding comments that, at least in conjunction with extant theories (and probably in any theory of composite propellant combustion which is to account for propellant heterogeneity effects on burning rate), two aspects of the combustion process are of particularly profound importance. These are the physical and chemical nature of the burning surface and the physics of the gas phase mixing process.

The importance of the burning surface and consequently of at least a partial knowledge of its nature in composite propellant combustion is apparent. Physically, its importance is that of a reactive phase interface with composition inhomogeneity which forces gas mixing prior to reaction in the gas phase. Further, the burning surface represents an obvious physical boundary in the midst of the zone affected by combustion. The composition discontinuity across the surface determines

* These rate expressions have generally been of the Arrhenius form.

(both chemically and physically) the nature of the reactant inputs to the gas phase flame. Mathematically, the burning surface is of obvious import as a boundary of the presumed major reactive region (the gas phase). In any differential treatment of the gas phase state the surface must be specified as a boundary condition in terms of transverse temperature and/or composition profiles and gradients. Likewise, integral treatments of the propellant flame must include specification of at least thermal gradients at the surface and mass flow from the surface in order to treat energy and overall mass conservation in the flame zone.

Similar to the burning surface, the subject of the gas phase mixing of fuel and oxidizer has a justifiably essential place in current theories of composite propellant combustion. Visual and photographic observation of the combustion of such propellants (at any but the lowest combustion pressures) has indicated inhomogeneity in the gas phase (see, for example, references (13)(14)(16)(17)(24)(25)(37)(38)(46)). The implications of this inhomogeneity on reactive heat release and consequent thermal flame propagation as described above are obvious. Experimental burning rate measurements indicate oxidizer particle size effects which also suggest mixing influences. Mathematically, inhomogeneity in the gas phase reactive region necessitates the introduction of two or three dimensional mass diffusion formulations into either differential or integral treatments of the composite propellant combustion situation.

As might, therefore, be expected, the various characterizations of gas phase mass diffusion effects in composite solid propellant combustion mechanism theories are quite diverse.

This thesis describes two researches into the nature of: first, the burning surface, and second, the effects of inhomogeneities on composite solid propellant combustion. It deals with the development of a photographic research tool for gaining needed insights into the nature of the composite propellant burning surface and with some results of the use of this technique. Further, it describes burning rate measurements on composite propellants burning at low pressures which constitute an extension of previous researches into diffusive influences on composite propellant combustion. These two aspects of the overall combustion picture are dealt with separately in the following two chapters and experimental results are presented for each case. These results, while not comprehensive, do serve to establish clearly the feasibility of meaningful photographic studies of the propellant burning surface and to promote a more careful consideration of diffusive influences in composite propellant combustion.

CHAPTER II

COMPOSITE SOLID PROPELLANT BURNING SURFACE PHOTOGRAPHY

A. Background

There are a number of interesting aspects of the nature of a solid propellant burning surface with respect to combustion mechanism and burning rate theories. Insight into some of these various aspects is to be expected from reasonably-high-resolution photographic studies of the surface.

Surface shape has been involved both in mathematical characterizations of the surface, e.g., the "two-temperature" surface of the Nachbar "sandwich" model (3), and also in attempts at qualitative description of burning rate details, e.g., the surface "waviness" observed by Bastress and postulated by him to relate to particle-size-induced plateau burning effects (9).

Questions of phase of the surface material arise with some oxidizers and fuels, e.g., $KClO_4$ oxidizer or polyurethane fuel (10). These questions relate to such matters as physical mixing of reactants before gasification and change in gas phase scale of inhomogeneity due to material agglomeration at the surface.

Further, the actions and effects of numerous propellant additives including catalysts and metal particles have been either observed or postulated to depend on surface phenomena. For example such effects as protrusion from surface into flame zone (11)(40) and surface agglomeration of fine metal particles (12)(17) are of

considerable interest and are amenable to investigation by burning surface photography. Other interesting aspects of the burning surface include the intermittent and unsteady combustion of discrete oxidizer particles and the physical appearance of the surface as evidence of sub-surface reaction in the solid phase. From these numerous and interesting considerations, one is, therefore, led to investigate the possibility of applying photographic techniques to observations of the propellant burning surface.

While considerable previous work involving photography of burning solid propellant and of extinguished solid propellant surfaces has been reported, up to this time little concerted effort has apparently been made to observe the burning surface itself during combustion. Such work as has been reported involves one of three approaches, i.e., such low resolution surface observation as is possible via flame illumination itself (10), profile observation via backlighting of very thin propellant strands (13), or relatively low resolution photography of surfaces via external artificial light sources (10). Without exception previous efforts have had serious limitations due to the abnormality of the burning situation in which surface observations are made.

In those cases where flame luminosity serves as the light source for surface photography, it is generally difficult to observe the surface except near an edge of the burning sample. Likewise,

observations on very thin propellant samples force observations on the sample edge where combustion may be quite abnormal as compared with the central portion of a large sample. Edge effects as indicated, for example, by the dependence of burning rates (measured by combustion of small strands of propellant) on sample size (14) can be important in distorting the combustion process by various means such as heat loss from the solid phase, mixing of ambient gases with the flame zone immediately above the propellant sample, etc. Thus, both surface observation by self illumination and by profile views of thin samples have a serious drawback in leaving the observer uncertain of how well his observations really characterize the surface of a normally-burning propellant sample.

Past efforts at photography of burning propellant surface via artificial light sources likewise raise serious questions regarding validity of the observations made. To date, in each situation where artificial illumination was provided for photographic observation, the continuous light sources used were of such intensity as to allow ignition of the propellant sample solely by the radiant energy flux of this illumination (10) (15). Clearly, the radiant energy influx inherent in such illumination affects the combustion process and the burning surface structure to an indeterminate extent. This fact must cast serious doubts on surface observations made under such circumstances.

Further comments on previous attempts at burning surface photography may be made with respect to the resolution of surface detail. Previous efforts may be roughly classified into two types: those involving relatively low magnification (up to about two times) with relatively large depth-of-field (10)(12)(15)(17) and those involving relatively high magnification (from ten times to twenty times) and small depth-of-field (13)(16). No previous work of this sort at intermediate magnifications, say, three to ten times is known.

The first of these types of past photographic effort has the disadvantage of yielding observations on only grossest structure of the burning surface to an extent that will be made clearer in later portions of this thesis. Though gross features are of interest with respect to some aspects of surface phenomena, e.g., metal additive agglomeration, it is certainly desirable to attain higher resolution for study of other aspects, e.g., oxidizer-fuel surface configuration.

The second type of photographic studies (high magnification, low depth-of-field), while providing greater resolution of detail, suffers from decreased depth-of-field such that frequently only regions with dimensions of the same order of magnitude as a typical oxidizer particle size are "in-focus". Further, it is this second type which typically has the thin sample edge effect uncertainty described above. Thus, it is appropriate to seek to develop a better photographic

system for burning surface photography not only because of the previously-described effects of sample configuration and artificial illumination, but also because of resolution vs. depth-of-field considerations.

B. Experimental Program

1. Approach

The basic concept from which the research program described in this chapter grew is that of photographically viewing the burning surface using an artificial light source for illumination. This light source should be of such intensity that the photographic effect of flame illumination is negligible under the photographic exposure conditions used. This concept also included a configuration minimizing the possibility of observations of uncertain validity because of edge effects and light source radiant energy effects.

2. Concept Feasibility

To evaluate the feasibility of the photographic technique, an experiment was carried out in which strands of solid propellant were photographed while burning at atmospheric pressure in a stream of nitrogen gas. The experimental arrangement is depicted in Figure 1.

For this preliminary experiment, existing equipment was used which limited the magnification on the film to five times actual size. The camera used was a 35 mm. single lens reflex

equipped with an apochromatic $f/1.8$ lens and extension tubes. Figure 2 is a photograph of a typical composite propellant containing a relatively coarse ammonium perchlorate oxidizer and was taken with the apparatus of Figure 1. While Figure 2 and other similar photographs constituted only a preliminary test of the concept, it was apparent that the depth of field and spatial resolution obtainable offered encouragement for further efforts.

Placement of an electronic flash gun sufficiently close to the burning strand made ample light intensity available, even though the nominal aperture setting was the largest possible with the apparatus used ($f/22$). The use of an electronic flash as the source of illumination had the added advantage of limiting the exposure time to about $1/1000$ th second, thus providing time resolution of the moving burning surface similar in order of magnitude to the spatial resolution sought.

On the strength of successful photographs such as that of Figure 2, the following experimental program to allow surface photography at higher resolution and over an appreciable range of combustion pressures was initiated.

3. Apparatus

Since the relation between combustion chamber pressure and propellant burning rate is a major interest in composite

solid propellant combustion, burning surface observations at different pressures are desirable. To this end, a pressure vessel and compatible optical system were required.

a. Optical Strand Burner

The following pressure vessel specifications allowing comprehensive burning surface photography were considered in selecting the optical strand burner:

1. Pressure range from sub- or at least atmospheric to approximately 2000 psia.
2. Provision for ignition of the propellant inside the pressure vessel.
3. Optical windows appropriate to both photography and auxiliary lighting requirements, e.g., an oblique or normal view of the burning surface itself was required rather than merely a profile view.

In order to eliminate the need for applying a restrictive coating to the propellant sides (which would obscure the view of the burning surface), a continuously-purging chimney-type propellant strand burner selected for this investigation.

The burner used was a modification of an existent propellant strand burner equipped with slot windows in the

axial direction. The primary burner modification required was provision for an inner chimney to allow more uniform gas flow past the burning propellant and assure ease in cleaning optical surfaces open to possible soiling by combustion products. The slot window of the burner provided a range of directions from which to supply auxiliary photographic lighting to the strand surface. However, because of the thick windows required for high pressure containment, attempts to view the strand via an optical path oblique to the window surfaces suffered from excessive distortion in photographic image quality (particularly considering the high level in resolution desired in this study). Consequently, a novel technique for igniting the propellant strand was developed. This technique forced the propellant surface to burn at an angle to the bomb windows and to the optical axis of the photographic system. Since the burning surface tended to direct itself during the combustion process toward a plane normal to the axis of the strands, the surface was viewed shortly after ignition (long enough after ignition, however, to assure the end of ignition transients causing variation in the shape of the burning surface).

The original strand burner arrangement provided for purge gas inlet at the bottom of the burner but this was found to produce an ejector effect which lowered the pressure

between the inner chimney and burner pressure body. This pressure decrease promoted a slight leakage of product gases from inside the inner chimney to the annular region between it and the pressure windows. Leakage resulted in a deposition of soot and smoke on the inner surfaces of the pressure windows. In the final arrangement as illustrated in Figures 3 and 4, gas was introduced at the top of the burner and forced to flow down through the annular passage thereby precluding such leakage.

b. Optical System

1. "Depth-of-Field" Versus "Resolution"

Preliminary photographic studies (see page 11) indicated "depth-of-field" to be a major influence on the apparent usefulness of burning surface photographs. That is to say, visual observation of projected color transparencies and enlargements of black-and-white negatives showed only a narrow region of the obliquely-viewed propellant surface in any detail.¹ Clearly, this effect had to be accounted for in attempting rational optical

1. This, of course, only reflects what photographers know well, i.e., that while the detail ultimately observable through enlargement of a photograph of a planar object (located at a photographic systems plane of perfect focus) depends solely on the quality of the film, lense, etc., detail in the photographic image of a non-planar object (of finite depth) is also influenced by the geometrics of optical image formation. Thus, the image of every point of an object is not, even for "perfect" optical systems, a point but rather a finite area. The visual effect of this area is attributed (if the human eye can resolve the finite dimensions of the area) to the subject point's being "out-of-focus".

system design for the given instrumentation problem. Thus it was obviously not sufficient that the photographic optical system be fabricated from components capable of resolving small detail only at the geometrical plane of perfect focus. It was required further that the resultant object depth over which such a detail was "in focus" had to exceed the actual dimensions.

Rather than consider "depth-of-field" in the classical photographic sense, it appeared rational to consider "resolution" as the combined result of both geometric ("depth-of-field") effects and non-geometric (diffraction, optical aberration, film grain, etc.) effects. Such treatment was expected to substitute for the classic calculated "depth-of-field" values a functional relationship between resolved detail and displacement from the plane of perfect focus. This result would be in contrast to the typical photographer's definition of "depth-of-field" as that single object displacement from the plane of perfect focus which results in an arbitrary resolved detail scale (with actual numerical values dependent on subjective factors e.g., degree of photographic enlargement, resolving power of the human eye, perspective, etc.).

c. Detailed Description of Nitrogen Purge System

Nitrogen purge gas was supplied to the optical strand burner by the same pressurizing system used in previous

studies at this laboratory (see References (9), (26)). The control panel for the nitrogen flow is shown in Figure 5 .

For the purposes of this study, nitrogen purge gas for the optical strand burner was routed through the temperature conditioning coil of another strand burner before being admitted to the optical strand burner. This arrangement was required for two reasons, both due to the high nitrogen supply pressure (2000 psig.) at the control panel. In being throttled at the control panel from a high supply pressure to the lower pressures used in this study, the purge gas was found to be cooled substantially. This cooling caused, first, difficulty due to condensation of moisture on the interior window surfaces of the burner when the cooled burner interior was opened to the atmosphere after one firing and in preparation for the next. Further, it was felt that a cold purge flow environment might possibly result in lack of reproducibility of burning due to the varying times of strand exposure to the cold purge flow during normal burner operation. Hence, the conditioning coil was inserted into the nitrogen supply system.

Temperature conditioning of the nitrogen purge gas was accomplished by electrical heating of the nitrogen supply conditioning coil via a circulating hot water bath. The coil was found to be long enough that nitrogen emerging from it was essentially at the surrounding water bath temperature (which was thermostatically controlled at 70°F.). This fact was established for the range of flows actually used in this study

by immersion of a thermocouple in the gas flow between the conditioning coil outlet and the optical strand burner inlet.

2. Optical System Analysis and Results

A simplified analysis of a single lense photographic system was carried out in order to determine: the minimum scale of resolved object detail (d_m) as a function of primary optical system magnification (M), combined film and optical system scale of resolution (d_{of}), effective F-stop (F)¹, and object displacement from the plane of perfect focus (D). The analysis was aimed at determining the maximum object displacement (D) from the plane of perfect focus for which object detail of scale d_m might be expected to be recorded on the film. In classical photographic terms, this corresponds to finding the functional relationship between "depth-of-field" and "circle-of-confusion" where this "circle-of-confusion" results from both geometrical and non-geometrical effects (and is considered a variable) and where 2D corresponds to a pseudo-"depth-of-field".

Two facts are apparent from the results of the analysis which is described in detail with typical numerical values in Appendix A. First, it is clear that below a certain dimensional object scale a major loss in the amount of surface viewed in detail is the penalty paid for a high resolution requirement. This fact is empirically apparent qualitatively to anyone who has used a microscope. Second, it must be noted that a fundamental

¹Effective F-Stop = $F_s(M+1)F_{nom}$, where F_{nom} = Nominal F-Stop of lense.

limitation exists in that, within the range of d_m reasonably associated with small oxidizer particles (say, $d_m = 10$ to 30 microns), the distance over which such resolution is possible (2D) may easily be of the same order as d_m itself.

3. Optical System Details

In the light of the factors discussed above and associated calculations, the optical system shown schematically in Figure 5 was constructed. Basically the optical system consisted of a 4" x 5" view camera body with two 2" diameter black felt-lined extension tubes of 16" and 30" lengths as well as appropriate lens, shutter, and film-holding adapters¹. The complete assembly was mounted on an optical bench and directed at the propellant strand burner as indicated in the figure.

The lens used was an enlarging lens of 100 mm. focal length with diaphragm aperture openings nominally between f/5.6 and f/45. This quality enlarging lens was chosen because of its correction for non-infinite object distance, and it was mounted in reverse to insure operation close to its design conditions². Its 100 mm. focal length was chosen to suit the

1. Though the apparatus was built with a capability for burning surface cinemacrography, motion pictures were not attempted in this study.
2. Higher quality, so-called "process" lenses with correction for non-infinite object distance are commercially available. These lenses are, however, typically designed for use at quite low magnification (frequently unit magnification). It was, therefore, felt that an enlarging lens (typically designed for magnifications in the range desired) probably offered a better alternative lens choice.

range of magnifications desired and the access available to the optical strand burner (nearest approach approximately 4 1/2 inches). An iris shutter with synchronization for electronic flash up to shutter speeds of 1/500 sec. was mounted behind the lens. Electronic flash synchronization at high shutter speeds was required in order to minimize flame radiation photographic effects while still allowing photographic observation of the burning surface via electronic flash lighting. The 4" X 5" camera body with bellows and interchangeable extension tubes provided ease of focussing and an appreciable range of possible magnifications. It further allowed use of diverse film emulsions and formats via interchangeable sheet film holders, a Polaroid film back, and a 35 mm. single lens reflex camera body mounted on an adapter plate. Focussing was accomplished using either the 35 mm. reflex camera body viewing system or a ground glass screen mounted in the image plane.

c. Photographic Light Source

Careful consideration was given to the problem of choosing a light source to supply the necessary level of illumination to the strand surface and allow photographs of the burning surface to be taken through the propellant flame. Major initial

concerns were the short exposure times required to render burning surface motion negligible during exposure and the high levels of illumination required to render flame emission photographically negligible.

For a propellant burning rate of 1 inch/second (high combustion pressure), calculations show that exposure times of the order of 100 microsec. are necessary to stop motion of the burning surface effectively at 5X to 10X magnification. Shorter exposure times than this are readily obtained with spark and electronic flash tube sources. Exposure time was, therefore, not deemed to represent a major obstacle to light source choice unless it became one in conjunction with illumination level requirements.

Analysis of preliminary photographic results (Section B-2 above) indicated that the luminous flux required from the photographic light source was approximately 10 lumens/cm^2 / exposure at the strand surface in order to allow use of color and/or high-resolution black-and-white films with 5X to 10X magnification on the film. This requirement has two aspects of particular importance: first, the basic problem of accomplishing surface illumination at a relatively high level, and second, the implications that such a high level radiant energy flux may have on the combustion process.

The ultimate illumination level available from a light source depends on its size and brightness. A source's "effective" size may be increased by the use of reflectors, focussing optics, etc., but only within the limits set by geometrical and physical optics considerations. The brightness of a source cannot be increased optically. More specifically, the radiant energy flux which can be provided at a single point (infinitesimal area) in space depends only on the geometrical solid angle through which energy is incident on the point and on the brightness of the illumination source. This solid angle of incidence depends on the effective size of the source.

Though the effective source size (solid angle of illumination at the lighted object) may be increased by optical means, it may also be decreased by optical "stops" between the source and the illuminated point or area; such was the case with the slot window optical strand burner used in the photographic studies involved here. The geometrical solid angle available for strand lighting was limited due to the relatively narrow slot windows of the burner. Source brightness, therefore, effectively limited available illumination and near-maximum illumination level (for this configuration) was achievable with relatively high brightness (6500°K color temperature), low total energy per flash (30 watt-second) electronic flash tube and reflector. Commercial

flash tubes do not typically operate at higher brightnesses than than corresponding to about 6500°K . color temperature. Therefore, without specially built lighting equipment, the capability of the modest source used in these studies could not be expected to be appreciably improved upon. Fortunately, in both numerical estimate and use, this source was found practical for the photographic efforts described in this study.

Only attempts at cinemacrography or higher magnification single-frame photography were anticipated to require careful, source-limited (rather than window limited) illumination system design (in the first case, because of the low energy flash light outputs of high repetition rate electronic flash light sources, and in the second case, due to the higher required illumination level). The flash source used was found to operate with an effective flash duration of about 500 microseconds which proved amply short considering the relatively low propellant burning rates to which surface photography was limited by other problems (see page 29). Analysis showed that illumination from this source is comparable to or slightly greater than that which might be obtained using a carefully-designed cinematographic flash light source. Hence, with respect to lighting, the single-frame photographic conditions and results reported later in this study were similar to those to be expected from multiframe photography involving a considerably more complex light source.

The use of an auxiliary photographic light source for even the relatively low magnification (5X to 10X) burning surface photography considered here is restricted by the possible effects on propellant combustion of the high radiant energy flux required. If an appreciable portion of this energy flux is absorbed by the propellant, the possibility exists of seriously altering the nature of the propellant combustion process, thereby invalidating observations of surface structure made in this situation. This fact has not been given appropriate consideration in some of the previous photographic investigations of propellant burning. As mentioned above, a luminous flux on the order of 10 lumens/cm^2 /exposure incident on the burning surface was found to be required for photomicrography with low speed, high resolution films. At a typical high intensity light source color temperature of $6500^\circ\text{K}.$, this flux might result in radiant energy absorption by the propellant surface (assuming a propellant surface emissivity near unity) of approximately 0.02 cal./cm^2 /exposure. A simple criterion for judging the effect of this flux on propellant combustion is its quasi-steady effect on surface temperature. Roughly:

$$r \rho c \Delta T_s = E_n \quad (\text{II-1})$$

where: r = propellant burning rate
 ρ = propellant density
 c = propellant specific heat
 ΔT_s = quasi-steady change in propellant surface temperature due to radiant energy input
 E = energy input/exposure
 n = exposures/sec.

Considering the following typical values: -

$r = 0.10$ cm/sec.
 $\rho = 1.6$ gm/cm³
 $c = 0.4$ cal/gm-°C
 $E = 0.02$ cal/gm²/exposure

then, from equation (II-1)

$$n = 3.2 \Delta T_s \quad (\Delta T_s \text{ in } ^\circ\text{K.})$$

This indicates that for negligible effects on combustion, say:

$$\Delta T_s \leq 100^\circ \text{ K (high)}$$

n must be limited to approximately 320 exposures/sec.¹ Thus, the application of high speed photography is limited by the maximum number of frames which may be exposed before the necessarily high artificial light flux seriously alters the combustion

process. This limit may, of course, be extended by use of

¹It is interesting that 320 exposures/second would result (with an incident flux of 0.02 cal./cm² exposure) in a time-averaged flux of 6.4 cal./cm²/second. This flux is of the same order as those steady radiant fluxes observed by Levy and Friedman (22) to affect appreciably the deflagration of pure ammonium perchlorate.

higher speed film and/or lower magnifications, but only at the expense of considerably decreased resolving power.

4. Procedure

a. Strand Preparation

After assembly of the experimental apparatus described above was completed, test photographs of non-burning, cut-surface propellant samples located in the optical strand burner were made using films of different speeds (and resolution)¹ and varying the optical system effective f-stop (aperture). The results of these tests indicated that the best combination of resolution and depth of field for 35 mm. photography with the illumination available were obtained with Eastman Kodak Plus-X film (developed, as recommended by the manufacturer, in Kodak Microdol-X developer) and an effective f-stop of 176 (nominal f/22 at 7X magnification). This combination was quite successfully used for all succeeding high resolution photographs of burning strands.

In order to assure an oblique photomacroscopic view of the propellant burning surface while retaining a distortion-minimizing optical line-of-sight (as discussed on page 14 above), propellant strands were ignited and allowed to burn on a bevelled surface as shown in Figure 5. To accomplish this, 1/4" square strands of about 4" length were cut with a bevel (approximately 45°) on one end and a length of Nichrome igniter wire was cemented

¹Eastman Kodak Panatomic X, Plus-X, and Tri-X; Adox KB-14 and KB-16.

to this surface using several coats of butyl acrylate "dope".

The propellant strands were restricted from burning down the strand sides by leaching the ammonium perchlorate from the exposed strand sides before cutting the bevel on one end of the strand. A short cold water rinse was used to leach the strands, and excess moisture was eliminated after the leaching process by blotting of the strand sides and drying in air for a few minutes.

b. Flash Synchronization

In order to photograph strands burning at high rates (at elevated pressures), it was necessary to synchronize the camera shutter and light source flash with the passage of the propellant surface through the photographic field of view. A photoelectric trigger device was developed to sense the flame luminosity as the burning surface passed the field of view. Its arrangement was as is shown in Figures 5 and 6. A schematic of the trigger circuitry used is shown in Figure 7. As the burning surface regressed during combustion, it was imaged by the sensor assembly optics at about 5X magnification on a plane at which was mounted a small semiconductive photo-resistor as approximately 2 mm. in diameter which, in the 5X-magnified burning strand image plane, corresponded to only about 400 microns motion of the burning surface. Thus, this trigger device was capable of suitable reproducibility in triggering of the optical system shutter. Trigger sensitivity was adjustable to insure that stray light during burning did not trip the shutter

before the burning surface actually entered the field of view of the photo-resistor. Sensitivity adjustment also allowed compensation for variations in level of this stray light from propellant to propellant and in flame luminosity as pressure was varied.

For most photographic runs, the voltage drop across the photo-resistor was monitored by Polaroid photographs of an oscilloscope trace. This assured that triggering was occurring properly and that the luminosity profile thus recorded appeared to be normal.

c. Firing Procedure

To obtain burning surface photomacrographs the following procedure was used.

A prepared strand with igniter on its bevelled end was placed in the optical strand burner strand holder as shown in Figure 4 . Continuity of the igniter leads was checked before the burner was closed. Also, before burner closing, the strand side facing the photomacroscopic camera was focussed on either a ground glass screen (when Polaroid or 4" x 5" cut film was being used) or in the view finder of a 35 mm. single lens reflex camera body adapted to the photomacroscopic camera body (when 35 mm. frames were to be taken). The optical strand burner, being located on a table equipped with horizontal micrometer screw adjustment, was

then moved about 1/16" so that a portion of the propellant burning surface interior to the strand side originally focussed upon would be in focus. The burner was then closed, nitrogen flow started, and the shutter on the photoelectric trigger monitor oscilloscope camera was opened. After about one minute, ignition was accomplished. The photoelectric trigger circuit was manually energized very shortly after ignition was visually apparent through the optical strand burner windows. After the photoelectric trigger fired the photomacroscopic camera shutter and flash lamp, the trigger circuit was immediately de-energized by interrupting the plate circuit of its thyratron (see Figure 7), and the shutter on the trigger monitor oscilloscope was closed. The propellant strand was allowed to burn out before the nitrogen purge flow was shut off. The burner was then opened, chimney windows were removed and cleaned, and another strand was loaded.

d. Interference by Carbon Continuum Radiation

A major problem was encountered in attempts at burning surface photography, i.e., masking of the burning surface by strong carbon continuum radiation from thermally-emitting carbon particles in the gas phase above the surface. In photographs of a PBAA-ammonium perchlorate propellant burning at low pressures (up to about 100 psig.), the surface was observable through the flame luminosity. Figure 8 shows this PBAA ammonium perchlorate propellant burning at 250 psig. and photographed under the same exposure conditions as those which had allowed a view of the surface during

at 100 psig. This increase in flame luminosity and consequent increased masking of the burning surface with increasing pressure was particularly evident with PBAA propellants.

The observed increase in flame luminosity with increasing pressure was paralleled by an increase in soot deposits on the strand burner interior after each run. As pressure was increased during a series of runs, the luminosity appeared first in the photographs as streams or jets emanating from various locations over the entire burning surface. This indicated that the emission was not a result of flame quenching by the relatively cold nitrogen purge gas stream at the burning strand edges. Substitution of air as a purge gas appeared to reduce this luminosity only negligibly. Attempts to alleviate the luminosity problem by changing oxidizer mass concentration and particle size (and distribution) also failed to yield major decreases in flame luminosity although increasing oxidizer-fuel ratio did result in a slight decrease in luminosity.

The use of a fuel binder yielding higher propellant flame temperature resulted in a significant reduction in carbon continuum radiation's interference with surface photography. While PBAA and polyester-polystyrene fuels gave evidence of considerable carbon radiation at combustion pressures above 100 psig., a polysulfide propellant allowed views of the burning surface at pressures up to about 500 psig. A photograph of a strand of a polysulfide-ammonium perchlorate propellant burning at 300 psig. is shown in Figure 9 ,

where it may be compared with a similar photograph (same exposure conditions) for the previously-mentioned PBAA propellant. Because of the wider pressure range observable with the polysulfide binder, it was selected for immediate study, and nearly all the observations reported in this study are derived from experiments with polysulfide-ammonium perchlorate propellant.

C. Results and Discussion

Single-frame photographs of burning propellant surfaces were obtained in black-and-white for a polysulfide-ammonium perchlorate¹ propellant with bimodal oxidizer distribution (see Table I for compositional details). Figures 11 and 12 show detailed, enlarged views of the surface reproduced here after enlargement to 49X from 35 mm. frames taken at 7X magnification.

The following observations regarding the burning surface are based on a limited number of photographs but serve to point out the detailed observations that can be made utilizing the technique described.

1. The surface is very heterogeneous, this heterogeneity being of two scales presumably due to the bimodal oxidizer distribution present.
 2. A few large oxidizer particles are apparently lying rather free on the burning surface. Even fewer appear to be present during burning at higher pressures (say 200 to 500 psig) than at lower (near atmospheric) pressures. In almost all cases, a "haze" is apparent
-
1. Several low-resolution photographs of a potassium perchlorate-polysulfide propellant were made in addition, but this propellant was not observed in detail. It is noteworthy, however, that photographs of this propellant indicated the presence of liquid globules (of approximately 300 μ diameter) much larger than the potassium perchlorate itself. A photograph of such a propellant's burning surface was obtained and it was apparent both that liquid phases can be identified from single frame photographs and that agglomeration may be studied by the burning surface photography technique.

in the vicinity of each large particle. This "haze" is not self-luminous. This fact was established by photographing surfaces under the same combustion conditions but without auxiliary illumination. All such photographs showed little or no image of such haze, indicating that such images in photographs with auxiliary light were caused by reflected not emitted light.

3. A large-scale crater-like surface structure is apparent. Small or intermediate bright centers (apparently within the crater depression) are usually observable along with such individual craters. Within some craters, there is no evidence of bright areas whatsoever. Where present, these local bright areas are in some cases fairly distinct, while in others, they are indistinct, and a haze like that reported above is apparent.
4. The hazy, cloud-like appearance mentioned above is observed to be considerably less predominant at higher pressures. It is considerably less apparent at 100 psig (Figure 12) than at 20 psig (Figure 11). However, the phenomenon appears to be observable up to 500 psig (above which no photographs were taken).

5. At low pressure, some free-lying perchlorate crystals show bright spots within an overall haze closely hugging the crystal.
6. Fine-scale particle structure is apparent between craters. It is presumably due to small perchlorate crystals lying partly or fully exposed, but whether the small crystals are accompanied by a small scale equivalent of the large particle craters discussed above is not clear.

On the basis of these observations, it appears that several different modes of surface structure are present in the combustion of polysulfide-bimodal ammonium perchlorate propellants burning at pressures between atmospheric and 500 psig.

First, some large oxidizer particles appear essentially free on the surface. These have also appeared on early photographs of propellants with other binders. Their presence would seem to be due to fuel pyrolysis at such a rate as to leave large crystals without surrounding binder. If such is the case, it is quite reasonable that, under the action of gravity, these free crystals will "ride" the surface during its regression until finally they are completely consumed. This phenomenon has been observed by other workers (16) .

Second, a number of equally large oxidizer particles appear to pyrolyze faster than the fuel binder leaving craters in the surrounding fuel-fine particle oxidizer matrix. It is supposed that the bright spots

appearing in these craters are partially-pyrolized perchlorate crystals and that their variation in size may be accounted for by variations in the extent of pyrolysis of the individual crystals in different craters. This suggests that the observations of Bastress on the surface structures of extinguished polysulfide-bimodal ammonium perchlorate propellant probably do not characterize the propellant surface during combustion. Specifically, unless the higher fuel concentration and slightly different bimodal oxidizer particle size distribution of Bastress' propellants promote gross changes in burning surface structure, it can only be assumed that the propellant surface changes during the extinguishment process. Further, if this is the case, one is led to question the value of other workers' observations on surface structure of extinguished propellant samples (40).

Small particles, though indistinct in the present photographs, indicate less evident crater-like surroundings. This is reasonable considering size influences only, and it is not yet clear to what extent small particles may pyrolyze in a different local environment than the larger crystals. Thus, it is particularly evident from the photographs that, at least in the case of large oxidizer particles, a time-unsteadiness of "surface" regression occurs. The extent to which this must be accounted for in burning mechanism theory is not clear a priori and warrants further investigation.

The haze observed to surround a number of large perchlorate crystals is difficult to interpret but is likely to bear on the chemistry of oxidizer pyrolysis at the surface and may be characteristic of polysulfide binder only. The cloud-like appearance is not likely to be due to carbon particles formed as intermediate products in the flame. Observation of the haze by reflected light implies a high reflectivity (low emissivity) for it, whereas carbon particles would be expected to exhibit low reflectivities. Color photographs have shown this haze to be white or colorless.

Operating experience with the optical strand burner in which these propellants were burned indicated that a fine white smoke deposit remains after firing of the propellants. More smoke is deposited on the burner interior surfaces at low pressures (near atmospheric) than at higher pressures (say, 300 psig.). Although, due to changing purge flow conditions inside the burner (with changing burner pressure), this increased deposition does not necessarily evidence increased production of this smoke at low pressures, the increased deposition, in paralleling photographic observation of haze near the surface, may be significant. Deposits on the burner interior surfaces after firing of these propellants have not been chemically-analyzed but solutions of similar smoke deposits (resulting from sub-atmospheric combustion of both PBAA and polysulfide propellants) have been made and tested for ammonium and chloride ions with positive results in each case. Thus, it appears that the smoke deposits are at least

partially ammonium chloride. Ammonium chloride smoke might quite reasonably be expected to be formed during strand burning in a relatively cold nitrogen environment. Cold surroundings introduce the possibility of quenching of intermediate combustion species at the strand edges. Since flame zone dimensions are expected to decrease with increasing pressure, the admixing effect involved in quenching may be expected to be less at higher pressures, thereby explaining the decreased deposition of smoke on strand burner interior walls at higher combustion pressures. The formation of ammonium chloride can easily be explained chemically by considering the chemistry of the combustion situation. Ammonium perchlorate decomposition involves the release of ammonia molecules into the gas phase (49), and HCl is a known product of ammonium perchlorate-oxidized solid propellant combustion. The spatial coexistence of these two species in the propellant flame zone is, therefore, virtually certain, and edge-effect quenching of the two is likely to result in ammonium chloride precipitation.

The simultaneous formation of white smoke thought to be ammonium chloride and a white "haze" apparent in burning surface photographs raises the question of whether the haze or "clouds" might not also be ammonium chloride formed as a product or intermediate in the ammonium perchlorate pyrolysis or in the fuel-oxidizer redox reaction. Eventual disappearance of the smoke in the convective field immediately above the propellant

surface (resulting in cloud-like formations rather than streams of smoke) is attributable either to convective and/or diffusive dispersion or to thermal decomposition (or sublimation) in the higher temperature regions of the flame zone. It appears unlikely, however, that this near-surface haze is ammonium chloride. The low sublimation temperature of ammonium chloride (-35°C . at 1 atm.) (39) makes it difficult to rationalize the formation or the presence of condensed ammonium chloride within a gas phase which is probably over 500°C . (composite solid propellant surface temperature measurements are typically near or above this temperature (42)). The fact that these clouds were not observed in preliminary photographs of propellants with fuels other than polysulfide while white strand burner depositions have been observed at sub-atmospheric pressures with various fuels further suggests that the smoke deposited on strand burner interiors and the near-surface clouds need not be of the same composition. Polysulfide-AP propellant combustion at low pressures already appears to be somewhat unusual in the light of recent experiments at this laboratory involving "flame-less" combustion at subatmospheric pressures (48). It is therefore quite possible that the white smoke clouds observed in photographs of the burning surface of polysulfide propellant are similarly unique, but further elucidation of the nature of these clouds is not offered at this time.

Considering the possible importance of the white haze or clouds near the burning surface at low combustion pressures with polysulfide

propellant, it would appear that low pressure combustion may represent a chemically different burning mechanism regime than that of higher pressures. This is particularly possible in the light of so-called "flame-less " combustion" mentioned in the discussion above. It is recommended that a useful first step toward further understanding of this possibility could be made by more careful chemical analysis and investigation both of the white smoke formed during strand burning experiments and of the gaseous products of combustion formed during low pressure burning. This should be carried out with respect for the fact that the observed smoke may be solid ammonium chloride, condensed ammonium perchlorate following sublimation, or a mixture of the two. The possibility of its being, at least in part, condensed ammonium perchlorate is particularly interesting with respect to the combustion mechanism implications of such a vapor pressure-controlled sublimation-recondensation process.

C. Conclusions and Recommendations

It must be concluded on the basis of the results presented above that the technique described herein for burning surface photography has demonstrated considerable promise for elucidating the nature of the solid propellant burning surface and its place in overall mechanism of solid propellant combustion. Several interesting burning surface observations have been made, and there is every reason to believe that extension of these observations to different fuel-oxidizer combinations and to

additive-containing propellants can yield other valuable insights into agglomeration, liquid phase effects, etc., on the burning surface. The technique has been proven and tried, and a logical recommendation is that it be used to extend observations into new, interesting areas.

A noteworthy extension of the work reported here would be the development of a light source appropriate to sequential, multi-frame photography of the burning surface. Although single frame photography, such as that dealt with here, is valuable, the dynamics of metal agglomeration and oxidizer particle pyrolysis, for example, can really only be studied photographically by successive, time-resolving photographs of a given area on the propellant surface. It is quite likely that a light source suited to this purpose can be developed reasonably economically, and this would allow worthwhile extension of the above proven feasibility of high resolution burning surface observations in a normal combustion situation.

It further appears promising to extend photographic surface observations to "artificial" systems as well as practical propellants. Investigation of systems of the sort utilized by McAlevy (41) (which employ, for example, burning packed beds of fuel or oxidizer particles with oxidizer or fuel gas, respectively, passed through them) may provide valuable insights into solid fuel and oxidizer pyrolysis processes.

CHAPTER III

COMPOSITE SOLID PROPELLANT BURNING STUDIES

AT LOW PRESSURES

A. Background

Solid propellant burning rate and combustion mechanism studies at low pressures (near and below atmospheric) are of interest for several reasons.

Low pressure combustion is a major interest with respect to mass diffusion processes which result from composite propellant heterogeneity in the solid phase. Earlier in this study the extent to which current burning rate theories call upon mass diffusion concepts and formulations was pointed out. Diffusion flame concepts depend on the assumption that chemical kinetic reaction rates are so fast that the supply of reactants to the flame reaction zone limits the overall rate of reaction and heat release. It has already been pointed out that all current theories of composite propellant combustion involve such diffusion controlled (or at least diffusion influenced) combustion regimes. Since, in general, mass diffusion processes occur faster at lower pressures while chemical reactions occur more slowly, it is clear that low combustion pressures constitute approach to a limiting combustion regime. Hence, a reasonable approach to testing the validity of postulated diffusive combustion mechanism concepts is to study propellant combustion at such low pressures as can be attained without exceeding the typical low pressure deflagration limits of solid propellants. This procedure should allow

extension or modification of previous experimental observations and theoretical formulations related to particle size effects on composite propellant burning rate.

Low pressure solid propellant combustion is also of interest for another important reason. Since chemical reactions are generally slower at lower pressures, it is common for the time and distance scale of a flame zone to increase with decreasing pressure. This expectation is borne out by flame zone observations over pressure ranges above atmospheric pressure (see, for example, reference(19)). Thus, flame zone structure studies by photographic, spectroscopic, and thermometric methods are facilitated by low combustion pressures. Low combustion pressure studies of flame zones must, however, be made with cognizance that controlling chemical kinetic reaction steps and product gas compositions may change with pressure. This possibility has been established for example, in ammonium perchlorate decomposition and deflagration studies (18). Thus, although flame structure studies are experimentally convenient at low pressures, care must be taken in attempting to extrapolate experimental observations to higher pressures.

Another reason for interest in low pressure solid propellant combustion studies is the so-called "low pressure deflagration limit". Typically, deflagration of solid propellants cannot be effected at arbitrarily low pressures. Each propellant appears to have a limiting

low pressure at which combustion ceases. This pressure has been termed the "low pressure deflagration limit" and has been investigated theoretically (20) (21) and experimentally (11)(14)(22) for propellant systems. To date, however, the physical and/or chemical causes of the limit are uncertain. It is obvious that "low pressure" in the deflagration-limit sense need not imply sub- or even near atmospheric pressures since some propellants reportedly experience a low pressure limit at rather high absolute pressures (e.g., 22 atm. for pure ammonium perchlorate) (22). Many practical propellants do, however, exhibit such a limit near or below atmospheric pressure. As with other "abnormal" combustion situations, propellant combustion near this deflagration limit is of interest not only in itself but also for the insights it may provide into the mechanism of more "normal" combustion at higher pressures.

B. Previous Subatmospheric Composite Propellant Combustion Studies

Few experimental subatmospheric composite propellant combustion studies have been carried out. Of these only the work of Webb (23), Silla (24), Powling and Smith (25), and Barrere and Nadaud (46) appear in the unclassified literature. A summary of the burning rate data from these sources is shown in Figure 13.

The results of Webb show burning rates for strands of 20% polyester-polystyrene - 80% ammonium perchlorate propellants

with two, broad, unimodal oxidizer particle size distributions; one, coarse (approx. 120 micron mean particle size) and one, fine (approx. 16 micron mean particle size). Webb's results extend downward in pressure to 6.5 psia and are from experiments carried out in a stagnant nitrogen environment.

Silla's results are for strands of a propellant of the same fuel and the same fuel-oxidizer mass ratio as Webb's but with a bimodal oxidizer particle size distribution of unreported particle size. Burning rates were measured by Silla between 2.5 psia and atmospheric pressure in what apparently was a near-stagnant environment with a pressure controlling bleed and a small vacuum pump connected to the vacuum burner.

Powling and Smith report data for burning rates of pressed pellets containing 10% paraformaldehyde-90% ammonium perchlorate between approximately 2 psia and atmospheric pressure.

Barrere and Nadaud's results are for two unidentified propellants; one, metallized and one, unmetallized; with unspecified sample dimensions and test configuration.

C. Previous Studies Of Particle Size Effects In Composite Solid Propellant Combustion At Low Pressures

Before 1961 little comprehensive experimental research on oxidizer particle size effects in composite solid propellant was reported. In both the classified and the unclassified literature, the

particle size effects reported deal largely with variation of coarse and fine oxidizer proportions in the widely-used bimodal oxidizer blends, e.g. (26). In the few instances where propellants containing unimodal oxidizer distributions were studied, oxidizer was used (as ground) in very widely-distributed unimodal samples (4)(23)(26). Particle sizes were rarely measured and carefully recorded in such studies.

The work of Bastress (9) in 1961 probably represents the first systematic and comprehensive investigation of particle size effects in composite propellant combustion. Bastress investigated burning rates with both propellant strands and rocket motors. He also observed the surfaces of strands extinguished by sudden depressurization. The propellants used featured several different fuels, narrow- and broad-cut unimodal oxidizer fractions between 9 and 265 microns mean particle size as well as some bimodal oxidizer fractions, varying oxidizer loadings, and varying degrees of fuel polymerization.

Most of Bastress' investigations were performed with a 35% polysulfide - 65% ammonium perchlorate propellant containing narrow, unimodal oxidizer cuts. The results of burning rate measurements on these propellants burning at pressure between 15 and 1800 psia. (as well as some observations on extinguished propellant surfaces) led Bastress to delineate several different combustion regimes determined by combustion pressure and mean oxidizer particle size. These regimes as postulated by Bastress are shown in figure 14. Some of his burning rate curves are shown in figure 15 with a cross-plot in Figure 16.

A similar cross plot is shown in Figure 17.

Bastress discussed his observed particle size effects at the lower pressures of his experimental range largely with reference to the "granular diffusion flame" theory of Summerfield (4). The burning rate data Bastress reports for polysulfide-ammonium perchlorate propellants were analyzed with respect to the Summerfield burning rate expression:

$$\frac{P}{r} = a + bp^{\frac{2}{3}} \quad (\text{III-1})$$

Values of the parameter "b" (which is expected to vary with oxidizer particle size) are presented by Bastress as varying with the mass mean particle size as shown in Figure 18. These values of the parameter were obtained from a plot of p/r vs. $p^{2/3}$ as shown in Figure 19.

As has been pointed out previously (6), Equation [III-1] in practice a correlation equation based on similarity concepts. The "chemical kinetic" parameter "a" and the "diffusional" parameter "b" in Equation III-1 may be derived in terms of the pertinent variables of the combustion situation. Analytical expressions for these parameters at best, however, contain factors involving currently unknown propellant chemical kinetic effects and the unknown mass of gas phase oxidizer or fuel "pockets" ("granules") caused by solid phase heterogeneity. It is not surprising, therefore, that numerical values of the parameter "b" (which derives from mass diffusion effects dependent on the scale of the solid phase heterogeneity) have not been completely reconcilable with numerical value estimated from analytical expressions for "b".*

* This point has been discussed at some length but with inconclusive results (27).

Numerical estimates of "b" require assumption of the relation between oxidizer particle size and the scale of gas phase heterogeneity, a relation which is not at all clear either a priori or even a posteriori. This difficulty in actually predicting the values of parameters "a" and "b" does not, however, constitute a decrease in the usefulness of Equation III-1 as a correlative tool. It does make clear, however, that other means must be sought to check the validity of the similarity concepts employed in deriving it.

As Bastress comments, the values of "b" he obtained were for different pressure regions for each of the different oxidizer particle sizes (as indicated on Figure 19), i.e., from about 15 to 50 psia. for the largest particles size to about 50 to 200 psia. for the smallest particle size. These pressure regions and particle sizes correspond to those indicated as Bastress' combustion regime map (Figure 14).

If particles size effects are primarily due to mass diffusion phenomena, they should disappear or at least tend to decrease strongly as combustion pressure is decreased. In this light, there are two aspects of Bastress' data to be considered: the first, qualitative, and the second, quantitative.

First, as is apparent from Figure 16, at pressures less than about 200 psia. and for particle sizes under 20 to 60 microns, the burning rate of polysulfide-ammonium perchlorate propellant is apparently insensitive to oxidizer particle size. The situation is somewhat less clear regarding polyester-polystyrene propellants

(see Figure 17). Nonetheless, a measure of qualitative substantiation of postulated mass diffusion-controlled particle size effects can be considered to be established by this trend toward insensitivity to particle size. The extent of verification of the postulated mechanism remains, however, somewhat uncertain especially due to a lesser observed trend with the second fuel type and due to scatter in the data (both random and systematic) for the first fuel type.

It might further be expected qualitatively that increases in propellant combustion pressure should lead to increased particle size dependency if mass diffusion is the phenomenon involved in particle size effects. That is, increased combustion pressure should first, render small particles of effect similar to larger particles at lower pressures and second, render the heterogeneity resulting from smaller and smaller particles more and more influential when superimposed on the typically faster reaction kinetics of higher pressures. Qualitatively, this trend is observable but not strongly so in the data of Figure 16 where only mild increases in slope occur at a given particle size with pressure increases of more than an order of magnitude. Contrary to the previously-discussed comparative trends toward insensitivity at small particle sizes with Bistrass' two propellant fuel types, more pressure effect on particle size influences is evident in the polyester-polystyrene data of Figure 17 than in the data of Figure 16.

This difference in trends may, however, be attributed to different regime boundary values of pressure and particle size for the two propellants with different fuel binders. Hence, the different comparative trends are probably not of profound importance regarding the mechanism of particle size effects. Qualitatively, therefore, there is some measure of verification of the importance of mass diffusion concepts in composite propellant particle size-burning rate relationships. It is questionable, however, whether such qualitative support is either useful or conclusive with respect to a mechanistic description. Thus, it is valuable to consider a second aspect of Bastress' data.

To look further into mass diffusion concepts of particle size influences than simply at trends toward insensitivity of burning rate to particle size at low pressures and increasing sensitivity with increasing pressure requires either consideration of a specific, detailed model or diagnostic data from special burning situations*. At present, only one moderately successful burning rate vs. pressure vs. particle size model of composite solid propellant combustion exists, i.e., that of the "granular diffusion flame" mentioned above. It is instructive, therefore, to look further into particle size effects on burning rate by specific reference to this model.

*. i.e., attempts to test the effects of other variables than particle size which are known to influence mass diffusion rates, e.g., the molecular weights of fuel pyrolysis products, the mean temperature in the gas phase, etc. Unfortunately, it is not known to what extent attempts to make such tests would evidence effects other than that due to altered mass diffusion alone.

The detail of the "granular diffusion flame" model of composite propellant combustion allows a look beyond qualitative trends and toward quantitative consideration of particle size effects. It is at this point, however, that Bastress' data became difficult to invoke as arguments for mass diffusion - controlled particle size effects. To be sure, qualitatively, the data of figure 16 are consistent with the prediction of the "granular diffusion flame" model, in that burning rates appear to become insensitive to particle size at low pressure. However, one may look, by use of this particular model, at the regime just before particle size effects appear to vanish and one may test whether they disappear "fast enough" to be compatible with the model. For this purpose, reference to the P/r vs. $P^{2/3}$ plots of Figure 19 is useful. These curves show that, as combustion pressure is decreased, particle size effects remain in effect to appreciably lower pressures than would be expected on the basis of "granular diffusion flame" model. The curves for different particle sizes, rather than even continuing to converge at the same rate in the "premixed flame" regime as in the "granular diffusion flame" regime, actually appear to tend away from convergence and merge less quickly with decreasing pressure. Thus, in terms of the "granular diffusion flame" theory, Bastress' results not only fail to confirm a predicted trend but, in fact, appear contradictory to it.

In summary, then, it must be said that while Bastress' results lend some qualitative support to mass diffusion phenomena as a basis for particle size effects in composite solid propellant combustion, within the realm of the most successful, current mechanistic model, they do not do so quantitatively.

Other studies of oxidizer particle size influences on composite solid propellant burning rate are those of Sutherland (27), Taback (26), and Webb (23) (all summarized in Reference (4)) as well as those by Adams, et. al. (28). In all of these studies oxidizer particle size distributions either were broad, unimodal or bimodal ones, or were not varied over a large particle size range. Thus, these additional results must be also termed inconclusive with respect to particle size effects on combustion mechanism. Not only is there little in any of the results to support concretely any of the current burning theories" concepts of the influence of oxidizer particle size via mass diffusion effects, but similar to the results of Bastress, these results hold up some indication that such concepts may, in fact, not apply as explanations of particle size effects in composite solid combustion.

With regard to the preceding comments on experimental observations of particle size effects and particularly in the light of those comments on the results of Bastress, it appeared quite valuable to extend particle size effect observations to lower pressures. Considering the extensive experimental program of Bastress, it was thought reasonable to begin this extension by means of subatmospheric combustion pressure experiments with propellants of the same formulations as those of Bastress. The remainder of this chapter describes the development of an experimental program for this purpose and some of its results.

D. Experimental Program

1. Scope of Work

An experimental program for investigating the sub-atmospheric pressure combustion of composite solid propellants was undertaken, prompted by the observations of the preceding discussion. The following portion of this chapter reports on the development of a suitable apparatus for sub-atmospheric pressure burning rate determinations and on the results and observations obtained from it. Experimental experiences are reported which suggest modifications of the apparatus to allow complementary spectroscopic and photographic observations.

2. Apparatus

a. Subatmospheric Pressure Strand Burner

It was recognized at the outset of this program that an experimental item of primary interest would be sub-atmospheric pressure burning rate data.

A common approach to propellant burning rate determination is that of burning small strands of propellant, cigarette-fashion, in a stagnant-atmosphere, large volume chamber or in a chimney-type burner with inert gas purge flow coaxial with the strand. This approach typically involves constant or near-constant chamber pressure, and requires one firing for each point of a burning rate-pressure curve.

In the interest of simplicity and ease of operation and data reduction over a large number of runs as well as cost, such a strand burner was chosen as an appropriate burning rate measurement apparatus. Also bearing on the decision was the matter of optical accessibility of the propellant burning surface and flame zone for photographic, spectrographic, and visual observation.

The choice between a stagnant atmosphere and a continuously-purging strand burners was made in favor of the essentially stagnant environment design on the basis of ease of initial set-up. The hope was that a stagnant propellant sample environment would not greatly hinder either reproducible burning or optical accessibility. The burner as constructed included provision for strand mounting, ignition, and purging of the burner cavity of air and is shown in Figure 20. A further provision beyond that expected was made in that a small low-velocity purge flow of nitrogen coaxial with the propellant axis was included for reasons discussed on page 58.

The original choice of an essentially stagnant environment burner was made as a result of the vacuum pumping capacity required of a purged burner system. A reasonable approach to determining required purge flow in past experiences with chimney-type strand burners has been to attempt to match the purge flow velocity to the strand-burning

product gas velocity. Such matching has been found to minimize the propellant strand restriction required to keep the burning surface from spreading down the strand sides and also to minimize mixing of product gases with the cold gas environment near the strand. This velocity can be shown to vary essentially as $(\text{pressure})^{1-n}$, where "n" is the propellant burning rate pressure index. Calculations indicate that this velocity may be on the order of 80 ft./sec. at atmospheric pressure and require a vacuum pumping capacity of approximately 100 std. ft.³/min. near atmospheric pressure for a two-inch diameter burner chimney (though a smaller diameter chimney might be feasible, it was that a decrease below a two-inch diameter would introduce considerable risk of deposition on the burner windows required for observation of the burning strands). An investigation of water and steam ejector system with the desired vacuum pumping capacities was made, and these alternatives were discarded due to equipment cost and primary fluid mass flow requirements. Positive displacement vacuum pumps were deemed impractical for preliminary studies due to the complication introduced by the high mass-flow product gas scrubbing required to eliminate the possibility of pump damage by corrosive combustion products. On this basis, therefore, it was decided to assemble the essentially-stagnant environment system as illustrated in Figure 20.

A nitrogen supply system and vacuum draw-down capability as shown schematically in Figure 21 were used in conjunction with the strand burner itself. A surge tank was provided to minimize pressure fluctuations during propellant combustion. A small vacuum pump in the strand burner exhaust line was provided to maintain constant combustion pressure by exhausting the low-velocity purge flow and the combustion products during strand burning. The purpose of the simple sodium hydroxide pellet bed shown in the exhaust line (before the small pump) is that of minimizing corrosive vapors entering the mechanical pump.

Strand ignition was allowed for by the inclusion of electrical lead-throughs at the strand burner base and was provided by means of a Nichrome wire threaded through a hole near the top of the strand. A 24 v.d.c. rectifier supplied ignition power.

b. Instrumentation

A photographic system was used for measuring strand burning rates and is shown schematically in Figure 22. The system provided for burning rate measurement by photographically-recording successive images of the burning propellant strand at approximately 1.2x magnification with a scale grid¹ and stopwatch face superimposed on each film frame. The beam splitter used to accomplish this superposition

¹To minimize the interference between the grid scale image and the superimposed propellant sample image, a white-on-black-background grid was used. This grid was made by reflex-printing standard graph paper (ten-divisions-to-the-inch) onto high-contrast photographic enlarging paper.

of images was made by vacuum deposition of aluminum on a 1/16" thick glass plate. A trial-and-error procedure was used to determine the deposited film thickness which gave suitable density balance between flame and stop-watch and scale-grid images on the film.

Use of a Beatty-Coleman data recording camera with framing rate capability as low as two frames per second allowed simultaneous recording of burning surface position and time on 35 mm film. The framing rates actually used for data recording provided about twenty successive exposures during the passage of the burning surface through the camera's field of view (approximately one-and-one-half inches). This recording technique provided monitoring of propellant burning and checks on the steadiness of the burning surface regression rate.

The standard technique of burning rate determination by measuring the time period between melting of two fusible timing wires (of known separation along the strand axis) was not used for burning rate determination because of a reported tendency toward irregular fuse wire melting at low combustion pressures (low burning rates) (44). A series of typical burning rate record photographs of the type described here is shown in Figure 23.

c. Subatmospheric Strand Burner Operation

The propellants tested for sub-atmospheric pressure burning rates included two 25% polybutadiene-acrylic acid (PBAA) - 75% ammonium perchlorate propellants with narrow, unimodal oxidizer particle size distributions. Ammonium perchlorate of 13 micron and 188 micron mass mean particle sizes was incorporated in these PBAA propellants. Burning rates at sub-atmospheric pressures were also determined for a 35% polysulfide (LP-3) - 65% ammonium perchlorate propellant of 48 micron mass mean oxidizer particle size¹. All propellants used in these studies were prepared in the Princeton University Aeronautical Engineering Department Solid Propellant Processing Laboratory and were cast into blocks from which 1/4" square strands were cut. Sides of the approximately 4" long strands were inhibited (to prohibit flame spreading down the sides) by dipping once in a 5% solution of VYLF vinyl resin in methylene chloride.

The strand inhibition technique was determined through a series of strand combustion tests using both of the PBAA propellants described and a number of different inhibitors and inhibitor coating thicknesses. Inhibitor coatings generally interfere with both observation of the

¹ Propellant formulation details appear in Table

burning surface edge and with observation of the burning surface itself. Hence, minimal inhibition was found to be required. Simple leaching of ammonium perchlorate from the propellant strand sides, however, was found to be ineffective in eliminating flame spreading down the strand sides. This spreading was evidenced by the convex conical burning surface observed without strand inhibition. Such conical burning surfaces were observed (though to a lesser extent, even with inhibition in the case of the fine-oxidizer PBAA propellant. It is for this reason that provision was made in the strand burner for a relatively slow nitrogen flow directed from the strand holder base up along the burning strand. This flow was fairly successful in eliminating conical burning surfaces with the fine-oxidizer PBAA propellant.

Two check burning rate measurements using the coarse PBAA propellant were made; one with no nitrogen flow and one with such nitrogen flow as could be accommodated by the small vacuum pump at 1/2 atmosphere chamber pressure. Comparison of these two rates showed them to be equal within the experimental accuracy of the burning rate measurement technique. It was, thereby, judged that this small nitrogen flow probably did not affect burning rate measurement accuracy.

3. Procedure

The general procedure for burning rate determination was as follows: An inhibited strand of propellant of about 3-1/2" length was drilled (No. 60 drill) across the strand width about 1/16" from one end of the strand and a Nichrome igniter wire of about 10" length was inserted into this hole. Next, a 1/8" mounting hole was drilled on center at the other end of the strand. The strand was mounted on a mounting pin on the strand holder in the burner chamber. The igniter wire ends were then connected to two insulated pins provided on the strand holder base. Ignition circuit continuity was checked using a test light on the burner control panel, and the bell cover was lowered over the burner base (a thin coating of silicone vacuum grease was always used on the bottom edge of the bell cover and was cleaned off and replaced before each series of firings). Before evacuation of the chamber, the propellant strand was checked to have its front surface in focus by the recording camera by use of a ground glass camera slide in the film plane. Illumination for focussing was provided by a microscope illuminator lamp. Then, with the valve to the small vacuum pump closed and with the air bleed and nitrogen bleed valves closed, the large vacuum pump was used to evacuate the burner system to less than 1.0" Hg. absolute pressure. Upon attainment of this pressure or less, the large vacuum pump line was closed off by means of the valve provided in it, and dry nitrogen was bled

into the system to a pressure of at least 1.0" Hg. below atmospheric. The evacuation and nitrogen-filling processes were then repeated to further purge the system of air until the system was at the desired combustion pressure. At this time, the small vacuum pump was turned on, its line valve was opened, and the nitrogen-purge bleed valve was adjusted until (with the small vacuum pump drawing on the burner) the desired combustion pressure (or very near it) was maintained.

At this point the camera timer and stopwatch were started, and the lamps illuminating the stop watch and grid scales were turned on. Before ignition of the strand, the firing number was recorded by switching the recording camera on, letting it photograph several frames with a run-number card placed immediately in front of the stopwatch face, and then switching the camera off again.

Ignition of the strand was accomplished by passing a current through the igniter wire. When the propellant burning surface had regressed to a point slightly above the top of the recording camera's field of view, the camera was switched on once again and allowed to sequence photograph until the surface receded out of its field of view. During this time interval, chamber pressure, as indicated by a mercury U-tube manometer, was monitored visually, and estimated average pressure and variations from it during the run were recorded. After the strand had burned completely, the nitrogen bleed valve was closed, and the small vacuum pump was allowed to operate until chamber pressure was again reduced to less

than 1.0" Hg. absolute. When chamber pressure, reached 1.0" Hg. absolute or less, the small vacuum pump was turned off and the air bleed valve opened to return the burner system to atmospheric pressure for the loading of another strand for the next run.

Barometric pressure readings were taken at the beginning and end of each day's tests or at least every two hours, whichever period was shorter.

For one propellant - PBAA-AP (75%, 188 microns) - the low pressure deflagration limit was determined. This determination was easily effected by measuring burning rates at decreasing pressures until combustion extinction appeared (visually) imminent. A final test was then made without the previously-used nitrogen flow around the strand but with the small vacuum pump still in operation so as to decrease the chamber pressure slowly. The deflagration limit reported was that chamber pressure observed at the time of extinction of the visible flame at the propellant surface. No continued surface regression was apparent after that time.

4. Measurement Errors and Data Reduction

Burning rates were determined using contact prints of the film record of burning surface displacement vs. time. A typical contact print sheet is shown in Figure 23. In this figure, the stop watch and grid scale superimposed over the burning strand image are apparent. Left-to-right reversal of the stop watch face is due to

the optical system arrangement and did not interfere with time determination. Divisions on the grid scale are 0.05" apart and the usable strand image length can be seen to be slightly over 1.0".

Since the grid scale and front surface of the strand were located at equivalent focal planes (by means of the beam splitter), regression distances of the strand on the film record could be read directly from the grid scale image. These distances were always measured in the axial direction at a station near the midpoint of the strand. By this technique, it was estimated that burning surface location was measured to the nearest 0.01" using a hand magnifier. Thus, by using two frames showing a burning surface displacement of approximately 1", the distance regressed could be measured with a maximum error of about 2%.

The stop-watch-indicated time corresponding to each frame was also read directly from the contact print of the film record. Since the smallest stopwatch scale division was 0.1 second, the sweep hand was almost always stationary during the 1/50 second exposure time of the recording camera, and times from the two frames used for burning surface displacement measurement could be read to the nearest 0.1 second. Therefore, a typical run at approximately one atmospheric combustion pressure (with a burning rate of about 0.06"/second) yielded a 1" displacement of the burning surface in about 17 seconds. Hence, a maximum error in time interval of about 1.2% could be expected (with lesser percentage error - down to about

0.2% - at lower pressures due to the lower burning rates and consequently longer burning times).

Each burning rate film record was checked for obvious abnormalities of burning surface orientation or shape by observation of all intermediate frames exposed during the interval between exposure of those frames actually used for burning rate determination. Whenever such abnormalities occurred, they were noted. The constancy of burning rate during the time interval involved was always checked by separate burning rate calculation for the first and second halves of the total interval, and in some cases by checks over additional time intervals. In almost all runs, results were found to be consistent, and only a small percentage of the runs appeared to involve abnormal combustion.

As has been noted by others, an appreciable source of possible error in strand burning rate determination is that of tilted burning surface (23). This is true, naturally, of both fuse-wire-determined burning rate measurements and photographically-determined ones. An advantage, however, in photographic rate determination techniques such as that employed in this study lies in the possibility of partial correction for tilted burning surface errors. The correction procedure employed when necessary in this study was to measure burning surface inclination in each intermediate frame of the photographic sequence, calculate the average cosine of the burning surface angle, and correct the nominal burning rate

(calculated by the normal method described above) by this factor. Since it is apparent from the camera arrangement used that burning surface tilt toward the side of the strand observed by the camera may be difficult to detect due to flame luminosity and that tilt away from that side cannot be detected at all (without the use of another camera), it is obvious that attempts at burning rate correction for surface inclination were not complete. Nonetheless, it was felt that such partial correction as was possible conveniently was worthwhile and on the average could be expected to correct burning rates for up to half of the error possible without correction. Through the appropriate geometrical arguments, this error (without corrections) could be up to 3.4% for surface inclinations up to 15° . In most cases, observed inclinations were well below this value.

As was mentioned earlier, chamber pressure and pressure variations (if observed) were recorded during each run thus facilitating estimates of possible error in pressure measurement. For most runs, this variation was less than 1-1/2% even at the lowest chamber pressures, and rarely was this variation greater than 3%. Observed short period fluctuations of pressure as well as those too brief to allow manometer response (due to mercury column friction and inertia) were considered to be negligible in the light of averaging over the relatively long burning periods of the runs. Negligible error in combustion pressure measurement was expected

to be due to barometric pressure variations since careful readings of high accuracy (to 0.001" Hg.) were recorded frequently using a vernier-scale, laboratory-type, mercury column manometer.

In summary, then, the total error in burning rate determination by the technique described could be expected to be less than 6-1/2% particularly at lower pressures and after correction for observed burning surface inclination. Errors in recorded pressure were estimated to be less than 1-1/2% (at low pressures) and, in general, were probably appreciable lower than this figure.

5. Results

The results of a number of subatmospheric burning rate measurements are shown in Figure 2⁴ along with corresponding rates for higher pressures measured in a chimney-type strand burner*. The sub- and super-atmospheric rate curves are seen to blend smoothly indicating insensitivity of burning rates to the details of the burner construction. Scatter of the data points is, in general, within the 6-1/2% maximum estimated earlier in the preceding section.

The value of correction for burning surface inclination as described in the last section can be seen in the results for the PBAA-ammonium perchlorate fine propellant. Tilt correction appears to reduce scatter and to bring the subatmospheric results in line with those from super-atmospheric pressure. Nonetheless, the

* This burner had been widely used in the past, e.g., for Bastress' work, with no reason to doubt its satisfactory operation.

results for this particular propellant must be viewed cautiously since burning surface inclination was frequently high (up to 30°) with almost all strands**.

As indicated on the plot of the burning rate results (Figure 24), the lower pressure deflagration limit was determined for only one propellant.

A particularly notable characteristic of all the runs performed with both propellants was the production of appreciable quantities of whitish smoke in the burner chamber and the deposit of some of this smoke on the glass walls of the chamber. This smoke was not so dense as to interfere seriously with photographic burning rate determination, but it did cause attempts at surface photography via external illumination to fail due to reflection and scattering of the artificial illumination. Similar deposits during vacuum combustion were observed by Webb (23) and both white deposits on a strand burner interior and white "clouds" in the flame zone have been observed above atmospheric pressure during other propellant combustion studies (see page 33).

** The direction of this tilt was observed to be quite random. Several experiments involving addition of a 2-1/2" diameter hood to the exhaust line over the strand, total elimination of the exhaust line (inside the strand burner cavity itself), attempts at artificial inducement of tilt by leaving one strand side uninhibited and unleached, use of 1/2" square strands instead of the usual 1/4" square ones, etc. did not uncover the cause of this burning surface inclination. It was finally thought that this effect must be due to some characteristic of this particular propellant since equally-fine oxidizer in polysulfide-fuelled propellant (with a lower fuel concentration, however) only rarely burned with an inclined burning surface.

A solution of the deposit from the burner interior was readily made in both distilled water and in a sodium hydroxide solution. These solutions were then tested for the presence of chloride ion (standard AgNO_3 precipitation test) and for presence of the ammonium ion (NH_4Cl smoke test with HCl vapor and sodium hydroxide solution of the deposit). Results were strongly positive in each case. Further evidence for appreciable ammonium ion in this smoke was observed in the strong odor of ammonia evident upon opening of the sodium hydroxide pellet bed in the burner exhaust line.

6. Discussion

The results of the burning rate measurements of this study are not extensive enough to provide a basis for firm conclusions regarding subatmospheric composite solid propellant combustion. Use of the apparatus can easily be continued in order to produce further data. Nonetheless, on the basis of current data and observations, a number of important observations and speculations can be made.

From the burning rate results for both the PBAA and polysulfide propellants tested, there is still no clearcut evidence of the rather fast convergence of burning rate curves for different particle sizes which might be expected at low pressure in view of mass diffusion theories on oxidizer particle size effects. This point should be elucidated by more extensive testing of subatmospheric

pressure burning rates for particle-size-varied propellants. However, it is notable that a low pressure burning rate convergence discrepancy (previously discussed with respect to the results of Bastress) is still apparent in the lower pressure burning rates recorded in this study. Thus, the validity of this discrepancy as an objection to current concepts of mass diffusion effects in composite propellant combustion is reinforced, and the mechanism of particle size influence on solid propellant burning rate is still an open question. Since the mechanism of particle size has not yet been concretely related experimentally to mass diffusion in the unmixed gas phase, it is worthwhile to conjecture as to possible other causes of burning rate dependence on oxidizer particle size and distribution.

It is obvious that the presence of oxidizer as discrete particles within the fuel matrix requires microscopically unsteady burning and regression of the burning surface. Adams and other workers at E.R.D.E. in the United Kingdom (29) (32) have commented on this likelihood and also on the possibility that "the assumption of steady state flow, the attempt to make the problem one-dimensional, and the averaging and arbitrary linking of processes over the burning surface" may not be sufficiently realistic to allow a realistic solution to the composite propellant burning rate problem. An unsteady combustion process might well necessitate a time-dependent or time-averaged¹ configuration for modelling and burning rate

¹"Time-averaging" in this case must be done with the nature of the unsteadiness inherently accounted for in order to introduce at least its effects into a combustion mechanism formulation. It would not be sufficient, therefore, to "time-average" phenomena in the sense of any current burning mechanism theory which presumes "quasi-steady" burning or "effectively steady-state" conditions.

analysis. To date, however, no such analysis has been reported. This absence is understandable, unfortunately, considering the complexity of the burning propellant configuration, the uncertainty of the existence of readily-modelled controlling processes, and the lack of detailed knowledge of the individual propellant component pyrolysis phenomena and their interplay. Certainly, a more complete knowledge of the individual pyrolysis processes involved would be useful in attempting to eliminate these lacks. It is in this light that previous work on pure and fuel-modified ammonium perchlorate deflagration is worthwhile and continued efforts at further elucidating the mechanism of the thermal decomposition of ammonium perchlorate appear promising.

Another interesting prospect for at least rationalizing a description of particle size influences in composite propellant combustion relates to observations of particle size effects in the thermal decomposition of pure ammonium perchlorate (29)(30)(31). It is quite possible that suggestions of perchlorate decomposition control over burning rate at high combustion pressures (say, 1000 psia or more) apply also, at least in conjunction with oxidizer-fuel reactions, at lower pressures. Hence, it might be speculated that an attempt to interject particle size dependence in a combustion mechanism model might be successfully made by superimposing the solid phase decomposition reaction rate relations of Mampel, for example, (33), on a simple, unsteady model of successive pyrolysis

of stacked oxidizer and fuel thicknesses. Such an attempt requires first, preliminary theoretical studies of the likely trends of such a model and second, if suitable trends exist, experimental study of apparent particle size effects in oxidizer decomposition.

A further speculated origin of a particle size dependence of burning rate lies in the area of heterogeneous reactions. Such reactions have been postulated to bear on propellant burning mechanism (47) and probably warrant further development.

Aside from the question of particle size effects, the results of this study are interesting in another sense. From previous sub-atmospheric burning rates recorded by Webb(23), Silla (24), Powling and Smith (25), and Barrere and Nadaud (46), one observes that burning rate data for polyester-polystyrene and paraformaldehyde-fueled propellants show burning rate pressure indexes very nearly constant at a value of unity. The slopes for the PBAA and polysulfide-fueled propellants of this study are, however, constant or near-constant at about 0.7. Previous attempts at rationalizing the relative magnitudes of such burning rate pressure indices have been unsuccessful and no particularly useful speculation regarding them can be added at this time. The influence of fuel binder type may, however, be attributed to different pyrolysis rate temperature dependencies for various binder types, differing fuel volatilities, and differing fuel pyrolysis products though even qualitative descriptions of such origins of binder type influences are

essentially unsubstantiated. It is further suggested by the work of Nachbar on pure ammonium perchlorate (21) that, near their low pressure deflagration limits, solid propellant systems may exhibit changing pressure indexes due to radiative heat loss. Hence, it is possible that differences in index due to fuel binder changes might also result from consequent changes in burning surface emissivity.

7. Conclusions and Recommendations

It may be concluded from the previous results and discussion that a practical apparatus for determination of subatmospheric burning rates and low pressure deflagration limits has been developed. It has been found that the use of this essentially stagnant-environment burner is unsatisfactory for photographic observation of the burning surface (and probably for spectroscopic studies as well). Therefore, extension of low pressure observations beyond the measurement of burning rates would require a new burner arrangement. It appears likely that the most promising new arrangement would be one using a continuously-purged chimney-type burner requiring a vacuum system and product gas scrubber of high mass flow capability.

In light of the current results, it appears that existent theories of oxidizer particle size effects on composite propellant burning rate may not completely explain all the observed phenomena, but that further vacuum burning rate data would help to clarify

this question considerably. The burning rate particle size dependence results of this study as well as the previous results of Bastress suggest that explanations other than current concepts of mass diffusion might be worth considering in an attempt to explain oxidizer particle size effects in composite propellant combustion. In this light, it is recommended that simplified theoretical models of unsteady, step-wise fuel and oxidizer pyrolysis be investigated and that thermal decomposition be carried out with regard to particle size effects in pure ammonium perchlorate decomposition. Little work of this sort has been done previously, and no previous attempt at comprehensive treatment of such particle size effects has been reported.

Since the measured low-pressure burning-rate pressure indices of this study (for polysulfide and polybutadiene-acrylic acid fuels) are notably different than those observed at low pressures with other fuels, it would appear valuable to extend low-pressure burning rate studies to propellants using still different fuel binders (e.g., polyurethane) and to attempt binder type-pressure index correlations based on binder structure. Such extension might give some insight into the chemical kinetic aspects of propellant fuels since chemical kinetic effects are expected to predominate at low combustion pressures.

Considering the possible importance of the white smoke observed at low combustion pressures, it would appear that low

pressure combustion may represent a different burning mechanism regime than that of higher pressures. This is particularly possible in the light of recent experiments at this laboratory involving so-called "flameless combustion" at subatmospheric pressures (48). It is recommended that a useful first step toward further understanding of this possibility could be made by more careful chemical analysis and investigation of both the white smoke observed and the gaseous products of combustion formed during low pressure burning. This should be carried out with respect for the fact that the observed smoke may be solid ammonium chloride, condensed ammonium perchlorate following sublimation, or a mixture of the two. The possibility of its being, at least in part, condensed ammonium perchlorate is particularly interesting with respect to the combustion mechanism implications of such a vapor pressure-controlled sublimation-recondensation process.

REFERENCES

- (1) O. K. Rice, The Theory of Burning of Rocket Powders, OSRD 5574 (1945).
- (2) R. F. Chaiken, "A Thermal Layer Mechanism of Combustion of Solid Composite Propellants: Application to Ammonium Nitrate", Comb. and Flame, 3, 285-300 (1959).
- (3) W. Nachbar, "A Theoretical Study of the Burning of a Solid Propellant Sandwich", Solid Propellant Rocket Research, Vol. 1 of ARS Series on Progress in Astronautics and Rocketry, Academic Press, 207-226 (1960).
- (4) M. Summerfield, G. S. Sutherland, M. J. Webb, H. J. Taback, and K. P. Hall, "Burning Mechanism of Ammonium Perchlorate Propellants", Solid Propellant Rocket Research, Vol. 1 of ARS series on Progress in Astronautics and Rocketry, Academic Press, 141-182 (1960).
- (5) R. D. Geckler, "The Mechanism of Combustion of Solid Propellants", Selected Combustion Problems, Butterworths, London, 289-339 (1954).
- (6) R. D. Schultz, L. Green, Jr., and S. S. Penner, "Studies of the Decomposition Mechanism, Erosive Burning, Sonance, and Resonance for Solid Composite Propellants", Combustion and Propulsion, Pergamon Press, 367-427 (1958).
- (7) C. Huggett, "Combustion of Solid Propellants", Combustion Processes (editors: B. Lewis, R. N. Pease, H. S. Taylor), Vol. II of Princeton University series on High Speed Aerodynamics and Jet Propulsion, Princeton University Press, 514-576 (1956).
- (8) M. Barrere, A. Jaumette, B. F. De Veubeke, and J. Vanderkerckhove, Rocket Propulsion, Elsevier, New York, 239 (1960).
- (9) E. K. Bastress, Modification of the Burning Rates of Ammonium Perchlorate Solid Propellants by Particle Size Control, Ph.D. Thesis, Princeton University (March 1961).
- (10) D. R. Margetts and B. V. Connor, A Pressure Bomb for the Photography of Burning Strands of Propellant, Caltech JPL 20-119 (July 1958).
- (11) R. Friedman, J. B. Levy, and K. E. Rumbel, The Mechanism of Deflagration of Pure Ammonium Perchlorate, AFOSR TN 59-173 (February 5, 1959).
- (12) L. A. Watermeier, W. P. Aungst, and S. P. Pfaff, "An Experimental Study of the Aluminum Additive Role in Unstable Combustion of Solid Rocket Propellants", Ninth Symposium (International) on Combustion, Academic Press, 316-326 (1963).

- (13) R. Kling and J. Brulard, "Etude de la Combustion des Poudres Composites par la Microphotographie Ultra-Rapide", *La Recherche Aeronautique*, 80, 3-11 (January-February 1961).
- (14) D. L. Reid, The Dependence of Several Solid Propellant Burning Anomalies on Flame Structure, M.S.E. Thesis, Princeton University (July 1957).
- (15) A. Spencer, (Allegheny Ballistics Laboratory), private communication, August, 1963.
- (16) H. Selzer, "Ueber den Verbrennungsmechanismus von Compositen Treibstoffen", *Raketentechnik u. Raumfahrtforschung*, 2, 7, 41-46 (April-June 1963).
- (17) L. A. Povinelli and C. C. Ciepluch, "Surface Phenomena in Solid Propellant Combustion", Bulletin of the 18th Meeting of the JANAF Solid Propellant Group, Vol. II, 387-400 (June 1962) (Confidential).
- (18) A. E. Simchen, "Decomposition Equations of Ammonium Perchlorate", *J. Appl. Chem.*, 13, 369-374 (September 1964).
- (19) R. W. Lawrence and A. O. Dekker, "Structure of Flames from Ammonium Perchlorate Propellant", *Jet Propulsion*, 25, 2, 81 (February 1955).
- (20) B. I. Pliukhin, "On the Stationary Theory for Heat Balance of Powder and Explosive Condensed Phases", Eighth Symposium (International) on Combustion, Academic Press, 734-745 (1961).
- (21) W. E. Johnson and W. Nachbar, "Deflagration Limits in the Steady, Linear Burning of a Monopropellant with Application to Ammonium Perchlorate", Eighth Symposium (International) on Combustion, Academic Press, 678-689 (1961).
- (22) J. B. Levy and R. Friedman, "Further Studies of Pure Ammonium Perchlorate Deflagration", Eighth Symposium (International) on Combustion, Academic Press, 663-672 (1961).
- (23) M. J. Webb, The Dependence of Linear Burning Rate Upon Pressure for Ammonium Perchlorate - Polyester Resin Composite Solid Propellant, M.S.E. Thesis, Princeton University (May 1958).
- (24) H. Silla, "Burning Rates of Composite Solid Propellants at Sub-atmospheric Pressures", *ARS Journal*, 31, 9, 1277-1278 (September 1961).
- (25) J. Powling and W. A. W. Smith, The Surface Temperature of Burning Ammonium Perchlorate, ERDE Report No. 10/R/62 (1962).

- (26) H. J. Taback, The Effects of Several Composition Factors on the Burning Rate of an Ammonium Perchlorate Solid Propellant, M.S.E. Thesis, Princeton University (September 1958).
- (27) G. S. Sutherland, The Mechanism of Combustion of an Ammonium Perchlorate-Polyester Resin, Ph.D. Thesis, Princeton University (May 1956).
- (28) G. K. Adams, B. H. Newman, and A. B. Robins, "The Combustion of Propellants Based on Ammonium Perchlorate", Eighth Symposium (International) on Combustion, Academic Press, 693-705 (1961).
- (29) L. L. Bircumshaw and B. H. Newman, "The Thermal Decomposition of Ammonium Perchlorate", Proc. Roy. Soc., A227, 228-241 (1954).
- (30) A. K. Galwey and P. W. M. Jacobs, "The Thermal Decomposition of Ammonium Perchlorate at High Temperatures", Proc. Roy. Soc., A254, 455-469 (1960).
- (31) A. K. Galwey and P. W. M. Jacobs, "The Thermal Decomposition of Ammonium Perchlorate in the Presence of Manganese Dioxide", Trans. Far. Soc., 55, 1165-1172 (1959).
- (32) E. A. Arden, J. Powling, and W. A. W. Smith, "Observations on the Burning of Ammonium Perchlorate", Combustion and Flame, 6, 21-33 (March 1962).
- (33) K. L. Mampel, "Zeitumsatzformeln für heterogene Reaktionen an Phasengrenzen fester Körper", Z. Phys. Ch., A187, 43-47, 235-249 (1940).
- (34) C. Huggett, op. cit., 541.
- (35) D. B. Spalding, "The Theory of Burning of Solid and Liquid Propellants", Comb. and Flame, 4, 59-76 (1960).
- (36) G. P. Sutton, Rocket Propulsion Elements, Wiley (1949).
- (37) C. Huggett, op. cit., 565.
- (38) W. H. Andersen, K. W. Bills, E. Mischuck, G. Moe, and R. D. Schultz, "A Model Describing Combustion of Solid Composite Propellants Containing Ammonium Nitrate", Comb. and Flame, 3, 308, (1959).
- (39) Handbook of Chemistry and Physics (31st Edition), Chemical Rubber Publishing Company, 399, (1949).
- (40) C. Huggett, op. cit., 566-567.

- (41) R. F. McAlevy, III and S. Y. Lee, "A Porous Plug Burner Technique for the Study of Composite Solid Propellant Deflagration on a Fundamental Level and Its Application to Hybrid Rocket Propulsion", AIAA Preprint 63-496 (December 1963).
- (42) A. J. Sabadell, The Measurement of the Temperature Profiles of Burning Solid Propellants by Microthermocouples, M.S.E. Thesis, Princeton University, (September 1963).
- (43) J. Powling and W. A. W. Smith, "The Measurement of the Burning Surface Temperatures of Propellant Compositions by Infra-Red Emission", Comb. and Flame, 6, 173-181 (September 1962).
- (44) D. J. Sibbett and J. M. Lobato, Investigation of the Combustion of Composite Solid Propellants, Aerojet-General, 1782, 5, (April 1960).
- (45) R. Friedman, J. B. Levy, and K. E. Rumbel, "Factors Governing Burning Characteristics of Composite Solid Propellants", Bulletin of the 15th Meeting of the JANAF Solid Propellant Group, Vol. IV, 97-125 (June 1959) (Confidential).
- (46) M. Barrere and L. Nadaud, "Les Domaines de Combustion des Poudres Composites", La Recherche Aerospatiale, 98, 15-29 (January-February 1964).
- (47) A. R. Anderson, R. S. Brown, and L. J. Shannon, "Ignition Theory of Solid Propellants", AIAA Preprint 64-156 (January 1964).
- (48) J. Wenograd, W. J. Most, M. Summerfield, "Flameless Combustion of Polysulfide Ammonium Perchlorate Composite Propellants", Proceedings of the 1st Interagency Chemical Rocket Propulsion Group Combustion Instability Conference, 16-20 November 1964, C.P.I.A. Publication No. 68, 335-336 (January 1965).
- (49) G. A. Heath and J. R. Majer, "Mass Spectrometric Study of the Thermal Decomposition of Ammonium Perchlorate", Trans. Far. Soc., 60, 1783-1791 (1964).

APPENDIX A

I. Background

Analysis and specification of the so-called "resolving power" of optical systems is at best imperfect and rather arbitrary. Traditionally, the resolving power of optical system components, e.g., single or compound lenses, films, etc., has been specified as the empirically-determined ability of a component to image (or, to record, in photographic systems) discrete lines of known spacing located at the conjugate of the optical system's focal plane. Typically this specification is determined even at present by photographing test charts containing groups of black lines on white or gray backgrounds with each group having different line spacings. Use of high resolution film allows lens resolving power to be determined as that line spacing (usually specified in lines per mm.) which is just distinguishable as individual lines by microdensitometer measurements on a photographic negative. Similarly, use of high resolution lenses has allowed determination of the resolving power of most films in terms of resolved line spacings.¹

Interest in lens resolution led to development of various types of lens and film testing apparatus and techniques recommended and used by individual photographic and optical laboratories and also by the U.S. Bureau of Standards (A-2). No well-defined standard test configuration has, however, been accepted as a standard for such resolution tests. The

¹ A notable example, evidencing the difficulties of this procedure, is that of Kodak High Resolution Plate which has such high resolution that currently only a lower limit of its resolving power is quotable (A-1).

result has been that many film manufacturers, camera makers, etc. have specified resolving power of components in terms of the spacing of lines resolved but typically in diverse optical photographic situations. See References (A-3), (A-4), and (A-5) for examples of test results and specifications.

One of the reasons for lack of a widely-accepted standard resolution test is that the concept of specifying optical component resolving power in terms of line spacing has long been a subject of controversy. It is clear that measured optical resolving power as empirically-determined from images of spaced line groups is neither an absolute measure nor an incontrovertible specification of the capability of an optical system to provide "usable" image detail. The measured resolving power of a lens has long been known to depend rather profoundly upon position of the resolution line chart in the optical system field of view, test chart contrast, lighting, line separation (at a given spacing), test chart-to-lens distance, lens aperture, relative lens and film resolving powers, film type and processing, and other factors.

It has always been clear that, though test method standardization allows relative resolution rating and specifications by comparison, it is not by any means an "absolute" or even well-defined measure of "useful" optical component resolving power.¹

¹In fact, even the concept of resolution specification via line spacing is quite arbitrary considering, for example, the equally-valid use of resolved separation of point sources of light common in telescopic or diffraction-limited optical systems (a procedure which in most cases does not give resolving power specifications which are simply relatable to corresponding line spacing resolving power measurements).

In recent years, the desire for a more rational and less arbitrary measure of optical resolving power has led to the introduction of new concepts in optical system resolution analysis. New terms such as "point- and line-spread function", "modulation transfer function", "sine wave response", etc. have entered the optical engineers' and photographers' vocabularies. Reference to these terms has largely supplanted reference to optical resolution in terms of "resolved" line spacings.

A new technique for measuring and specifying film and lens resolving power has now become established enough to warrant its use in film resolution specifications by the largest film manufacturer in the United States (though such specifications are not readily available from other manufacturers).¹ At least until recently, however, only one lens manufacturer routinely tests by this method and makes such test results public². Consequently, the new technique is of limited practical benefit to the photographer, engineer, or scientist. The new concept involved is typically referred to as measuring the "sine wave response" or "modulation transfer function" (terms adopted from control theory) of a lens, film, processing procedure, or complete optical system and photographic process. Both the concept and its details have been discussed, reviewed, and developed rather extensively in the photographic and optical literature. It provides a more satisfactory approach to questions of

¹ See Reference A-6

² Unchallenged statement by Schneider representative at a Society of Photographic and Instrumentation Engineers meeting.

optical resolution only at the expense of: first, greater complexity of optical component description, and, second, information inputs corresponding to specific optical components. Thus, the "modulation transfer function" approach is not amenable to general studies aimed at outlining trends and optimum configurations for a desired photographic instrumentation task. For these reasons, no further review or discussion of this resolution analysis approach is presented here. Some references on the concept and techniques of the approach are noted in the accompanying partial bibliography ((A-7) to (A-10)).

II. Analysis

A. Introduction

The complexity and lack of generality of the intellectually-pleasing (but relatively intractable) "modulation transfer function" approach to optical system resolution analysis appeared of little value for the design problem inherent in solid propellant surface photography. On the contrary, it appeared reasonable (for preliminary design purposes) to investigate the influence of optical system parameters on resolution via the old (and admittedly imperfect) notions of resolving power and "depth-of-field" in terms of resolved line spacings, "circles of confusion", etc.

The envisioned purpose of this analysis was to attempt to determine:

- (i) the feasibility of fine detail observations on a solid propellant burning surface, and
- (ii) the extent of necessary trade-offs in resolution vs. depth of field as applied to solid propellant burning surface observations.

The analysis was carried out consistent with the concept of a photo-optical transformation (by an imperfect optical system) of infinitesimal light sources (at arbitrary locations in the object space) to areas of finite dimension in the image plane. After transformation back to the object space via a fictitious, perfect optical system, the scale of such a finite area then corresponds to a minimum resolved object scale.

Mathematical relations involving these point-source image

scales include the specification (via several different conceptual routes) of contribution to image degradation from several different sources. Diffraction effects are specified by reference to the well-known Fraunhofer diffraction pattern (dealing with circular diffraction patterns in the image plane and point light sources in the object plane (A-11)). The effects of film and optical component aberrations are specified together in the analysis as of a scale equal to the inverse of a resolving power specified in terms of a "resolved" line spacing. Geometrical optics depth-of-field effects are specified by a characteristic dimension equal to the diameter of the circular intersection of the image plane and a paraxial, conical bundle of light rays from a point source in the object space. These various scales of image degradation are, in this analysis, added together to specify an overall, combined scale of resolution as a function of object displacement from the plane of perfect focus¹. It must be noted that these individual contributions are from sources of different natures and should, therefore, be viewed cautiously as approximate dimensional scales (in numerical results) rather than as absolute, well-defined, physically-significant dimensions.

¹ Alternative approaches might involve a combined scale equal to the square root of the sum of squares of these various dimensional scales, or, more complicated yet, an attempt to inject radiant energy flux distributions from, for example, the Fraunhofer diffraction pattern. Such more complicated approaches were deemed unjustifiable in light of the preliminary, approximate nature of the desired analysis.

Another cause for caution in interpreting the numerical results of the following analysis is the lack of a clear-cut and usable definition of just what constitutes "resolution" in a practical sense (say, that of observing individual oxidizer particles in detail). It is well-known that an individual object can be sensed visually, for example, without sufficient detail being observed to allow actual identification of the object. Identification of details in optical images depends on a complex interplay between factors characteristic of both the optical system employed and the nature of the object viewed (e.g., object geometry, brightness, and contrast). Individually, these factors are incompletely understood, and together they form the subject of "object recognition", an active area of current research effort. Typical of analysis involving such complexity, the following one presumes a limiting case, i.e., it is assumed arbitrarily that an object of dimension smaller than that corresponding to the dimensional scale of the image of a point source cannot be considered as "resolved". In rather abrupt and arbitrary contrast, the analysis further presumes that objects larger than this scale can be observed in some detail, and, hence, considered "resolved". Thus, the analysis employs an artificially well-defined dividing line between "resolved" and "unresolved" object scales. Nonetheless, this arbitrary dividing line is of some use for qualitative, parametric studies and of some promise for useful order-of-magnitude quantitative results.

B. Derivation

1. Characterization of Film-Optical Aberration Effects

$$\text{Let: } d_{F-0} \equiv C_{F-0} \frac{1}{L_{F-0}}$$

where C_{F-0} is a constant of proportionality. Assuming, for simplicity, that $C_{F-0} = 1$, then:

$$d_{F-0} = \frac{1}{L_{F-0}} \quad [A-1.1]$$

2. Characterization of Diffractive Effects

Considering diffraction by a circular aperture via the Fraunhofer diffraction pattern approach (A-11):

$$d_D = \frac{0.61\lambda_0}{N} \quad M = 0.61\lambda_0 \frac{M}{\text{SIN}[\text{TAN}^{-1} \frac{a}{2X_1}]} \quad [A-2.1]$$

$$\text{Since typically: } \frac{a}{2X_1} \ll 1, \text{ then: } \text{SIN}[\text{TAN}^{-1} \frac{a}{2X_1}] \approx \frac{a}{2X_1} \quad [A-2.2]$$

$$\text{Therefore: } d_D \approx 0.61 \frac{\lambda_0}{n} \frac{2MX_1}{a} = 0.61\lambda \frac{2X_2}{a} \quad [A-2.3]$$

$$d_D \approx 1.22\lambda F$$

3. Characterization of Geometric Effects

From geometric optics, for $\frac{a}{2X_1}, \frac{a}{2X_2} \ll 1$; ($\frac{a}{2X_1} \approx \text{TAN}^{-1} \frac{a}{2X_1}$; $\frac{a}{2X_2} \approx \text{TAN}^{-1} \frac{a}{2X_2}$) and for paraxial rays (A-2):

$$\Delta_1 = \frac{d_G X_1}{aM - d_G} \quad [A-3.1]$$

$$\Delta_2 = \frac{d_G X_1}{aM + d_G}$$

Letting:

$$\Delta \equiv \Delta_1 + \Delta_2$$

Then:

$$\Delta = d_G X_1 \left(\frac{1}{aM - d_G} + \frac{1}{aM + d_G} \right)$$

But:

$$X_2 = MX_1 \quad \text{and} \quad F \equiv \frac{X_2}{a} \quad [\text{A-3.2}]$$

Then:

$$\Delta = \frac{d_G F}{M^2} \frac{2}{1 - (d_G/aM)^2}$$

Therefore:

$$\Delta \approx \frac{2d_G F}{M} \quad [\text{A-3.3}]$$

or:

$$d_G \approx \frac{M^2 \Delta}{2F} \quad \text{for:} \quad \frac{d_G}{aM} \ll 1; \quad \frac{a}{2X_1}, \frac{a}{2X_2} \ll 1 \quad [\text{A-3.4}]$$

4. Combined Characterization of All Image-Degrading Effects

Clearly:

$$d_{\Sigma} = \Phi(d_G, d_{F-0}, d_D)$$

For simplicity, consider a linear combination of effects:

$$d_{\Sigma} = a_G d_G + a_{F-0} d_{F-0} + a_D d_D \quad [\text{A-4.1}]$$

where the coefficients a_G , a_{F-0} , a_D represent the relative contributions to image degradation by the three assumed sources and are assumed to be constants.

Let:

$$d_M = \frac{d_{\Sigma}}{M} = \frac{a_G d_G + a_{F-0} d_{F-0} + a_D d_D}{M}$$

Substituting from [A-1.2], [A-2.3], and [A-3.4] into [A-4.2]:

$$d_M = \left(\frac{M^2 \Delta a_G}{2F} + 1.22 \lambda F a_D + \frac{a_{F-0}}{L_{F-0}} \right) / M \quad [\text{A-4.2}]$$

or:
$$\Delta = \left(\frac{d_M}{a_G} - 1.22\lambda F \frac{a_D}{a_G} - \frac{a_{F-0}}{a_G} \frac{1}{L_{F-0}} \right) \frac{2F}{M^2} \quad [A-4.3]$$

Δ can now be assumed equivalent to D , the axial object-space distance from the plane of perfect focus over which detail of scale d_M can be resolved. Twice this distance, $2D$, then describes the total object space distance over which d_M is resolved. (The symbol $2D$ is retained rather than being redefined in order to accent the displacement notion involved).

Therefore:
$$2D = \left(\frac{1}{a_G} \right) \left(\frac{2F}{M} \right) d_M - 0.61 \left(\frac{a_D}{a_G} \right) \left(\frac{2F}{M} \right)^2 \lambda - \frac{a_{F-0}}{a_G} \left(\frac{2F}{M} \right) \frac{1}{M} \frac{1}{L_{of}} \quad [A-4.4]$$

It is notable that the effect of the terms corresponding to optical aberrations (and film effects) and diffraction effects has been to decrease the effective "depth-of-field", $2D$, (over which d_M is resolved), to less than that predicted on a geometric optics basis alone.

It is further noteworthy that, excepting the term resulting from film-optical aberration effects, $2D$ in Equation [A-4.4] depends only on the parameters F and M via their ratio F/M . The contribution of the film-optical aberration term is seen to depend also on ML_{F-0} but not on r alone. Hence, a natural choice of variables for the $2D$ vs. d_M relation is F/M (or $2F/M$) and ML_{F-0} (rather than F , M , and L_{F-0} individually).

The choice of $2F/M$ as a variable is especially attractive since, for large d_M (relative to $\frac{a_D}{a_G} d_D$ and $\frac{a_{F-0}}{a_G} d_{F-0}$), $2D$

approaches $\frac{2F}{M} \frac{d_M}{a_G}$, and hence, $2D(d_M)$ depends in the limit only on the ratio $2F/M$ ¹. Thus, the expression:

$$2D = \frac{2Fd_M}{Ma_G} \approx 2D_{ult}^0. \quad [A-4.5]$$

expresses the ultimate maximum object distance, $2D$, over which d_M may be resolved at a given value of $2F/M$ and is the asymptote of any other, more complete expression for $2D(d_M)$ accounting for other types of image degradation. Equation [A-4.5] is represented graphically in Figure A-1 for several values of $2F/M$.

Considering next the effect of the diffraction term, $0.61 \left(\frac{a_D}{a_G}\right) \left(\frac{2F}{M}\right)^2 \lambda$ in Equation [A-4.4], it is clear that another, lesser limit on $2D(d_M)$ is imposed if diffraction is considered. This limit, though lower than that expressed by Equation [A-4.5], still depends only on the variable $2F/M$. Thus, a single curve (below that representing Equation [A-4.5]) appears for each value of $2F/M$ on the $2D$ vs. d_M plane corresponding to:

$$2D = \frac{2Fd_M}{Ma_G} - 0.61 \frac{a_D}{a_G} \left(\frac{2F}{M}\right)^2 \lambda \approx 2D_{ult}^1. \quad [A-4.6]$$

Several curves representing this limit are shown in Figure A-2.

Finally, the effects of film-optical aberrations enter into Equation [A-4.4] decreasing $2D(d_M)$ even farther. Since it has been

¹This obviously corresponds physically to the predominance of geometric image degradation (in the normal photographic "depth-of-field" sense) over diffractive and film-optical aberration effects.

assumed here that these effects are characterized by a constant scale at the image plane, d_{F-0} , the object scale to which they correspond, d_{F-0}/M (or $1/ML_{F-0}$) introduces a dependence of $2D(d_M)$ on ML_{F-0} (in addition to its previously-discussed dependence on the ratio $2F/M$). Thus, for a given value of $2F/M$, different values of ML_{F-0} (and therefore, of F) result in a family of curves in the $2D$ vs. d_M plane, each curve lower than that expressed by Equation [A-4.6] (and by Equation [A-4.5], of course). Several curves of these families representing the complete relation [A-4.4] are shown in Figure A-3.

An upper limit on $2D(d_M)$ clearly exists for given values of λ , $\frac{1}{L_{F-0}}$, a_G , $\frac{a_D}{a_G}$, $\frac{a_{F-0}}{a_G}$, since, maximizing $2D$ with respect to $2F/M$ and taking the limit as M approaches ∞ :

$$\lim_{M \rightarrow \infty} 2D\left(\frac{\partial 2D}{\partial F/M}\right) = 0 = \frac{d_M^2}{2.44\lambda} \equiv 2D_{ult.} \quad [A-4.7]$$

Equation [A-4.7] appears in Figure A-3 as the singular solution $M=F=\infty$ and is further shown numerically in Figure A-4 where $2D_{ult.}/d_M$ is plotted versus d_M with λ as a parameter.

Further, as might be expected from the linear image degradation model employed here and from the vertical asymptotes of Figure A-2, a minimum d_M is indicated for $2D$ approaching zero:

$$\lim_{2D \rightarrow 0} \left(\frac{1}{a_G} d_M\right) = 0.61 \frac{a_D}{a_G} \left(\frac{2F}{M}\right)\lambda + \frac{a_{F-0}}{a_G} \frac{1}{ML_{F-0}} \equiv \frac{1}{a_G} (d_M)_{min} \quad [A-4.8]$$

$$\left(= \frac{\frac{a_D}{a_G} d_D + \frac{a_{F-0}}{a_G} d_{F-0}}{M} \right)$$

$(d_M)_{\min.}$ is shown numerically versus $2F/M$ in Figure A-5 for the case:
 $a_G = 1$, $\frac{a_D}{a_G} = \frac{a_{F-0}}{a_G} = 1$, and $\lambda = 0.555\mu$ with $\frac{1}{ML_{F-0}}$ as a parameter.

C. Results

The results of the preceding analysis are essentially represented in Figure A-3. This figure represents the effects of limited variations in F/M and ML_{F-0} (for a typical value of λ as well as for assumed values of a_G , $\frac{a_D}{a_G}$, and $\frac{a_{F-0}}{a_G}$ of unity). The figure graphically portrays several pertinent aspects of the photomacrographic resolution - "depth-of-field" problem.

From Figure A-3, it is obvious that diffraction and film-optical aberration effects result in a serious decrement in the extent of the object space within which small particles can be expected to be resolved, i.e., classical calculations can be expected to overestimate "depth-of-field" considerably at resolution scales on the order of typical small solid propellant oxidizer sizes (5 to 50 microns). In fact, the steep approaches of the curves of Figure A-6 to $D = 0$ at a finite d_M indicate a finite resolution limit due to diffraction and film-optical aberration effects.

The particular characterization of these effects which were employed in the analytical treatment may, in their necessary simplicity, be insufficiently realistic due to the sensitivity implied by the steep approach to $D = 0$ at finite d_M . It is, for example, quite possible that a root mean square addition of these influences (rather than the

linear combination of Equation [A-4.1]) would result in appreciably different limiting values for d_M (and therefore, for $2D(d_M)$ near these limits). Similarly, an attempt to deal in greater detail (and with considerably greater analytical complexity) with the actual spatial distributions of radiant energy flux resulting from these effects (by adding image degradation contributions differentially and integrating spatially) would probably give somewhat different results. A finite resolution limit would nonetheless still be observed to result from any such analytical approach.

As sensitive as the numerical results of Figure A-3 may appear to be to effects which were but crudely approximated in the analysis, it must be allowed that these predicted relations are quite likely optimistic; real systems with corresponding nominal values of the various parameters dealt with in this analysis are quite likely to exhibit less resolution than the numerical results of the analysis indicate. Optimistic results are, however, quite within the spirit of the analysis, in that trends and, in an order-of-magnitude sense, the numerical values still have use in attempting to judge photographic concept feasibility and in the early stages of system design.

With the preliminary optical system design purpose of the analysis in mind, it is useful to consider typical orders of magnitude of the various parameters and variables which are pertinent to the resolution vs. "depth-of-field" problem.

The numerical calculations expressed by Figures A-2, A-3, and

A-5 were carried out for values of $\lambda = 0.555$ microns and a_G , $\frac{a_D}{a_G}$, and $\frac{a_{F-0}}{a_G} = 1$. The value of λ chosen is reasonable since visible light photography is much easier experimentally (focussing, etc.), since visible light optics and films are readily available in great variety, and since typical light sources are of color temperatures giving reasonable efficiencies in the visible light spectrum. Values of the combining parameters a_G , $\frac{a_D}{a_G}$, and $\frac{a_{F-0}}{a_G}$ were chosen as unity due to lack of a better value and due to the presumption that within the usable range of operating situations the details of image degradation effects are relatively unimportant. This presumption could only be validated by an experimental or analytical study well beyond the scope justifiable by the purpose of this analysis.

A typical value of the combined film-optical system aberration scale parameter, L_{F-0} , was chosen as an example for Figure A-3. This value represents a likely upper limit of practically attainable systems. It might be viewed, for example, as resulting from a linear combination of scales:

$$d_{F-0} = \frac{1}{L_{F-0}} = d_0 + d_F = \frac{1}{L_0} + \frac{1}{L_F}$$

where the optical and film effects are now separated. In these terms, $L_{F-0} = 100$ lines/mm. is rationalizable based on a typical fine-grain photographic emulsion¹, $L_F = 140$ lines/mm., and a rather optimistic high-quality photographic lens specification, $L_0 = 350$ lines/mm.

Typical usable values of F and M are somewhat less clearly

¹Kodak Panatomic-X (Reference A-7).

indicated. Usable focal length photographic lenses of high resolution are of apertures such that, generally, $5 < F' < 100$. A reasonable minimum approach distance to a burning propellant sample, say, $2'' < X_1$ requires that $f > 2''$. A reasonable maximum optical system length is $X_1 + X_2 = 200''$.¹ Then, $(M)_{\text{maximum}} = x_2/f = 200''/2'' = 100$. Since $M = 1$ is a reasonable lower limit on M , then, with $F = (M+1/M)F'$, $10 < F < 100$. Thus, reasonable values for F/M are: $0.10 < F/M < 100$. It is clear, however, that if several oxidizer particles are to be viewed on a burning surface:

$$1 \text{ to } 10 < \frac{2D}{d_M} \leq \frac{2F}{M}$$

and, therefore

$$0.5 \text{ to } 5 \leq \frac{F}{M}$$

Actually, the approximations of the preceding first-order analysis required that $\frac{a}{2X_1} \ll 1$ and, therefore, that $2F/M \gg 1$. This requirement, therefore, implies that $2F/M \geq 10$ or $F/M \geq 5$ which thereby places a minimum value requirement (for the purposes of this analysis) on F/M which, though slightly higher than that deduced on the preceding grounds is not so far above the reasonable $2D/d_M > 0.5$ to 5.0 requirement as to provide a major problem in a discussion of trends and orders-of-magnitude.

In summary, therefore, reasonable, attainable (though somewhat optimistic) values of the various optical system parameters are:

$$\lambda = 0.555 \text{ microns (based on operational case, lens and light source specifications, and visual focussing requirements)}$$

¹It must be allowed, however, that this is not a serious or fundamental limit and may be exceeded in design.

$$a_G = \frac{a_D}{a_G} = \frac{a_{F-0}}{a_G} = 1 \quad (\text{as a reasonable, though uncertain approximation})$$

$$L_{F-0} = 100 \text{ lines/mm.} \quad (\text{based on typical high-resolution lens and film resolving powers})$$

and: $5 \leq F/M \leq 100$ (maximum: based on a reasonable approach distance to sample)

or: $10 \leq 2F/M \leq 200$ (minimum: based on a required resolution of at least several particles)

Viewing the numerical results of the preceding first-order analysis with respect to these values of parameters and variables, then, it becomes apparent that useful burning surface photographs of solid propellant samples are probably feasible. Hopes for detailed views of more than a few individual small oxidizer particles are, however, unsupported. Clearly, it is unlikely that more than one or two particles of scale 10 microns or less can be viewed at a given time, but that an appreciably large field, say, 10 particles in depth can be viewed if the minimum particle size of interest is larger, say, 20 to 50 microns.

With these magnitudes in mind the optical system described in Chapter Two was assembled. Its final design and the lighting used with it would be predicted on the basis of the foregoing analysis to be approximately represented by the 2D-d_m plots shown in Figure A-6.

NOMENCLATURE

- d_D = dimensional image-plane scale of the distance between two point source objects just resolved despite diffraction at a circular aperture.
- d_{F-0} = dimensional image-plane scale (of a point source object) due to the combined effects of optical system image degradation (chromatic, spherical aberrations, etc.) and film resolution (due to emulsion thickness and granularity, etc.)
- d_G = dimensional image-plane scale (of a point source object) due to geometrical optics effects of an object location displaced from the plane of perfect focus (conjugate of the photographic film plane)
- d_Σ = total dimensional image-plane scale (of a point source object) due to all causes of image degradation
- d_M = minimum dimensional scale of "resolved" object detail
- D = axial distance (over which D_M is "resolved") on either side of the plane of perfect focus
- M = nominal optical system magnification ($\frac{\text{image scale at film plane}}{\text{object scale at plane of perfect focus}}$)
- Δ = object displacement from the plane of perfect focus (Δ_2 = displacement toward lens; Δ_1 = displacement away from lens)
- f = effective focal length of optical system¹
- a = diameter of effective aperture of optical system¹
- x_1 = axial distance from object plane to lens¹
- x_2 = axial distance from lens to image plane¹
- F' = nominal optical system F-stop ($= \frac{f}{a}$)
- F = effective optical system F-stop ($= F'(M+1)$)
- N = "numerical aperture" of optical system ($= \frac{1}{\sin^{-1}(2\frac{x_1}{a})}$)

¹It is presumed that all complex optical systems can be considered as equivalent in these terms to a single, simple lens system.

- n = index of refraction of object and image spaces
- λ_0 = wavelength of light in vacuo
- $\lambda = \frac{\lambda_0}{n}$ = wavelength of light in object and image spaces
- L_{F-0} = minimum line spacing of "resolved" image (in the traditional resolution chart sense) after film and optical image degradation but excluding diffraction effects.

APPENDIX A

REFERENCES

- (A-1) Kodak Photographic Films and Plates for Scientific and Technical Use (Eighth Edition), Eastman Kodak Company, Rochester, N. Y. (1960) p. 12.
- (A-2) National Bureau of Standards Circular NO. 533, Method for Determining the Resolving Power of Photographic Lenses, pp. 27.
- (A-3) Kodak Films (Fifth Edition), Eastman Kodak Company, Rochester, N.Y. (1951).
- (A-4) C. W. Kendall, War Department, Air Corps, Material Division, Memorandum Report on "Comparative Resolving Powers of Various Photographic Lenses", Library of the U. S. Congress, Washington, D. C. (1941), 5 pp.
- (A-5) R. N. Nierenberg, Army Air Forces, Material Command, Engineering Division, Memorandum Report on "Resolving Power and Illumination Data on Standard Motion Picture Lenses", Library of the U. S. Congress, Washington, D. C. (1943), pp 7.
- (A-6) Kodak Films for Cathode-Ray-Tube Photography, Eastman Kodak Company, Rochester, N. Y. (1962).
- (A-7) F. H. Perrin, "Methods of Appraising Photographic Systems: Part I - Historical Review", J.S.M.P.T.E., 69, 151-156 (March 1960).
- (A-8) F. H. Perrin, "Methods of Appraising Photographic Systems: Part II - Manipulation and Significance of the Sine-Wave Response Function", J.S.M.P.T.E., 69, 239-249 (April 1960).
- (A-9) D. P. Paris, "Approximation of the Sine-Wave Response of Photographic Emulsions", J.O.S.A., 51, 988-991 (September 1961).
- (A-10) D. H. Kelly, "Systems Analysis of the Photographic Process. II. Transfer Function Measurements", J.O.S.A., 51, 319-330 (March 1961).
- (A-11) M. Born and E. Wolf, Principles of Optics, Pergamon Press, New York (1959), page 418.
- (A-12) A. C. Hardy and F. H. Perrin, The Principles of Optics, McGraw-Hill, New York (1932), page 78.
- (A-13) Kodak Films for Black-and-White Photographs (Seventh Edition) Eastman Kodak Company, Rochester, N. Y. (1958), page 45.

APPENDIX A

LIST OF FIGURES

- Figure A-1 Depth of Field vs Resolved Scale (Considering Geometrical Effects)
- Figure A-2 Depth of Field vs Resolved Scale (Considering Geometric and Diffractive Effects Only)
- Figure A-3 Depth of Field vs Resolved Scale (Considering Geometric, Diffractive and Film-Optical Aberration Effects)
- Figure A-4 $\frac{2D_{ULT}}{d_M}$ vs d_M [Equation A-4.7]
- Figure A-5 $(d_M)_{MIN.}$ vs $\frac{2F}{M}$
- Figure A-6 Depth of Field vs Resolved Scale (For Assembled Optical System)

DEPTH OF FIELD vs RESOLVED SCALE

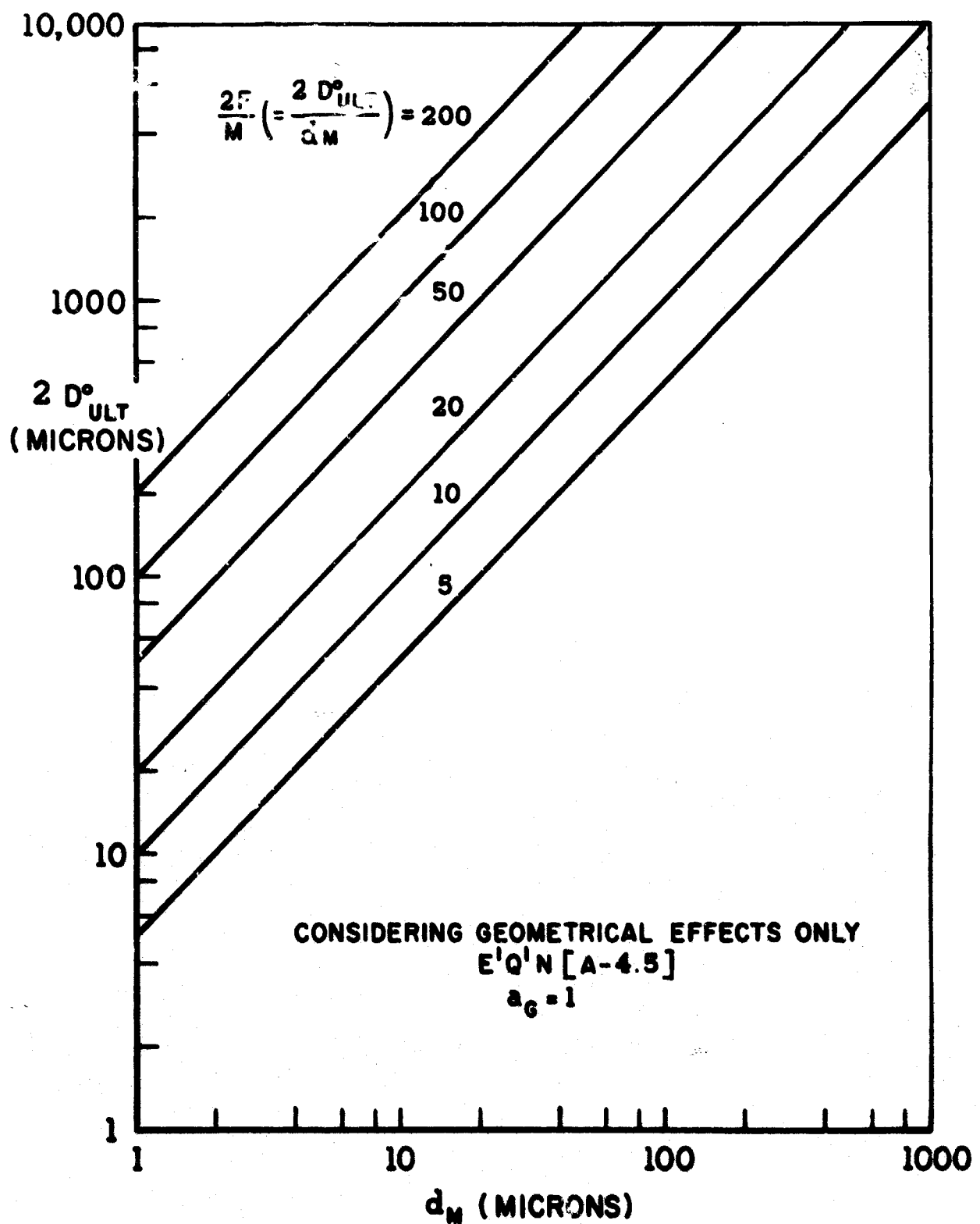


FIGURE A-1

JP19-4009-63

DEPTH OF FIELD vs RESOLVED SCALE

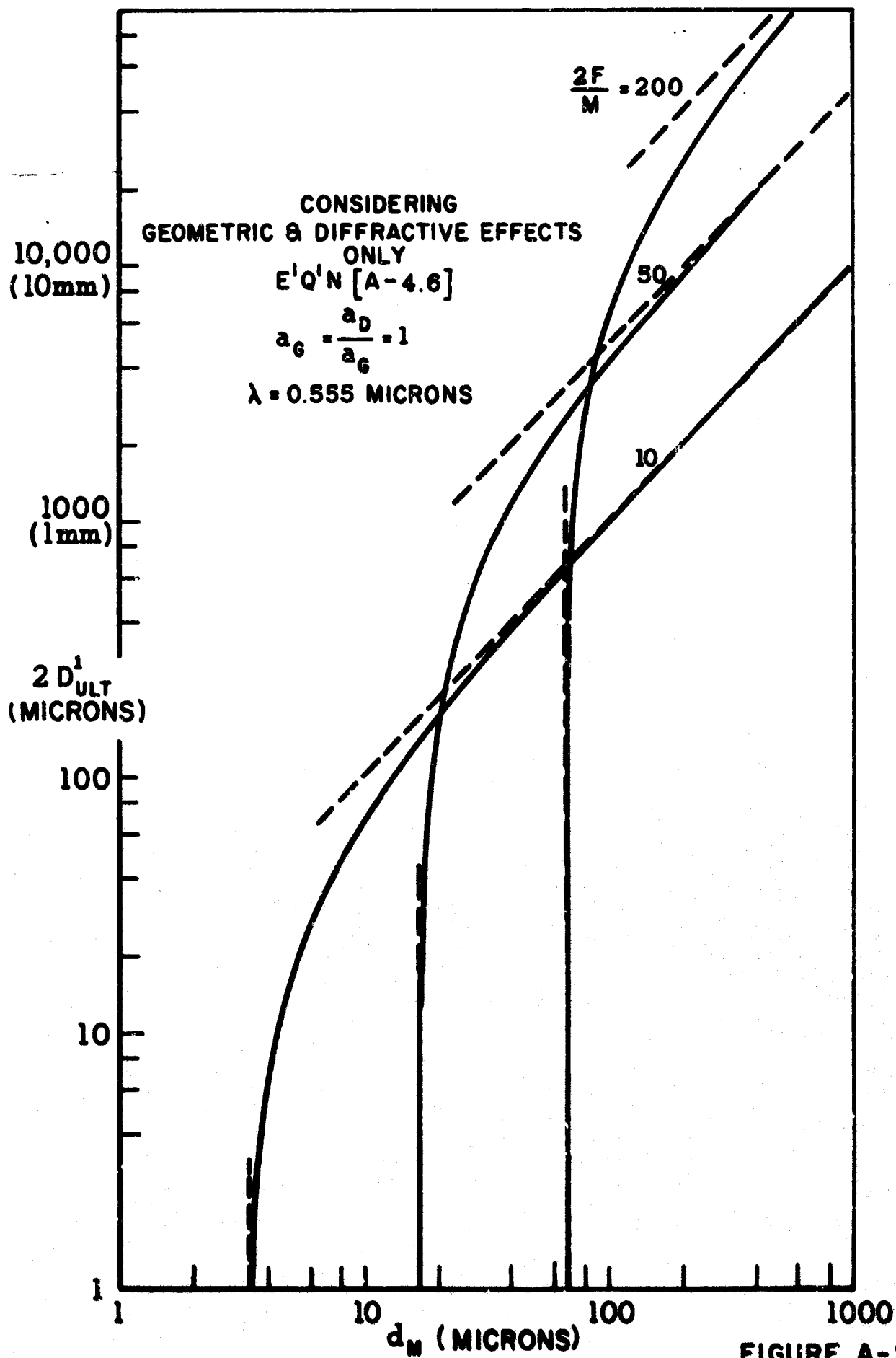


FIGURE A-2

JP19-4010-65

DEPTH OF FIELD vs RESOLVED SCALE

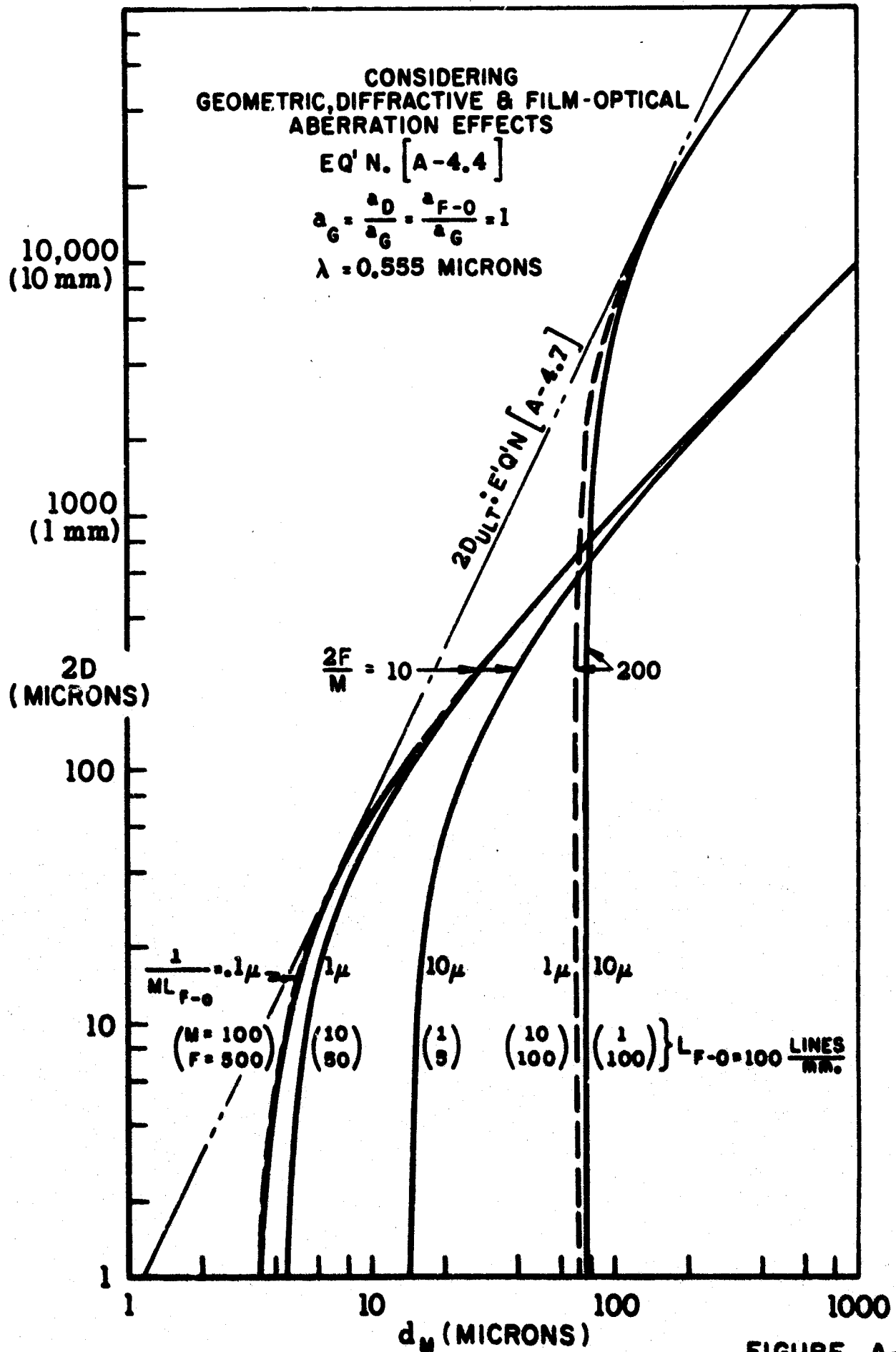


FIGURE A-3

JP19-4013-65

$\frac{2D_{ULT}}{d_M}$ vs d_M
EQ'N. [A-4.7]

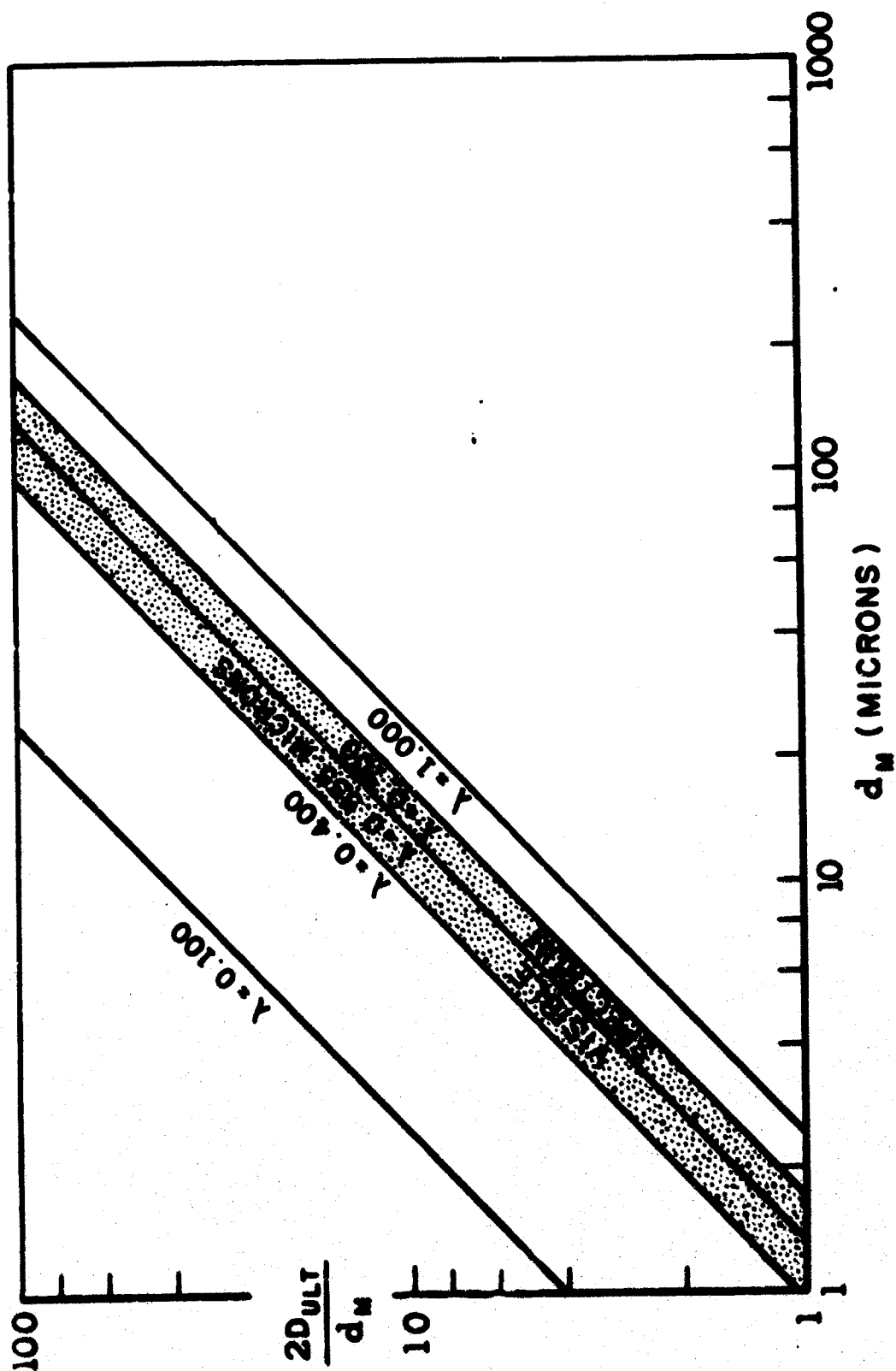


FIGURE A-4

$(d_M)_{\text{MIN.}}$ vs $\frac{2F}{M}$

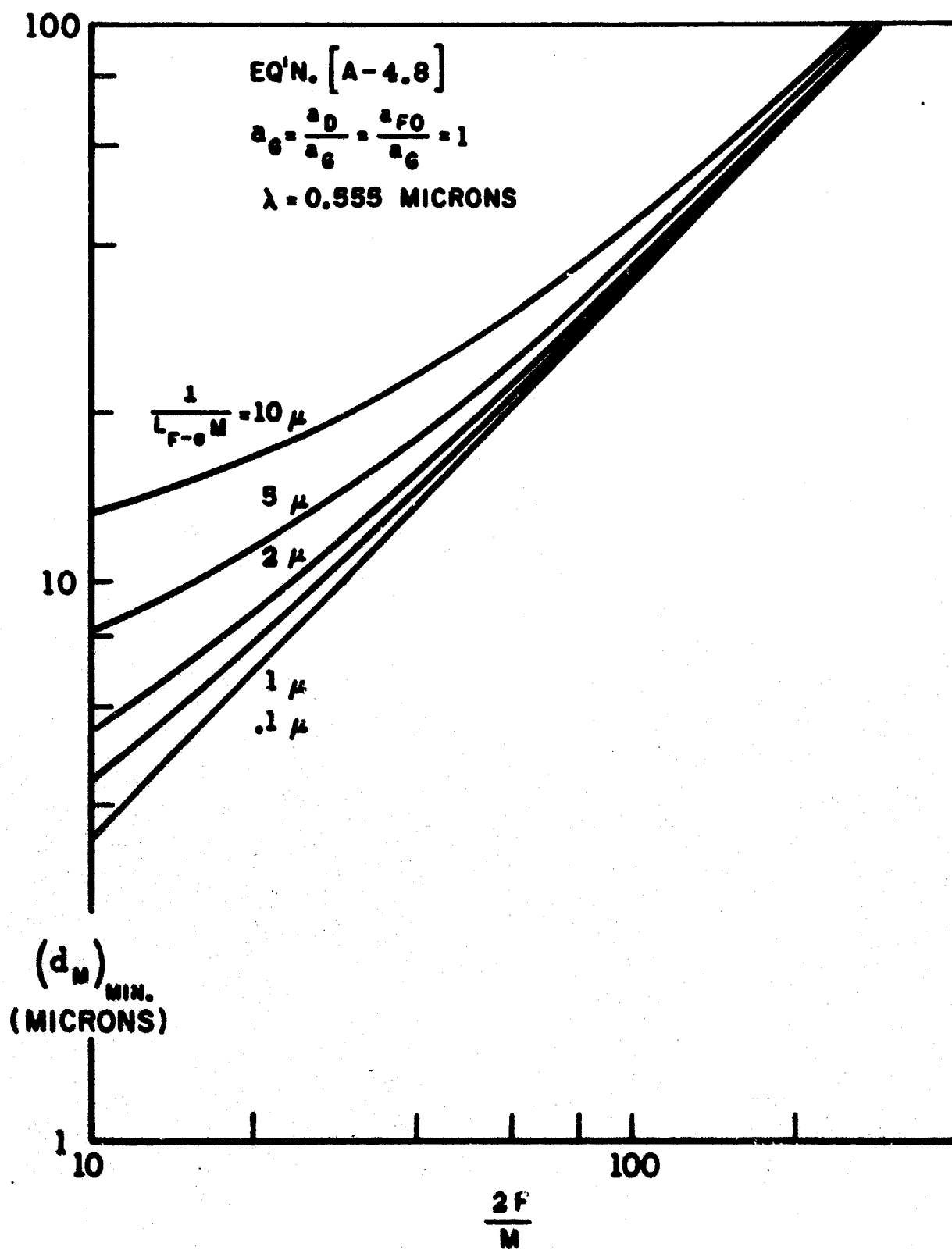


FIGURE A-5

JP19-4013-65

DEPTH OF FIELD vs RESOLVED SCALE

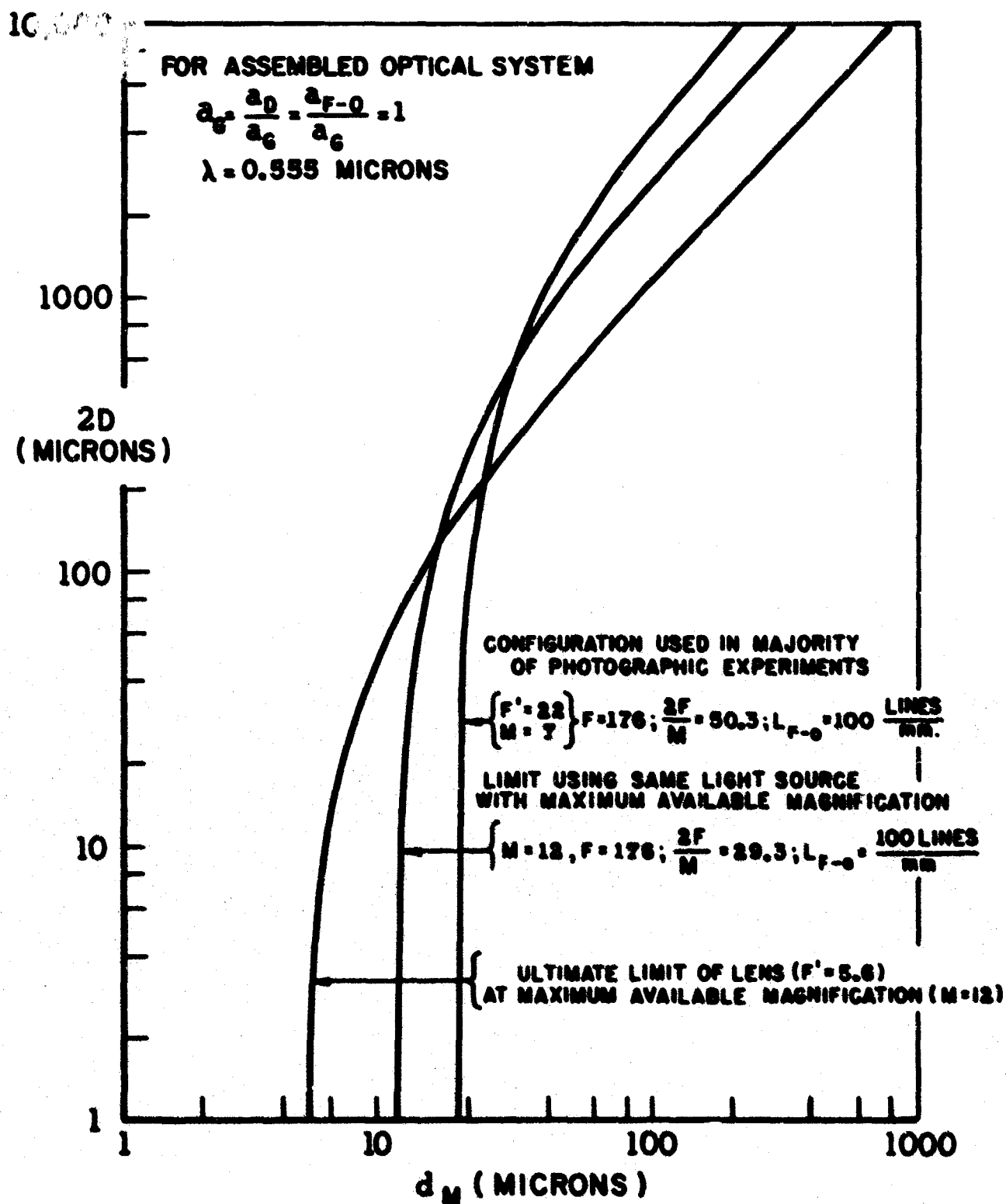


FIGURE A-6

JP19-4008-65

APPENDIX B - COMMERCIAL EQUIPMENT AND MATERIALS

<u>ITEM</u>	<u>Equipment</u>	<u>MANUFACTURER</u>	<u>USE</u>
Alpa 35mm. single lens reflex camera with extension tubes, Model 6B with	Pignons S. A., Ballaigues, Switzerland		Preliminary burning surface photography
Switar apochromatic camera lens, 50 mm. focal length, iris diaphragm (f/1.8 to f/22)			Objective lens for preliminary burning surface photography
Speed Graphic 4" x 5" press camera	Graflex, Inc., Rochester, New York		Camera body for photo-macroscopy
Componon enlarging lens, 100 mm. focal length, iris diaphragm (f/5.6 to f/45)	Schneider-Cogswell, Inc., Chicago, Ill.		Objective lens for photomacroscopy
Synchro-Compur shutter, 1 to 1/500 sec., electronic flash synchronized	Wollensak Optical Company Division of Revere Camera Company Rochester, New York		Shutter of photomacroscopic camera
Electronic flash unit. Model FR 150	The FR Corporation, New York, N. Y.		Flash lighting for burning surface photomacroscopy
Strobosnar electronic flash unit	Heliand Division of Minneapolis-Honeywell, Denver, Colorado		Flash lighting for burning surface photomacroscopy
Oscilloscope, Model 535A	Tektronix, Inc., Beaverton, Oregon		Monitoring of photoelectric trigger sensor output during burning surface photography

Appendix B

ITEM

MANUFACTURER

USE

High Gain Differential Calibrated
DC Preamplifier, Type D (plug-in)

Tektronix, Inc., Beaverton, Oregon

Monitoring of trigger
sensor output

Oscilloscope camera

Allen B. DuMont Laboratories
Clifton, New Jersey

Recording of trigger
sensor monitoring trace

Semiconductor light sensor,
Type 1 N 2175

Texas Instruments, Inc.
Dallas, Texas

Photoelectric trigger
sensor for burning surface
photography

Materials

Tri-X Pan film (35mm)

Plus-X film (35mm)

Panatomic-X film (35mm)

High-speed Ektachrome film (35mm)

Kodachrome II film (35mm)

Adox KB 14 film (35mm)

Adox KB 17 film (35mm)

Microdol-X film developer
D-76 developer

Acufine film developer

FR X-44 one-shot film developer

FR X-22 film developer

Ignition wire for Parr Peroxide
Bomb Calorimeters

us
-2

Eastman Kodak Company
Rochester, New York

Adox Fotowerke, Dr. C. Schleusser GMBH,
Frankfurt/Main, West Germany

Eastman Kodak Company
Rochester, New York

Bauman Photochemical Corp.,
Chicago, Illinois

The FR Corporation, New York, N. Y.

Fisher Scientific Company
New York, New York

Vacuum strand burner
recording and surface
photography

Surface photography

Burning surface photography

Recording film and surface
photographic film developing

Surface photograph film
developing

Surface photograph film
developing

Hot wire strand ignition

Appendix B

ITEM

MANUFACTURER

USE

Metering needle valves

Hoke, Inc., Cresskill, New Jersey

Nitrogen bleed control, vacuum strand burner

Loading valve, Type 15H

Grove Regulator Company, Oakland, California

Control loading of regulator for nitrogen bleed to vacuum strand burner

Mighty-Mite Pressure reducing regulator, Model 94

Grove Regulator Company, Oakland, California

Control of nitrogen bleed flow to vacuum strand burner

Test gauge, 0 600 psig.

U. S. Gauge, A Division of Ametek, Inc., Sellersville, Pennsylvania

Nitrogen bleed supply pressure indication, vacuum strand burner

Allstate battery charger Model 190.90020

Sears Roebuck and Company Chicago, Illinois

Hot wire ignition, power supply, vacuum strand burner

Beatty Portronic recording camera, Model JR

Photographic Products, Inc., Anaheim, California

Strand burning rate recording, vacuum strand burner

35 mm recording film magazine, Model C-54C

Beatty Coleman, Incorporated, Anaheim, California

Strand burning rate recorder, vacuum strand burner

Stopwatch, 0.01 sec. div.

Scientific Glass & Apparatus Company Bloomfield, New Jersey

Strand burner time measurement

Electronic repeat cycle

G. C. Wilson and Company Chatham, New Jersey

Strand burning recording camera framing control

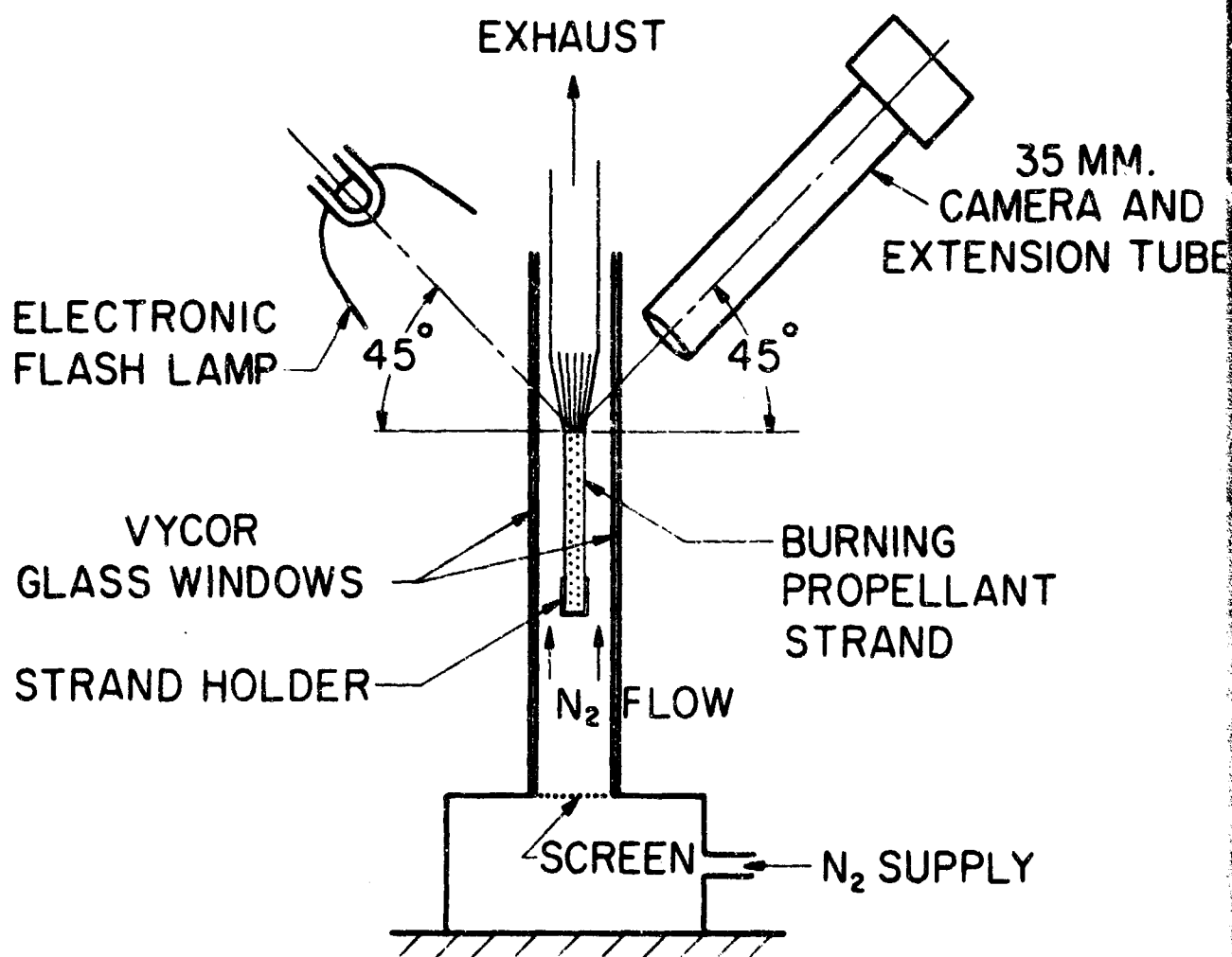
Universal illuminator, Model 359

American Optical Company Rochester, New York

Illumination of scale grid and stopwatch for vacuum strand burner

Appendix B

<u>ITEM</u>	<u>MANUFACTURER</u>	<u>USE</u>
LP-3 and LP-33 polymers (liquid)	Thiokol Chemical Corporation Trenton, New Jersey	Fuel binders
Polyester resin, Type P-13	Rohm and Haas Co., Philadelphia, Pa.	Fuel binders
Ammonium perchlorate	American Potash and Chemical Corporation New York, New York	Oxidizer
Copper Chromite	Harshaw Chemical Co., Cleveland, Ohio	Propellant additive
Carbon, lampblack	Fisher Scientific Co., Fairlawn, N. J.	Propellant additive
GMF (p-quinone dioxime)	Naugatuck Chemical Division of U. S. Rubber Company, Philadelphia, Pa.	Propellant curing agent
Sulfur, sublimed (sulfur flowers)	Fisher Scientific Co., Fairlawn, N. J.	Propellant curing agent
Di-Butyl Phthalate (n-Butyl Phthalate)	Fisher Scientific Co., Fairlawn, N. J.	Propellant plasticizer
Lupersol DDM (methyl ethyl ketone peroxide)	Wallace and Tiernan, Buffalo, New York	Propellant curing agent
Nuodex Cobalt accelerator	Nuodex Products Company, New York, N.Y.	Propellant curing agent
Lecithin, vegetable (technical)	Fisher Scientific Co., Fairlawn, N. J.	Propellant wetting agent
Polyurethane - Ammonium Perchlorate Propellant	Thiokol Chemical Corporation Elkton, Maryland	Sample Propellant
Potassium perchlorate	American Potash and Chemical Corporation New York, New York	Oxidizer



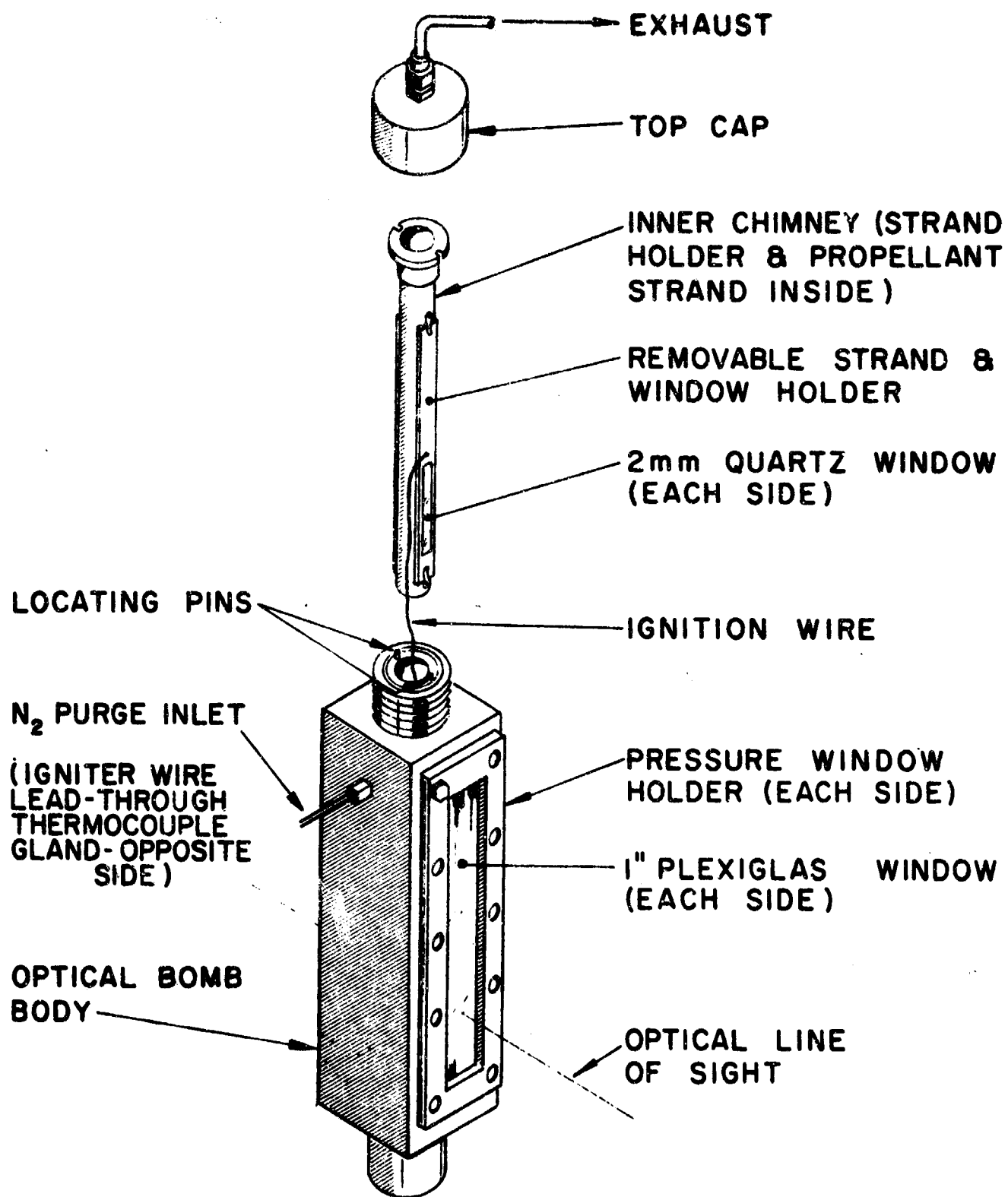
APPARATUS FOR BURNING SURFACE PHOTOGRAPHY
AT ATMOSPHERIC PRESSURE

FIGURE 1



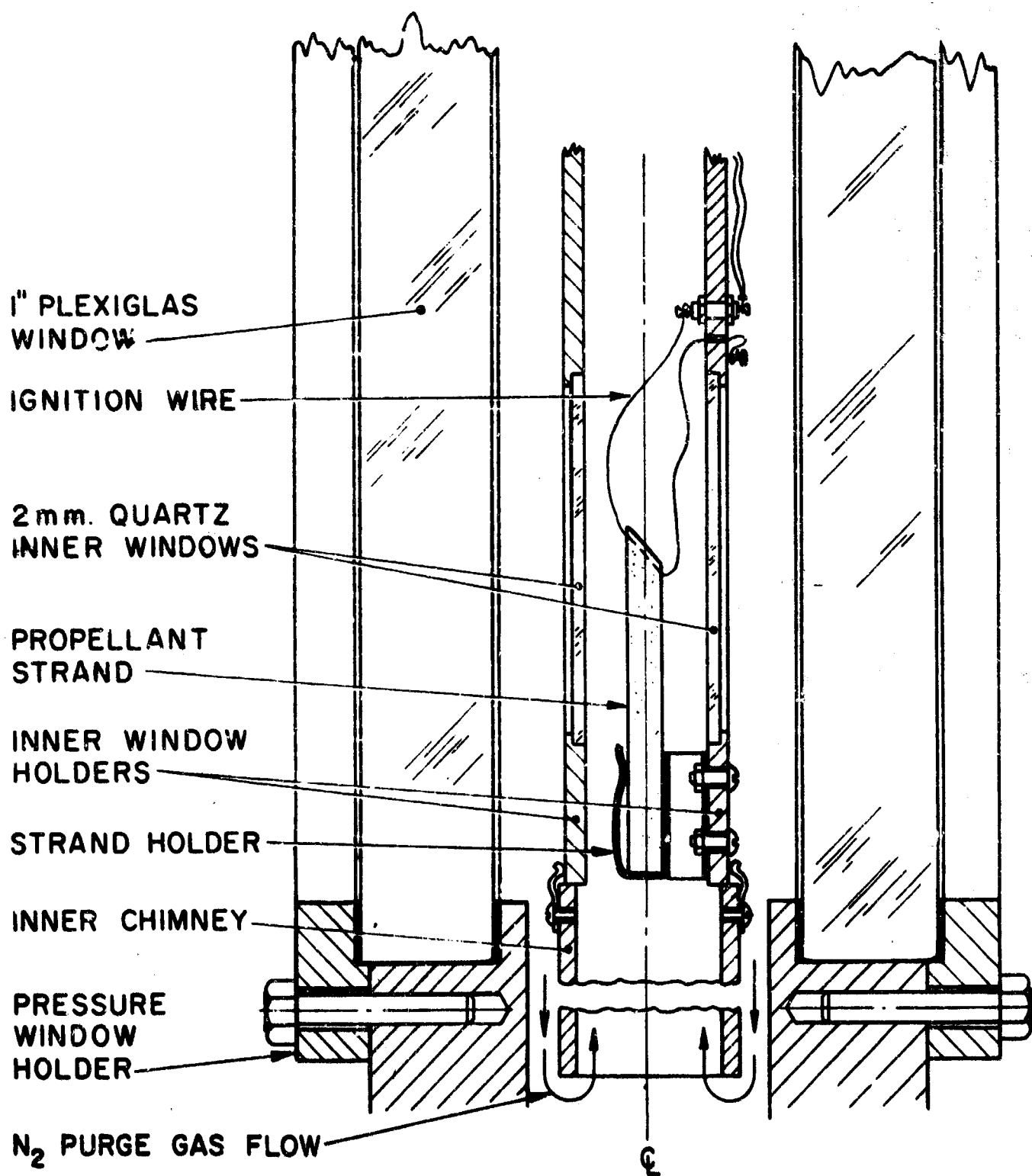
SURFACE OF POLYESTER-STYRENE PROPELLANT
PHOTOGRAPHED WHILE BURNING (1 atm. press. in N₂)
20x MAGNIFICATION AS SHOWN

FIGURE 2



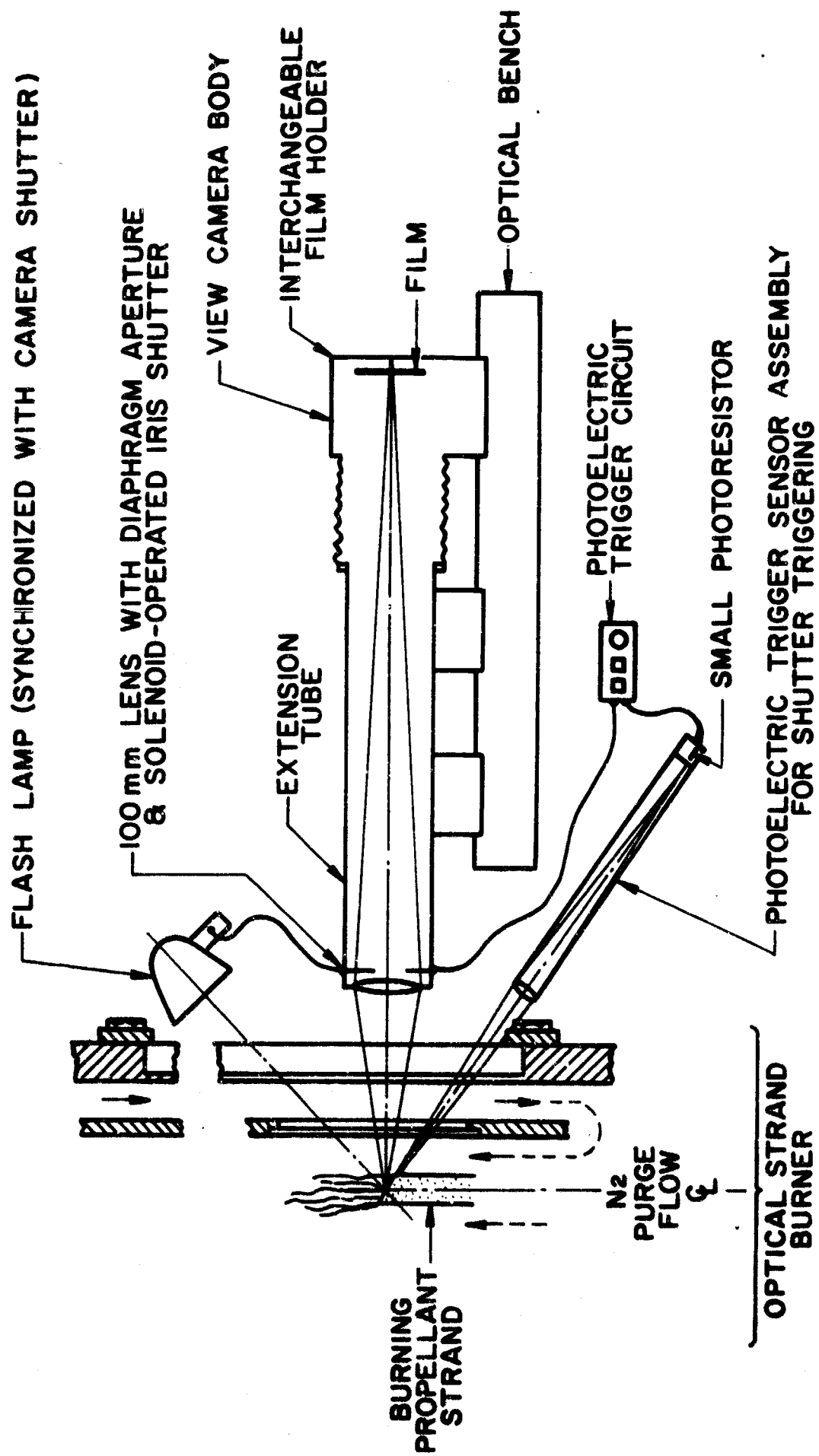
OPTICAL STRAND BURNER FOR PHOTOGRAPHY
OF BURNING SOLID PROPELLANT STRANDS

FIGURE 3



DETAIL CROSSECTION OF STRAND
LOCATION IN OPTICAL STRAND BURNER

FIGURE 4



OPTICAL SYSTEM FOR SOLID PROPELLANT BURNING SURFACE PHOTOGRAPHY

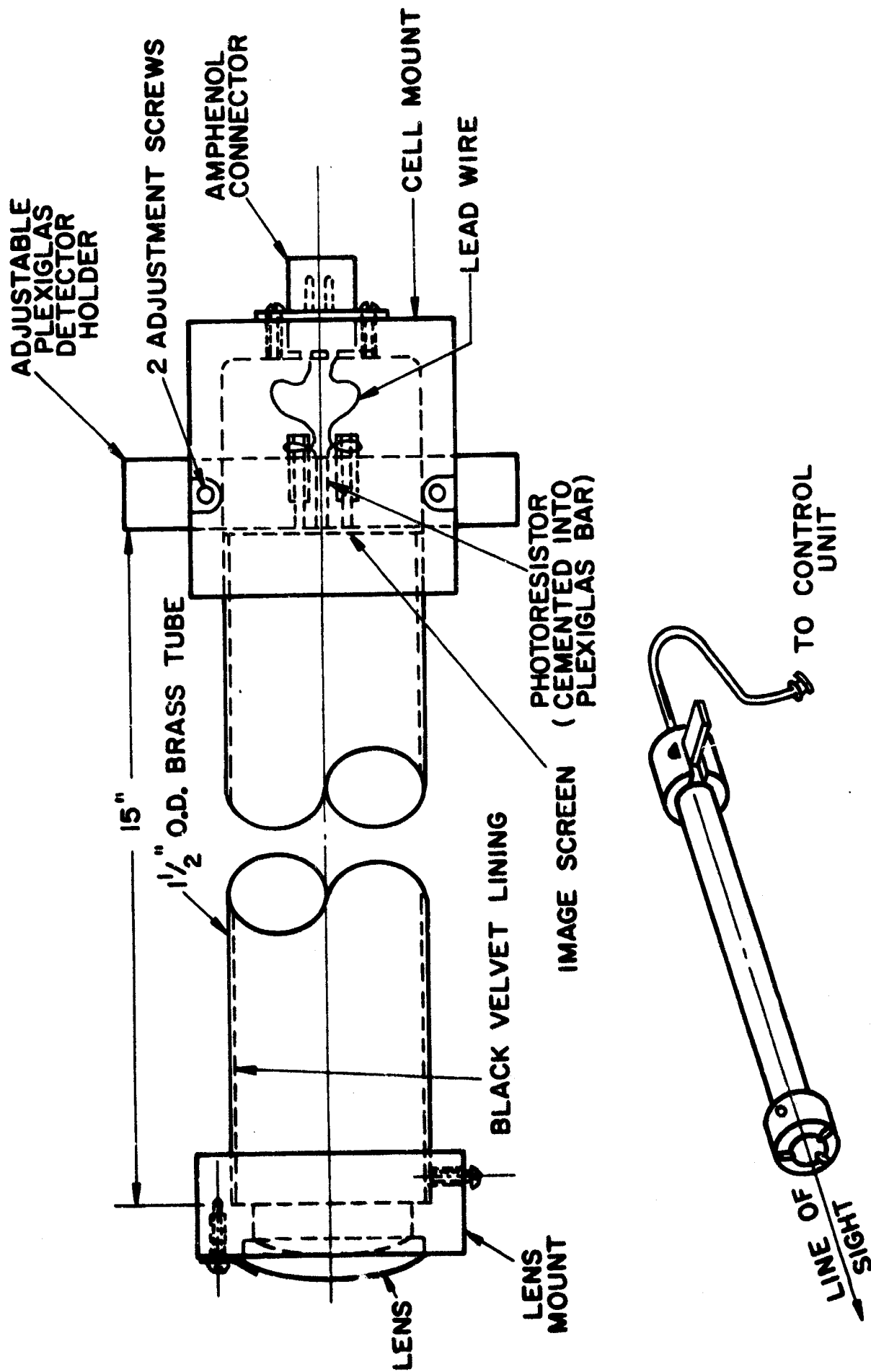
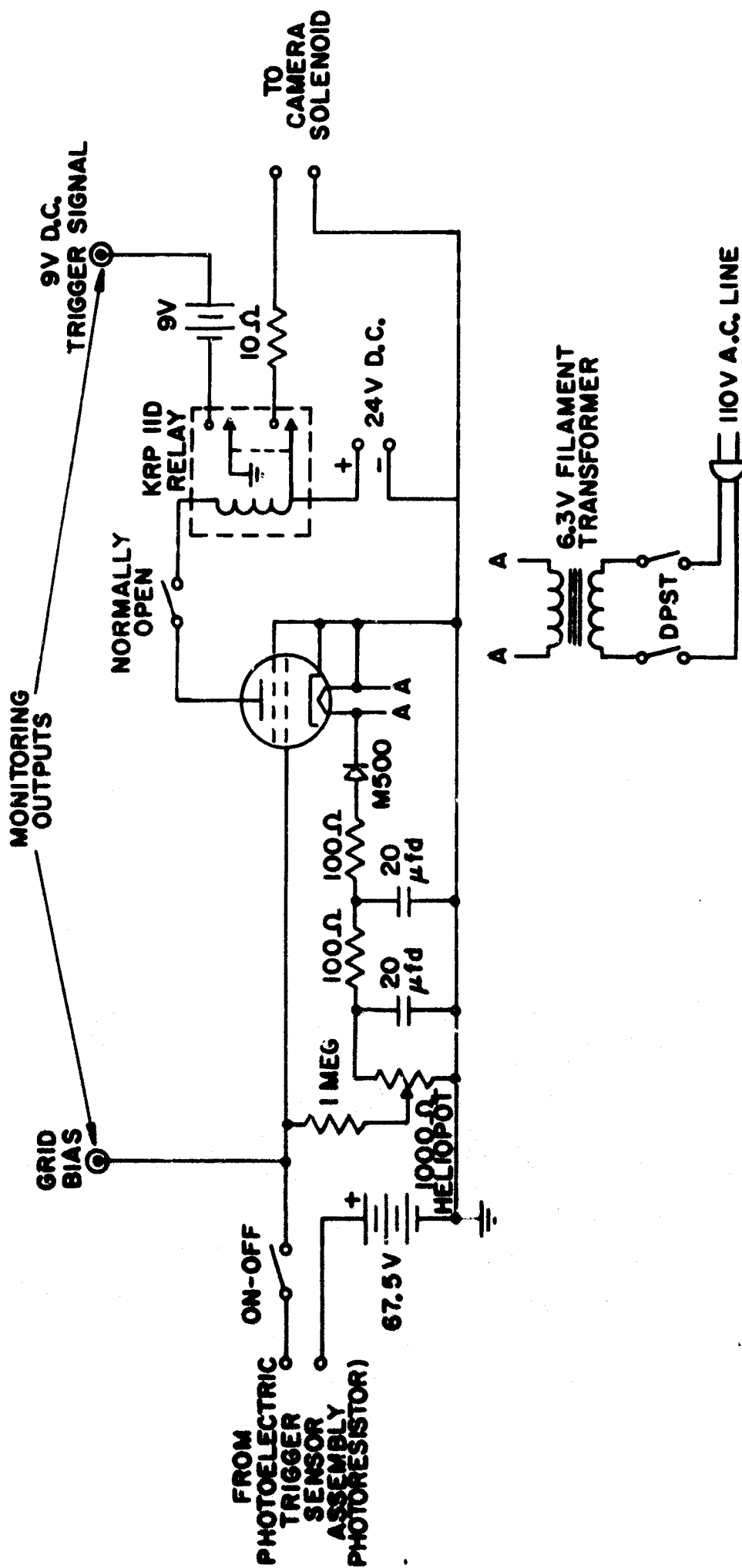


FIGURE 6

PHOTOELECTRIC TRIGGER SENSOR ASSEMBLY FOR SENSING PRESENCE OF BURNING SURFACE IN PHOTOGRAPHIC FIELD-OF-VIEW

JP19-4005-65

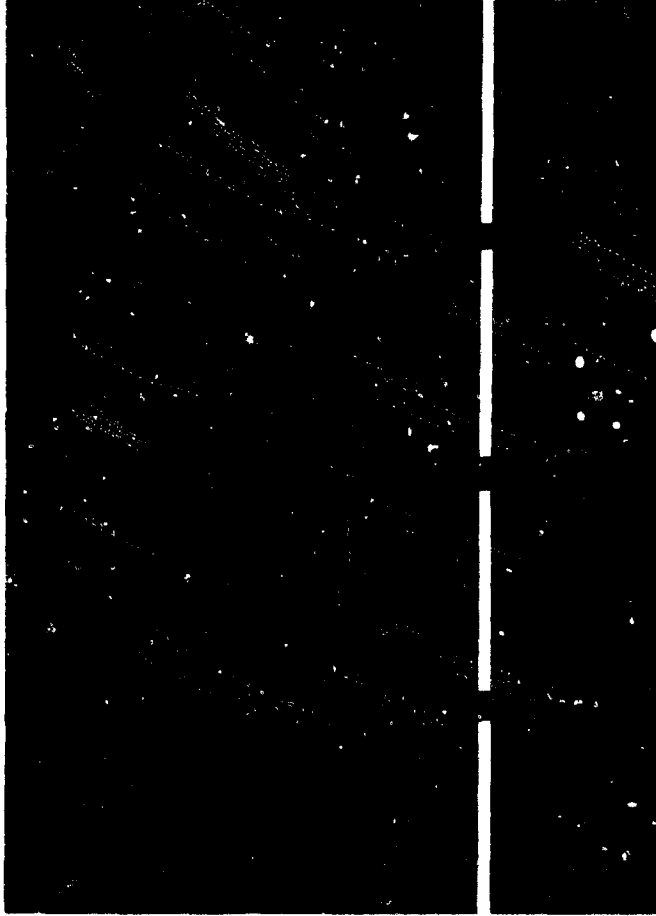


PHOTOELECTRIC TRIGGER CIRCUIT



PBAA PROPELLANT BURNING
AT 250 psig

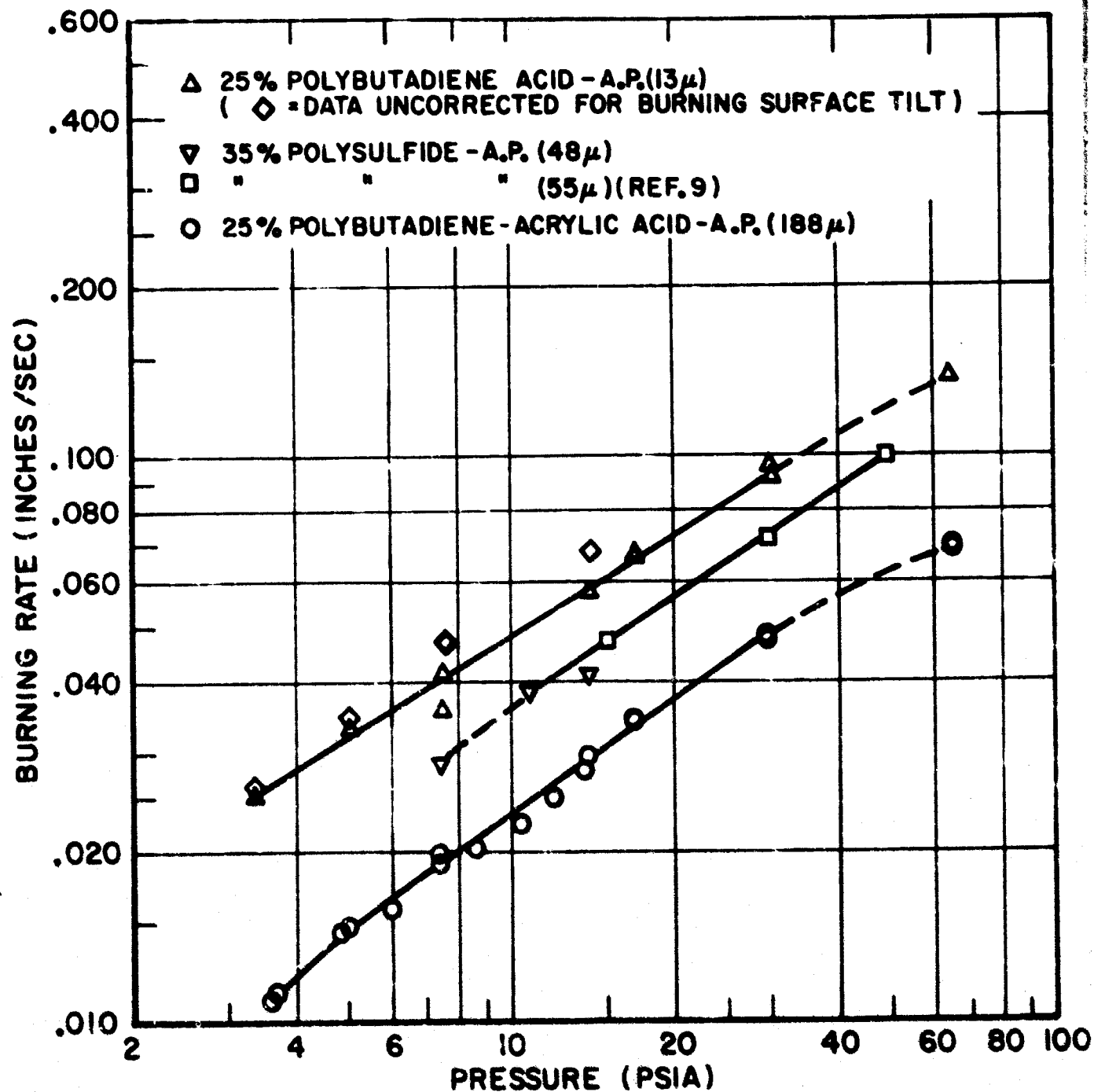
FIGURE 8



EDGE OF STRAND

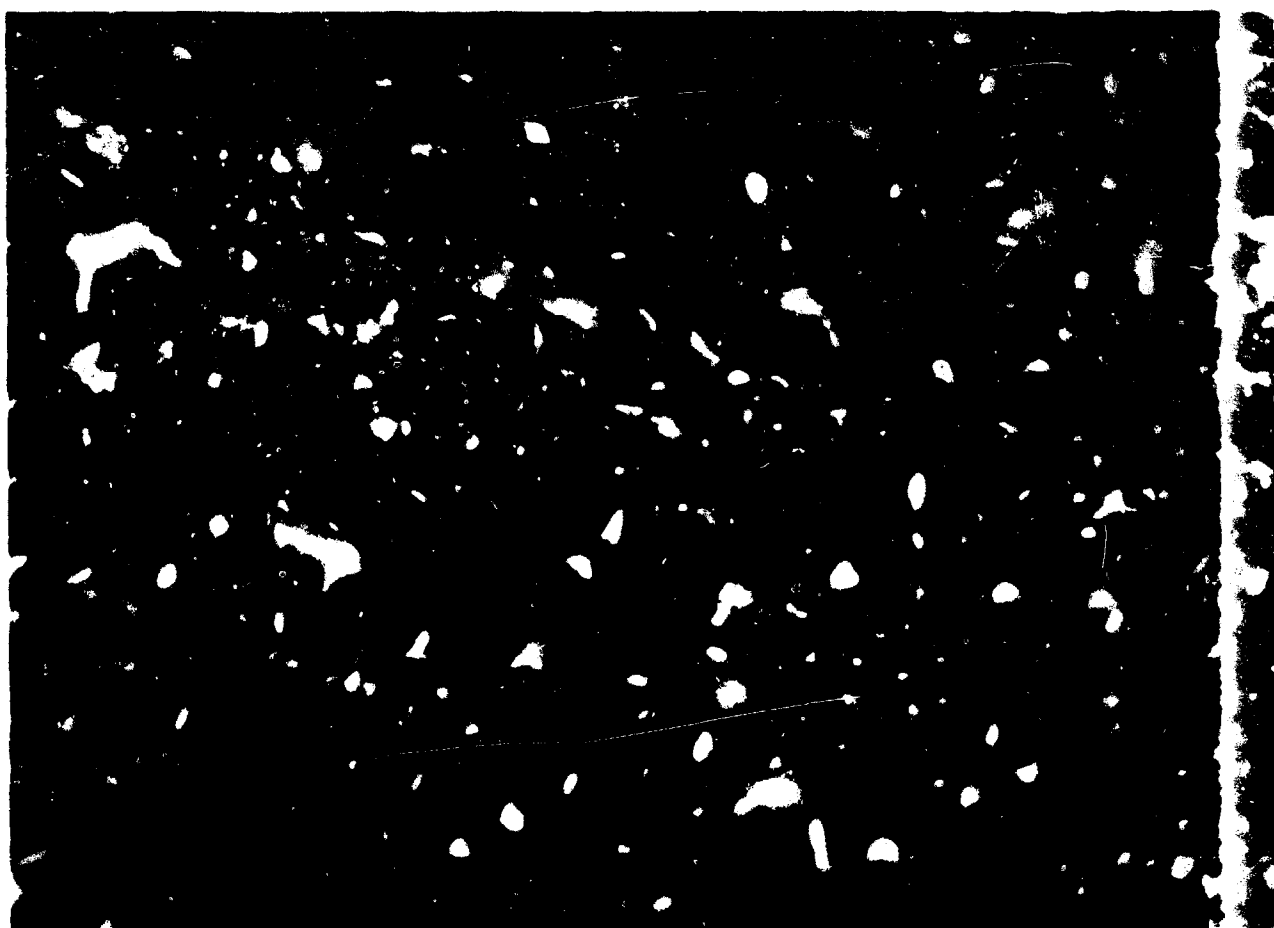
LP-3 PROPELLANT BURNING
AT 300 psig

FIGURE 9



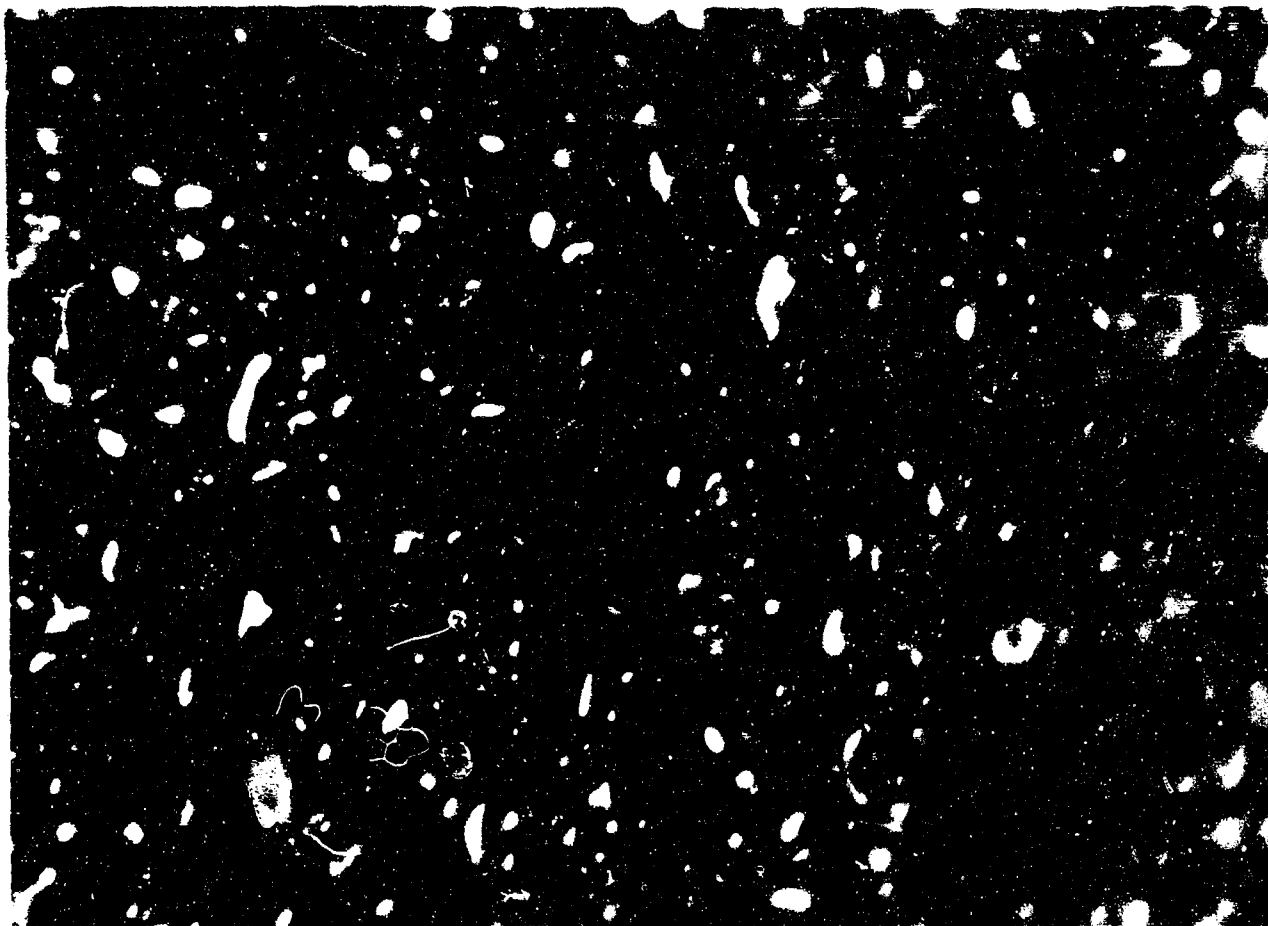
LOW PRESSURE BURNING RATES OF SEVERAL COMPOSITE
 SOLID PROPELLANTS OF NARROW, UNIMODAL
 PARTICLE SIZE DISTRIBUTIONS

FIGURE 10



**SURFACE OF POLYSULFIDE - AMMONIUM
PERCHLORATE PROPELLANT BURNING
AT 20 psig
(49 X MAGNIFICATION AS SHOWN)**

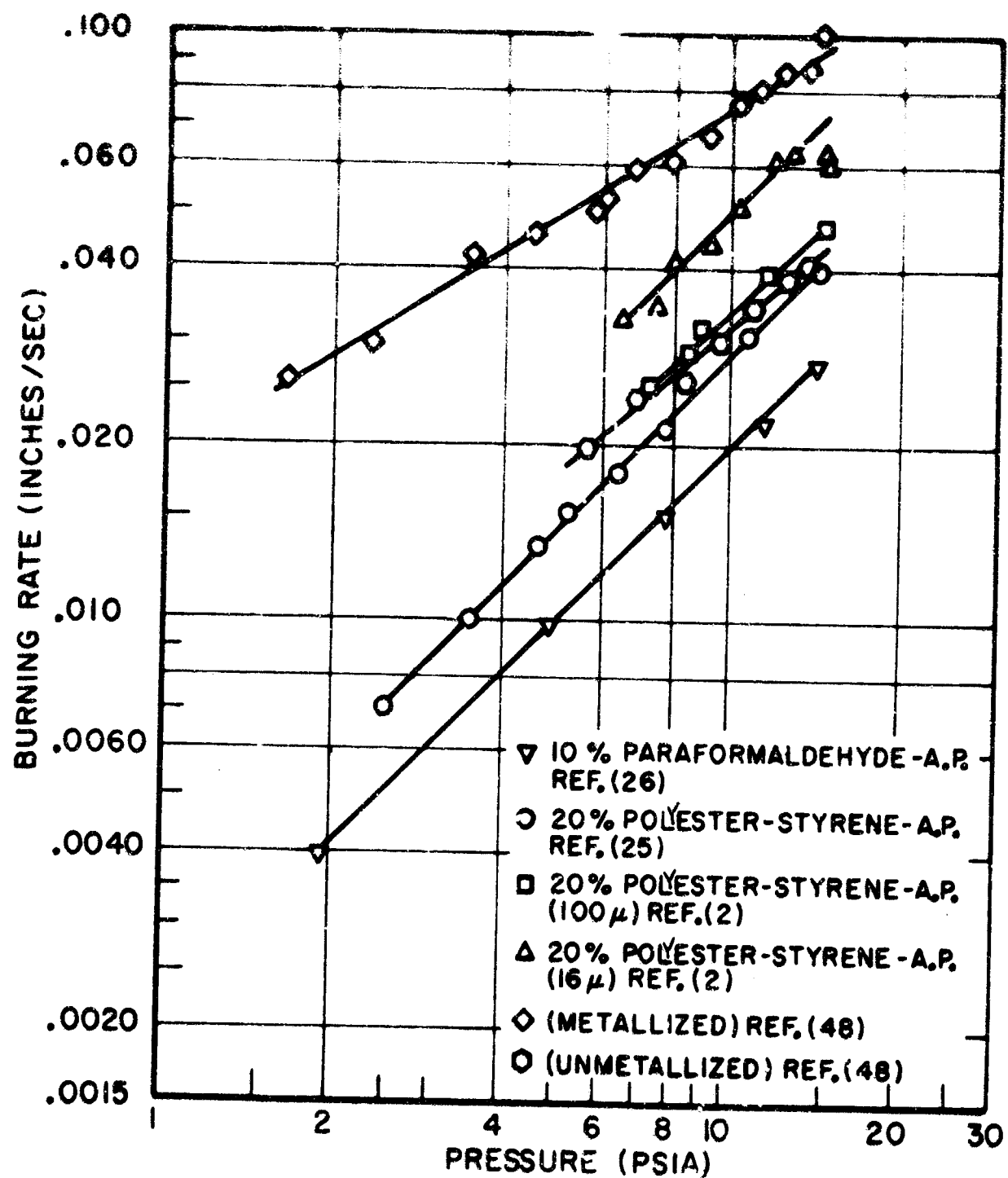
FIGURE II



SURFACE OF POLYSULFIDE - AMMONIUM
PERCHLORATE PROPELLANT BURNING
AT 100 psig
(49X MAGNIFICATION AS SHOWN)

FIGURE 12

VP19-1000-1



COLLECTED SUBATMOSPHERIC PRESSURE COMPOSITE
SOLID PROPELLANT BURNING RATES

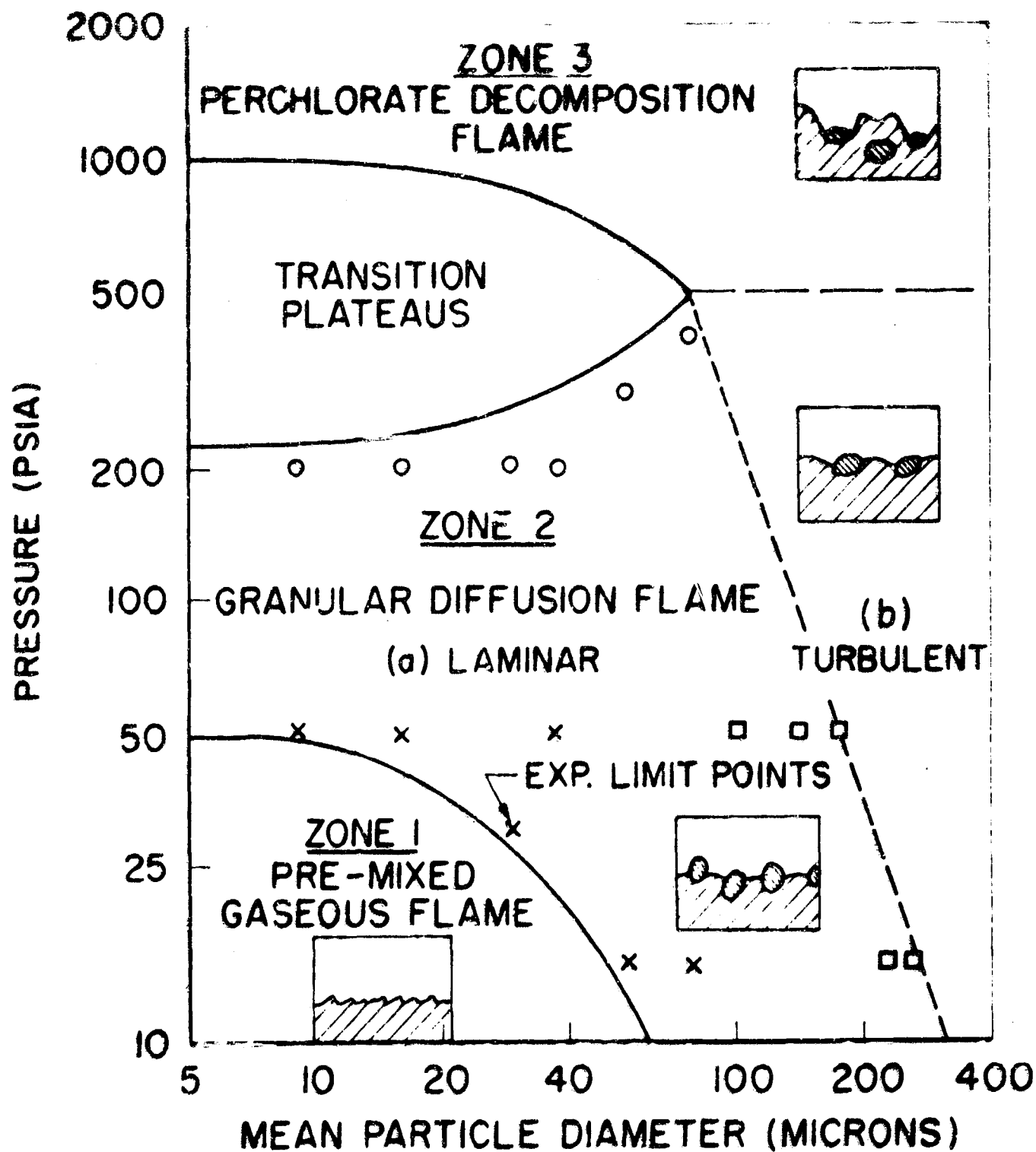
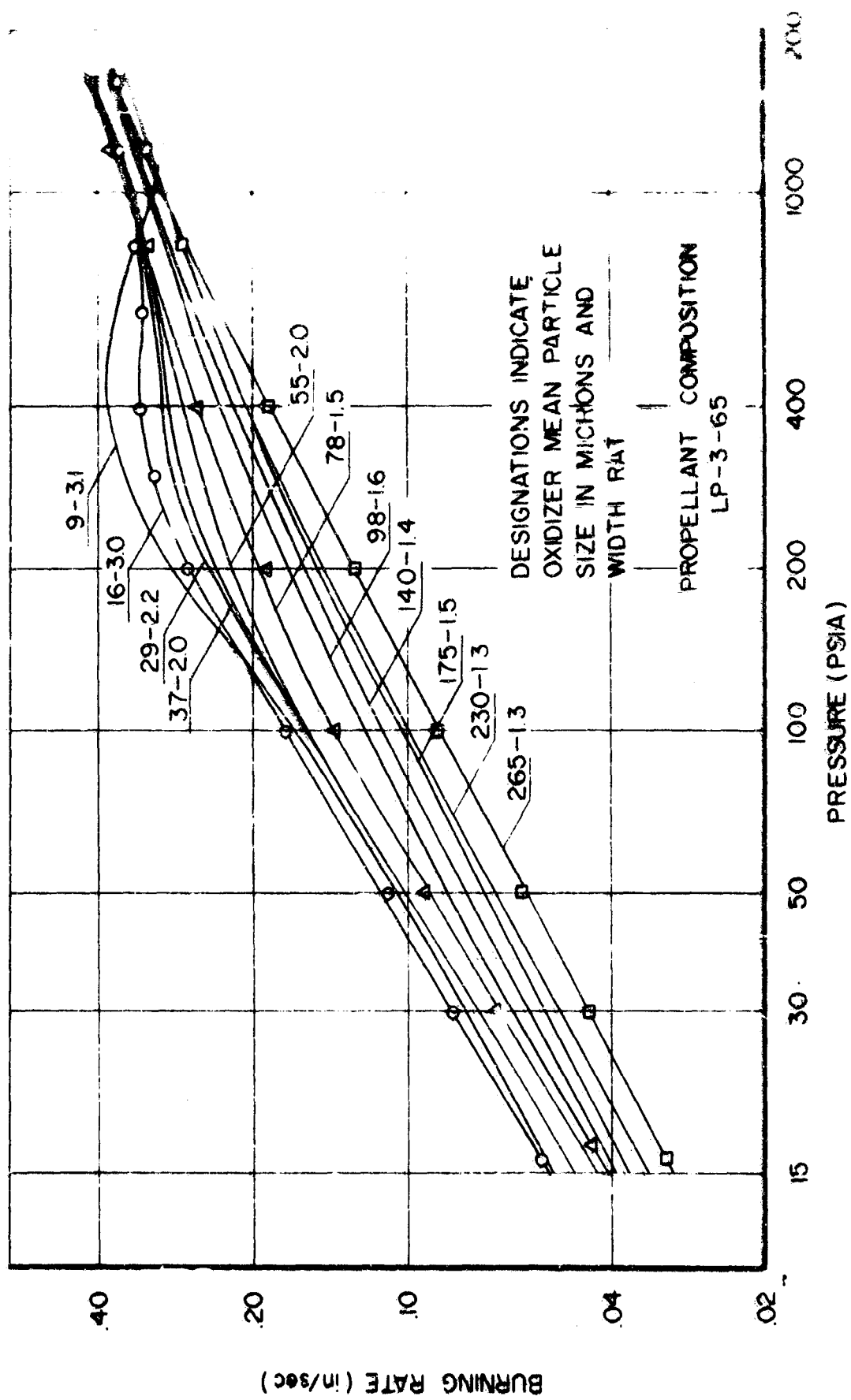


FIGURE 14



BURNING RATE VS PRESSURE FOR
POLYSULFIDE PROPELLANTS, NARROW UNIMODAL
PARTICLE SIZE DISTRIBUTIONS
(AFTER BASTRESS (9))

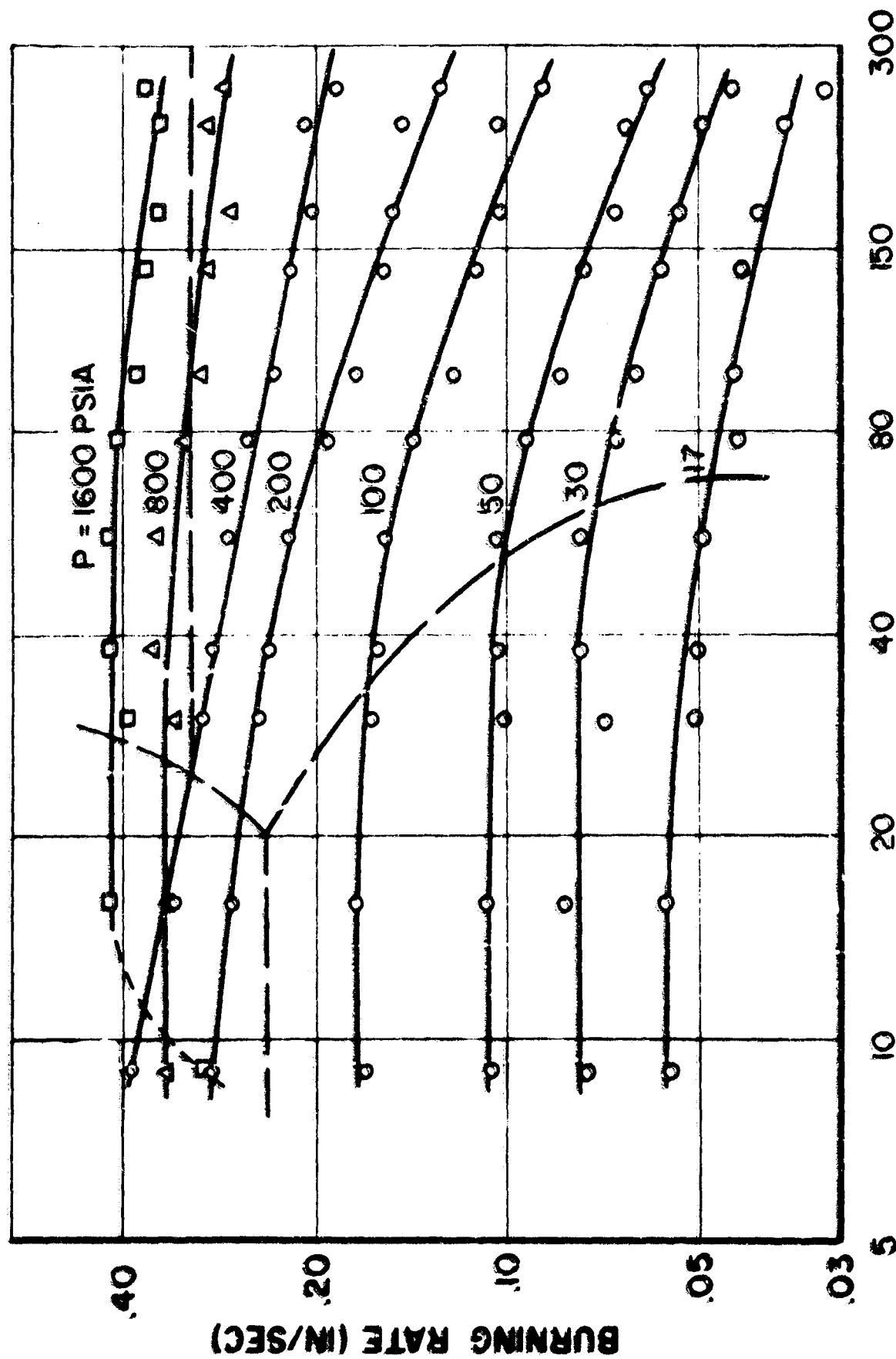
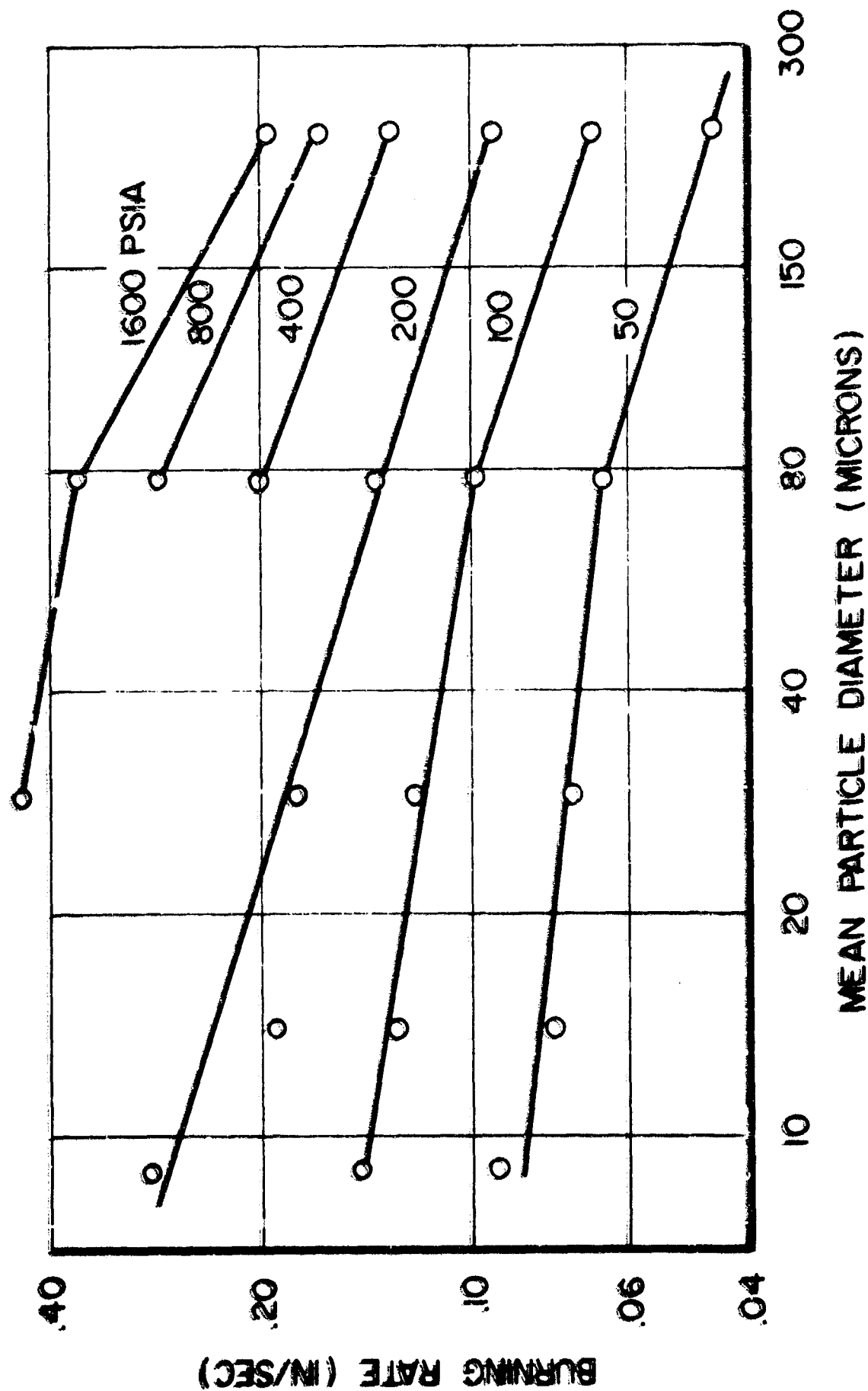


FIGURE 16

BURNING RATE VS PARTICLE SIZE, POLYSULFIDE
PROPELLANTS, NARROW UNIMODAL PARTICLE
SIZE DISTRIBUTIONS (AFTER BASTRESS (9))



BURNING RATE VS PARTICLE SIZE,
POLYESTER-STYRENE PROPELLANTS, UNIMODAL
PARTICLE SIZE DISTRIBUTIONS (AFTER BASTRESS (9))

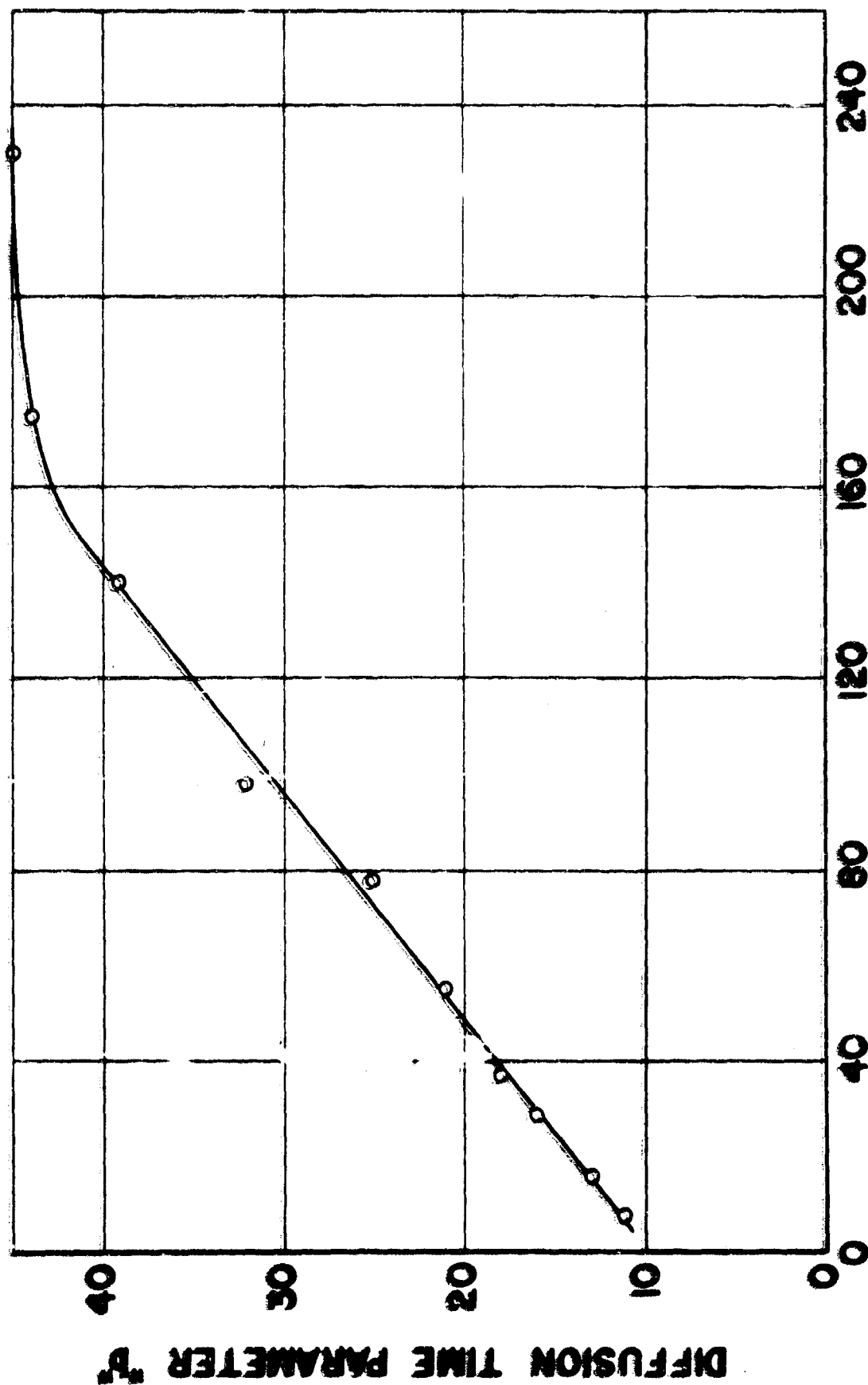
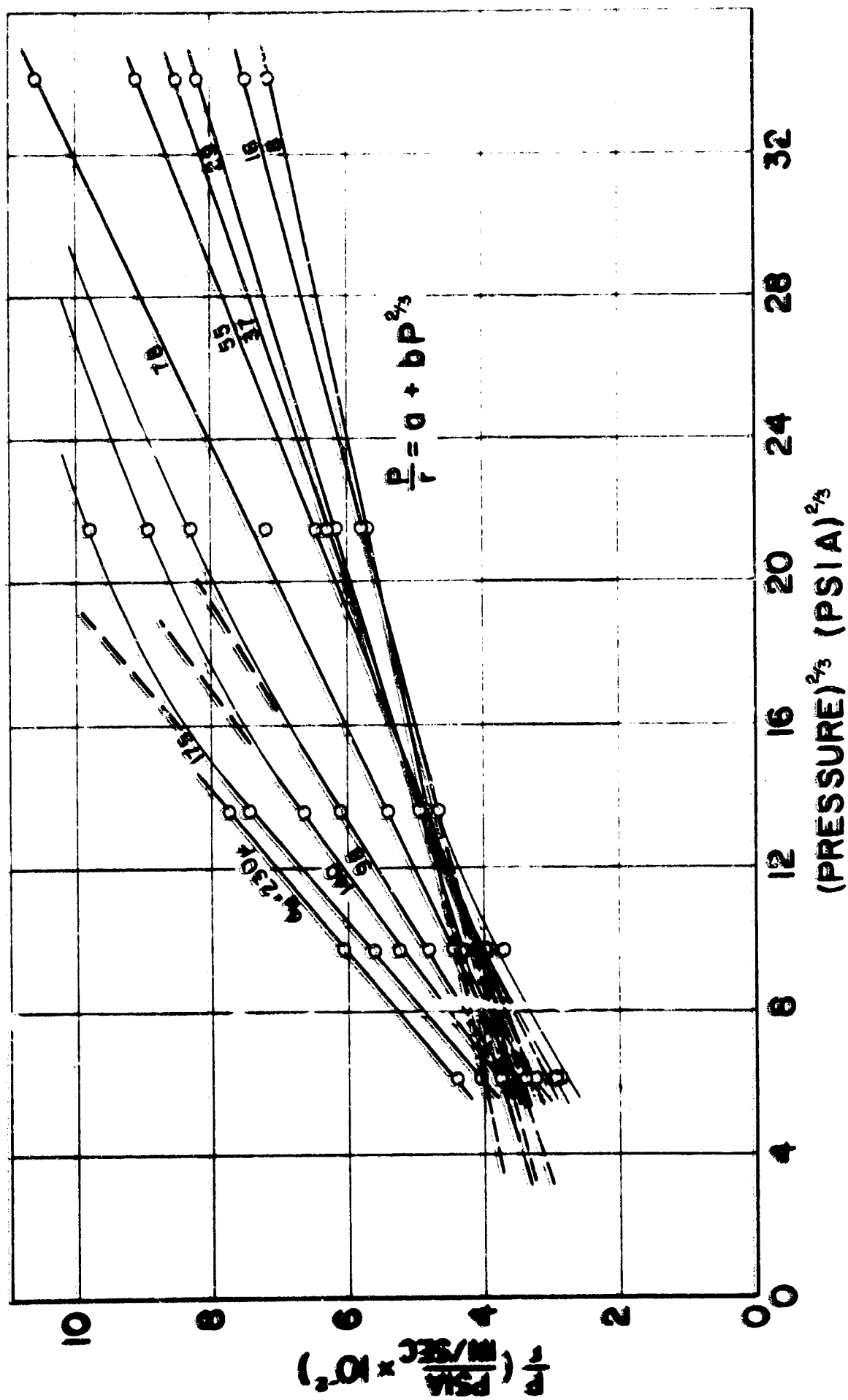
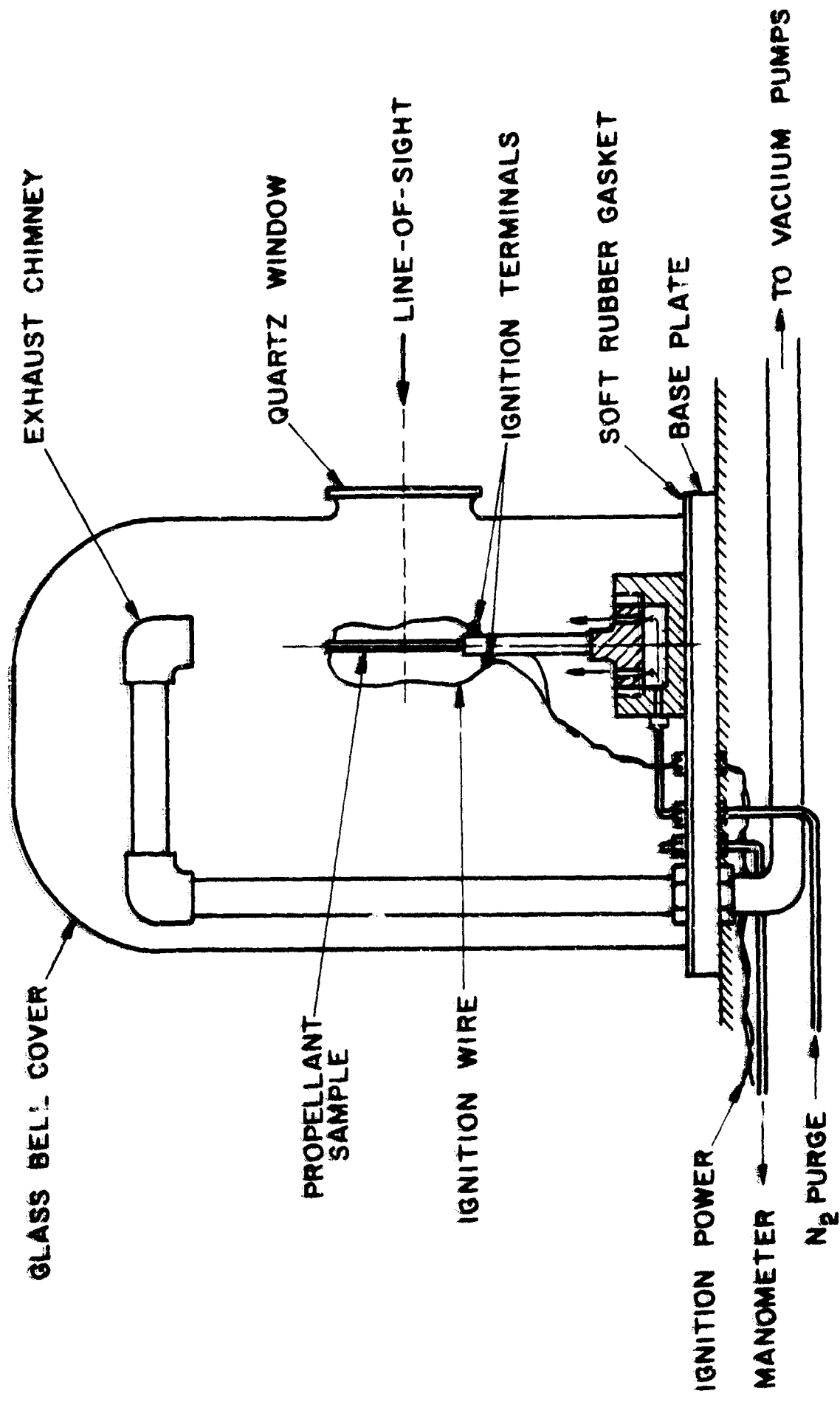


FIGURE 18
DIFFUSION TIME PARAMETER "b" VS PARTICLE SIZE,
POLYSULFIDE PROPELLANTS, NARROW UNIMODAL PARTICLE SIZE
DISTRIBUTIONS (AFTER BASTRESS (9))



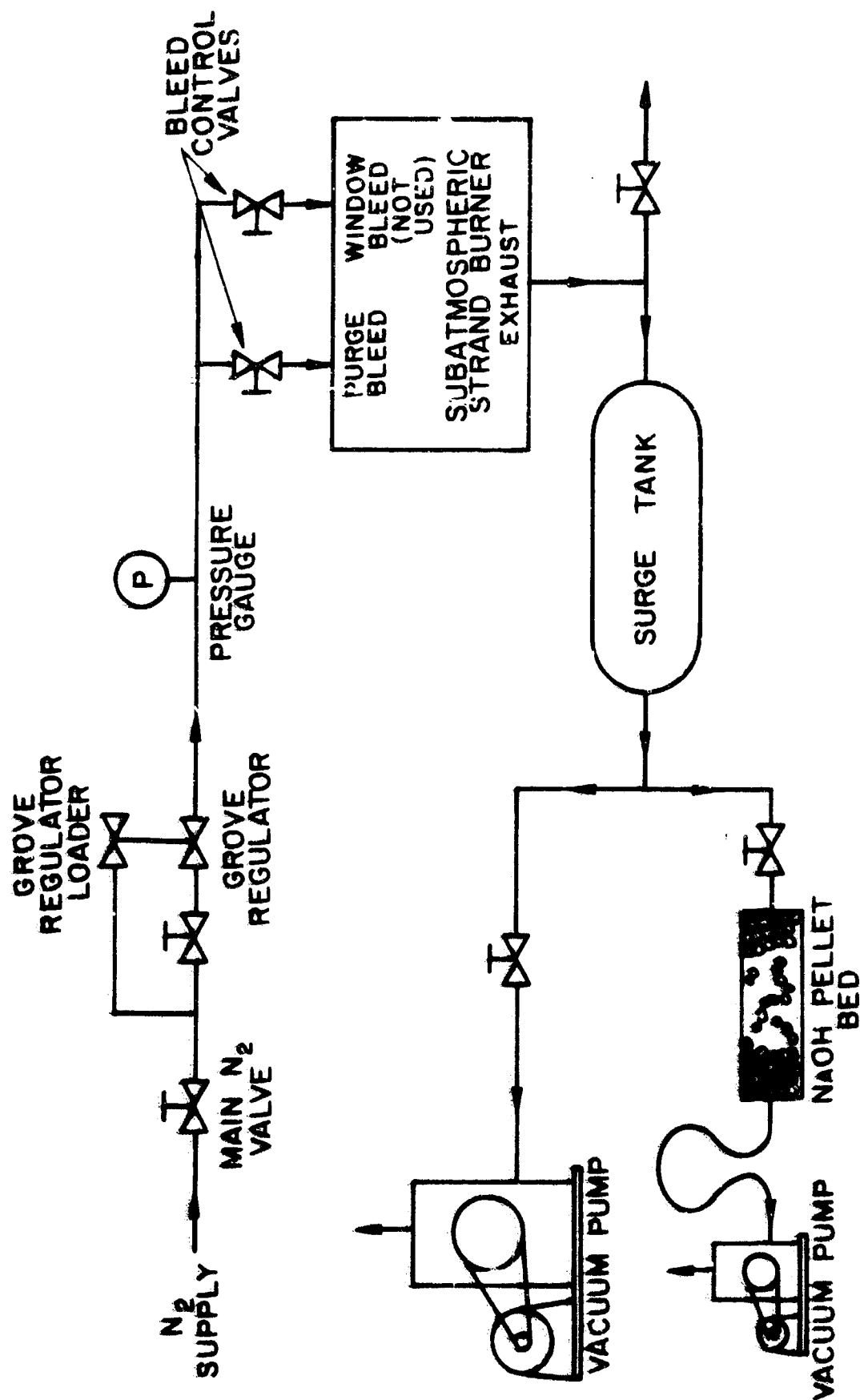
P/r VS $P^{2/3}$, POLYSULFIDE PROPELLANTS,
NARROW UNIMODAL PARTICLE SIZE DISTRIBUTIONS
(AFTER BASTRESS(9))

J219-4000-65

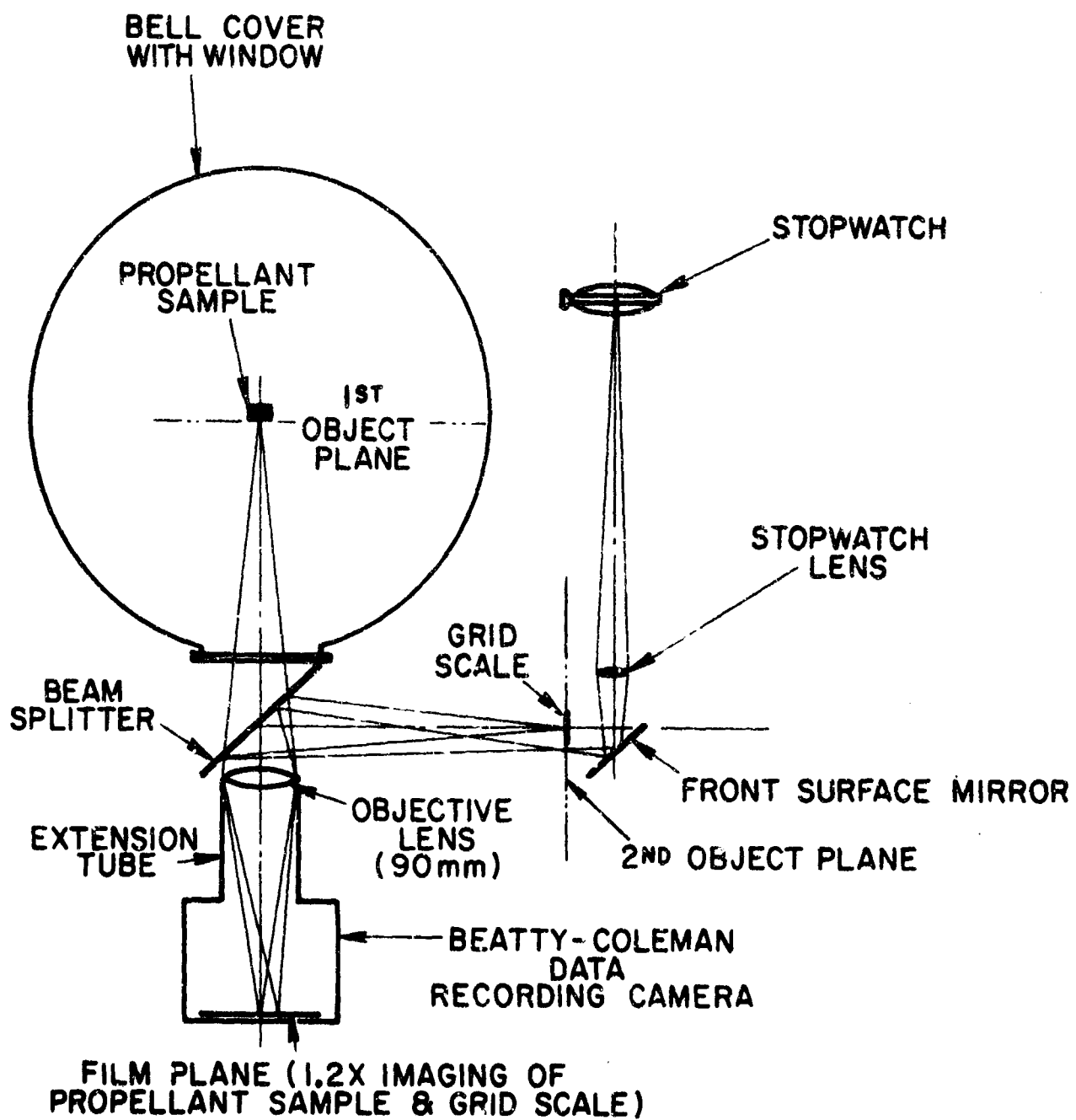


SUBATMOSPHERIC STRAND BURNER
(APPROXIMATELY TO SCALE)

FIGURE 20



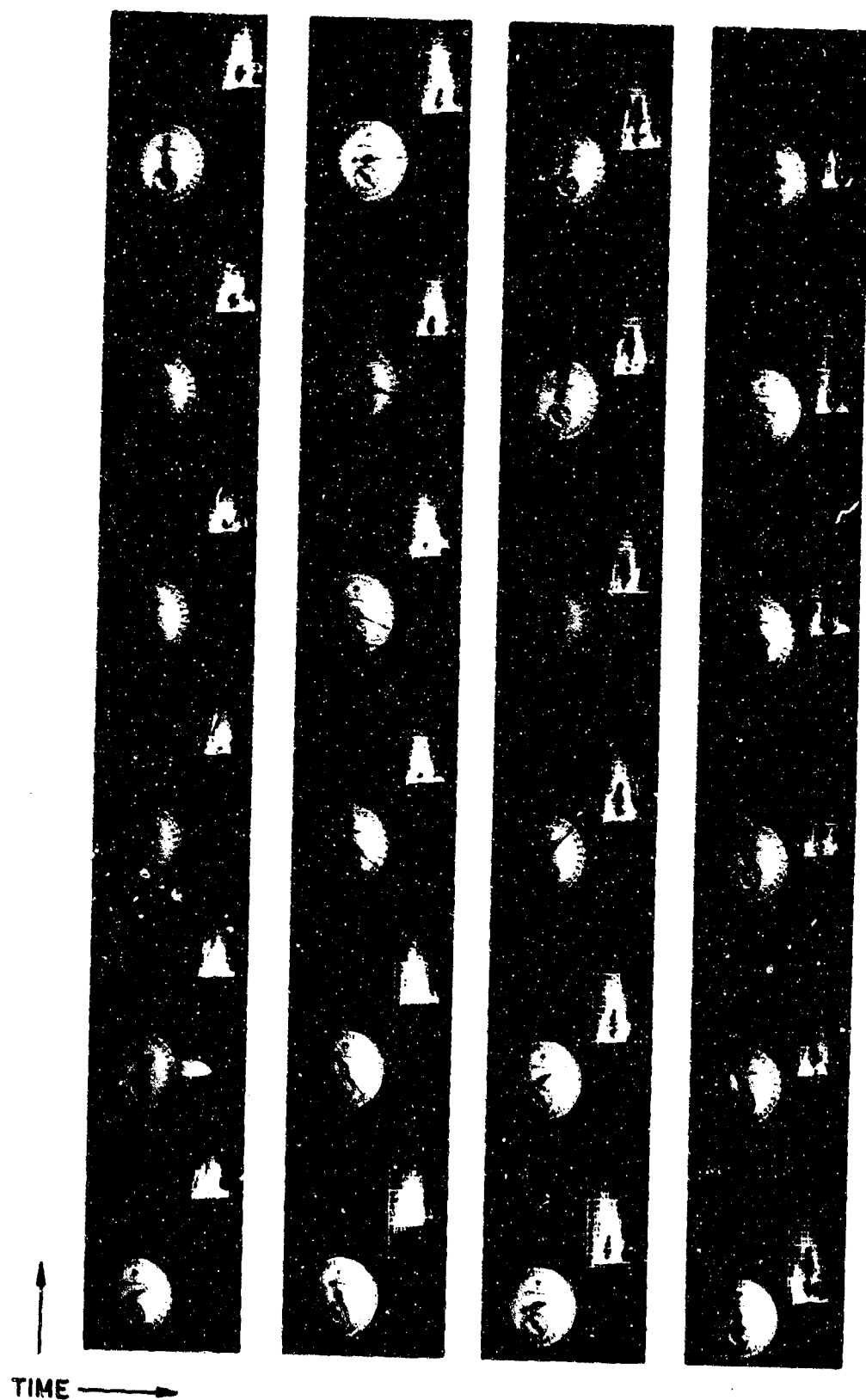
SUBATMOSPHERIC STRAND BURNER FLOW SYSTEM



PHOTOGRAPHIC BURNING RATE MEASUREMENT
OPTICAL SYSTEM

FIGURE 22

JP 19-4002-65



TYPICAL FILM RECORD USED FOR PROPELLANT
BURNING RATE DETERMINATION
(STOPWATCH FACE REVERSED DUE TO OPTICS)

FIGURE 23